Optical Properties of III-Nitride Semiconductors for Power Electronics and Photovoltaics

by

Hanxiao Liu

A Dissertation Presented in Partial Fulfillment
of the Requirements for the Degree
Doctor of Philosophy

Approved July 2020 by the
Graduate Supervisory Committee:

Fernando A. Ponce, Chair
Yuji Zhao
Nathan Newman
Alec M. Fischer

ARIZONA STATE UNIVERSITY

Augest 2020

ABSTRACT

This dissertation covers my doctoral research on the cathodoluminescence (CL) study of the optical properties of III-niride semiconductors.

The first part of this thesis focuses on the optical properties of Mg-doped gallium nitride (GaN:Mg) epitaxial films. GaN is an emerging material for power electronics, especially for high power and high frequency applications. Compared to traditional Si-based devices, GaN-based devices offer superior breakdown properties, faster switching speed, and reduced system size. Some of the current device designs involve lateral *p*-*n* junctions which require selective-area doping. Dopant distribution in the selectively-doped regions is a critical issue that can impact the device performance. While most studies on Mg doping in GaN have been reported for epitaxial grown on flat *c*-plane substrates, questions arise regarding the Mg doping efficiency and uniformity in selectively-doped regions, where growth on surfaces etched away from the exact *c*-plane orientation is involved. Characterization of doping concentration distribution in lateral structures using secondary ion mass spectroscopy lacks the required spatial resolution. In this work, visualization of acceptor distribution in GaN:Mg epilayers grown by metalorganic chemical vapor deposition (MOCVD) was achieved at sub-micron scale using CL imaging. This was enabled by establishing a correlation among the luminescence characteristics, acceptor concentration, and electrical conductivity of GaN:Mg epilayers. Non-uniformity in acceptor distribution has been observed in epilayers grown on mesa structures and on miscut substrates. It is shown that non-basal-plane surfaces, such as mesa sidewalls and surface step clusters, promotes lateral growth along the GaN basal planes with a reduced

Mg doping efficiency. The influence of surface morphology on the Mg doping efficiency in GaN has been studied.

The second part of this thesis focuses on the optical properties of InGaN for photovoltaic applications. The effects of thermal annealing and low energy electron beam irradiation (LEEBI) on the optical properties of MOCVD-grown $In_{0.14}Ga_{0.86}N$ films were studied. A multi-fold increase in luminescence intensity was observed after 800 °C thermal annealing or LEEBI treatment. The mechanism leading to the luminescence intensity increase has been discussed. This study shows procedures that significantly improve the luminescence efficiency of InGaN, which is important for InGaN-based optoelectronic devices.

To mom and dad for their love and support

ACKNOWLEDGMENTS

First, I would like to express my deepest gratitude towards my PhD advisor Prof. Fernando Ponce for giving me the opportunity to work with and learn from him in the past five and a half years. During this time, he has demonstrated to me the important principles of conducting scientific research: insatiable curiosity, rigorous research methodology, and academic integrity. I will always remember his invaluable teachings. I also want to give special thanks to Dr. Alec Fischer, who mentored me as I started my research at ASU, and taught me the use of cathodoluminescence, which became the main tool for my research.

I want to thank my collaborators, Prof. Yuji Zhao, Dr. Houqiang Fu, Dr. Kai Fu, Mr. Chen Yang, Dr. Rong Liu, and Dr. Zhihao Wu for their generous contributions. The samples and interesting problem they provided enabled me to conduct research and make discoveries that comprise much of this thesis. I also want to thank my group members, Dr. Hongen Xie, Dr. Shuo Wang, Dr. Shanthan Allugubelli, and Dr. Po-Yi Su for their collaboration spirit and friendship.

I would like to acknowledge the wonderful staffs at Eyring Materials Center at ASU: Mr. David Wright, Mr. Timothy Karcher, Ms. Diana Convey, and Dr. Emmanuel Soignard. Their expertise on various experimental tools and patient help have made my research experience at ASU much smoother and more enjoyable.

Finally, I would like to thank my parents for their unconditional love and encouragement through my education.

TABLE OF CONTENTS

Page

CHAPTER Page

LIST OF TABLES

Table Page

LIST OF FIGURES

Figure Page

Figure Page

Figure Page

Figure Page

Figure Page

Figure Page

Figure Page

Figure Page

Figure Page

CHAPTER 1

INTRODUCTION TO III-NITRIDE SEMICONDUCTORS

1.1 Background

III-nitride semiconductors have gained much attention in the recent decades. The successful development and commercialization of light emitting diodes (LED) utilizing wurtzite GaN has revolutionized the lighting technology by replacing the traditional incandescent lamps with more efficient and reliable solid-state lighting systems. This advancement has been recognized by the science community. The 2014 Nobel Prize in physics was awarded jointly to Shuji Nakamura, Hiroshi Amano, and Isamu Akasaki for their contribution in the invention of efficient blue light-emitting diodes, which has enabled bright and energy-saving white light sources.[1]

Since then, research on III-nitride materials have branched out into other applications, including photovoltaics[2,3] and more recently, power electronics.[4] The unique properties of III-nitride materials make them promising candidates in these areas of applications. However, many challenges still exist before III-nitride materials can be used to replace the existing technologies.

1.2 Physical properties of III-nitride materials

The III-nitride system consists of three binary compounds InN (E_g = 0.7 eV), GaN (E_g = 3.4 eV), and AlN (E_g = 6.2 eV) and their alloys. Their bandgap energies range from infrared to ultraviolet as shown in Fig. 1.1. In addition, they are all direct bandgap materials, which means that the radiative recombination and light absorption efficiency in these materials are much higher than indirect band gap materials, such as silicon. These properties make III-nitride materials a natural candidate for optoelectronic applications.

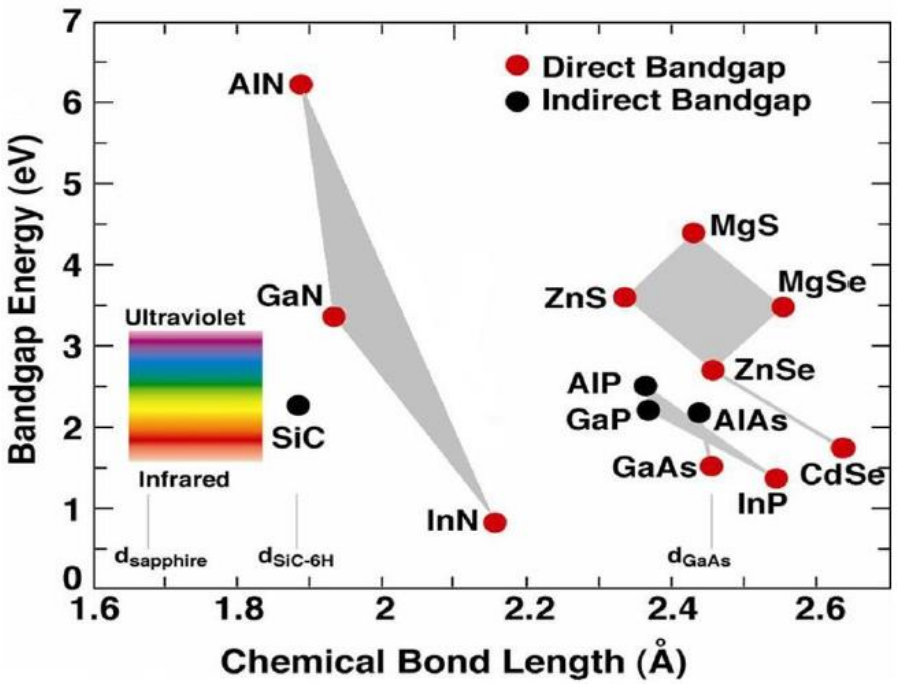

Figure 1.1. Bandgap versus lattice parameter for some semiconductor materials. [1]

III-nitride crystals exist in cubic zincblende and hexagonal wurtzite forms, with the wurtzite structure being more thermodynamically stable. The schematic diagram of a wurtzite lattice is shown in Fig. 1.2. Some basic physical properties of the III-nitride semiconductors are summarized in Table 1.1.

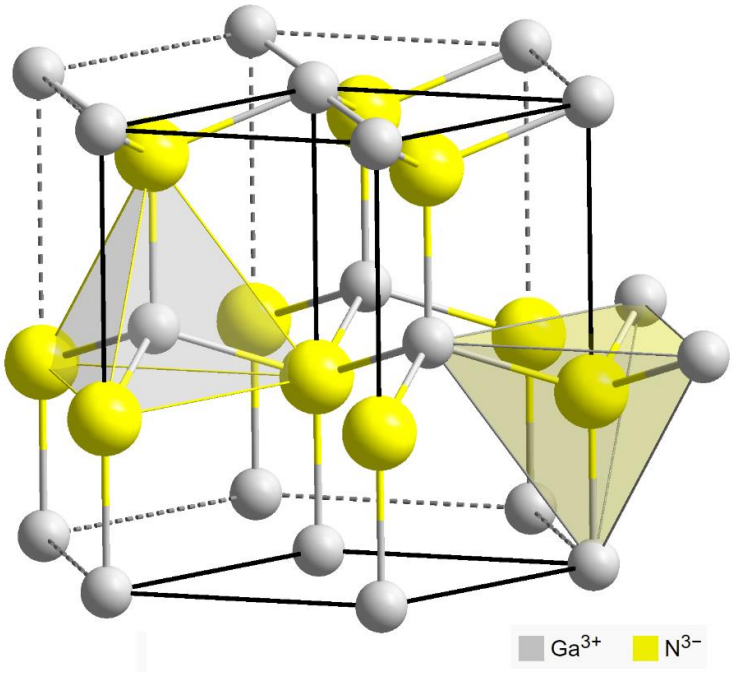

Figure 1.2. Schematic diagram of a GaN wurtzite lattice structure. (From Wikipedia)

Table 1.1. Basic physical properties of III-nitride semiconductors.[5,6]

Physical properties	**AlN**	**GaN**	**InN**
Lattice Constants (300K)			
a (Å)	3.111	3.189	3.538
c (Å)	4.979	5.185	5.703
c/a ratio	1.606	1.634	1.618
E_G(eV) (300K)	6.2	3.39	0.7
Thermal Expansion Coefficient (300K)			
a ($\times 10^{-6}K^{-1}$)	4.2	5.59	5.7
c ($\times 10^{-6}K^{-1}$)	5.3	3.17	3.7
Bond Length (Å)	1.89	1.94	2.15
Cohesive Energy per Bond (eV)	2.88	2.24	1.93
Melting Point (°C)	>3000	>2500	>1100
Bulk Modulus (Gpa) (300 K)	210	210±10	140

1.3 Introduction to Mg-doped GaN

For most solid-state device operations, two types of semiconductors are required: *n*-type and *p*-type. In *n*-type semiconductors, the material is doped with an element that has an extra valance electron. This leads to an abundance of mobile electrons that can conduct electricity. In silicon, this is typically done by substitutional incorporation of phosphorous. In *p*-type semiconductor, material is doped with an element that has a missing valance electron. This leads to a deficiency of electrons and unfilled bonds. The site where an electron is absent is positively charged and is called a hole. Holes can migrate in the lattice under an electric field. In silicon, this is accomplished by substitutional incorporation of boron.

In GaN, controlled *n*-type doing was achieved by substitutional incorporation of Si on Ga sites.[7] This results in shallow donors with an activation energy of 12-17 meV.[8] Since thermal energy at room temperature is 25 meV, the low activation energy of Si donors gives a near completion ionization of donors at room temperature, leading to very good *n*-type conductivity of Si-doped GaN.

P-type doping in GaN has proved to be more challenging. Several elements such as Zn, Be, Mg, and Cd were explored as acceptor candidates since the early 70s.[9,10] But the compensation of acceptors by unintentionally incorporated donors is very severe. In addition, acceptor level produced by most of these elements are deep within the band gap, leading to a high activation energy.[9,11,12] It was not until 1989, when Amano et al. first achieved *p*-type conductivity in GaN, by using low-energy electron-beam irradiation (LEEBI) on MOCVD grown Mg-doped GaN (GaN:Mg) thin films.[13] Later in 1992, Nakamura et al. discovered that *p*-type conductivity in GaN:Mg films can also be achieved

by thermal annealing the films in a nitrogen or vacuum environment at temperature higher than 500 °C. They observed six orders of magnitude drop in the resistivity of GaN:Mg films after annealing at 700 °C for 20 minutes in nitrogen (Fig. 1.3).[14]

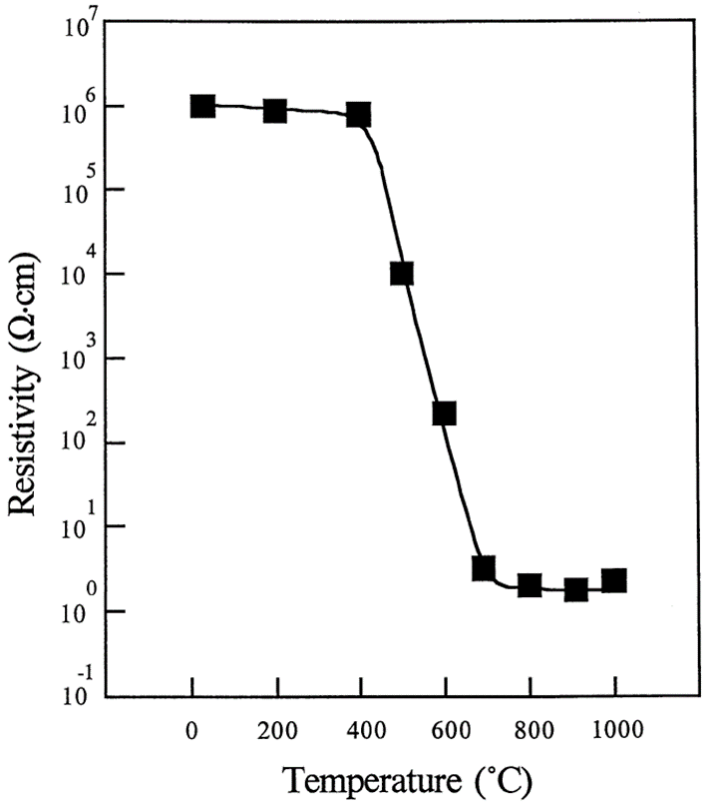

Figure 1.3. Resistivity of GaN:Mg as a function of annealing temperature. (Adapted from Ref. 14)

The mechanism leading to the resistivity drop in GaN:Mg after LEEBI or thermal annealing was not clear at that time. It was later discovered that Mg acceptors in the as-grown GaN:Mg films were passivated by H impurities, which form Mg-H complex that lowers the acceptor concentration.[15-18] Since H exists in most of the MOCVD precursors (e.g. NH_3, TMGa), there is a high degree of H incorporation into the GaN:Mg films during MOCVD growth. A H atom may bond with a Mg atom, donating its electron to make the

Mg atom isoelectric to a group III element. The Mg-H complex is stable at room temperature but can be dissociated under electron beam irradiation or thermal annealing, producing active Mg acceptors. Since thermal annealing is more economically feasible compared to LEEBI from a mass production point of view, post-growth thermal annealing has been adopted as a standard procedure to achieve *p*-type conductivity in GaN:Mg by the LED industry.

Despite the progress made, achieving high carrier concentration, high mobility GaN:Mg films is still challenging. One of the reasons is the activation energy of Mg acceptor in GaN:Mg is high. The Mg acceptor energy level in GaN:Mg films was measured to be around 170 meV above the valance band edge.[19] This leads to a low percentage of acceptor ionization at room temperature. A GaN:Mg film with a Mg concentration in the range of 10^{19} cm^{-3} will typically result in a hole concentration in the range of 10^{17} cm^{-3}. Further limitation on hole concentration in GaN:Mg is imposed by the solubility limit of Mg in GaN. It was reported that when Mg doping concentration exceeds the solubility limit of 1×10^{20} cm^{-3}, Mg forms precipitates that drastically reduce the *p*-type conductivity.[20,21] In addition, it was reported that self-compensation in GaN:Mg becomes significant when Mg concentration exceeds 2×10^{19} cm^{-3}.[22] It was speculated that increasing Mg doping concentration beyond this level will increase the concentration of nitrogen vacancies (V_N), which behaves as donors that compensate the Mg acceptor, leading to reduced hole concentration.[22]

1.4 GaN-based power electronics

In recent years, GaN has attracted a lot of attention for its applications in power electronics. Wide band gap semiconductor materials such as SiC and GaN offer many advantages in power electronic applications due to their unique material properties. For example, the critical electric field of GaN (3.3 MV/cm) is 10 times larger than that of Si. This means the drift layer thickness of GaN power devices can be made 10 times thinner that Si-based devices. This will reduce device size, decrease power consumption, and lower heat generation significantly. In addition, the intrinsic carrier concentration of GaN is much lower than Si due to its wide band gap. This makes GaN-based devices suitable for high temperature operations. Some of the physical properties for Si, 4H-SiC, and GaN are compared in Table1.2. Figure 1.4 shows the theoretical limit for specific on-resistance versus the breakdown voltage of these three materials when used in power electronics. Wide bandgap materials offer a smaller specific on-resistance (R_{on}) while maintaining a larger breakdown voltage.

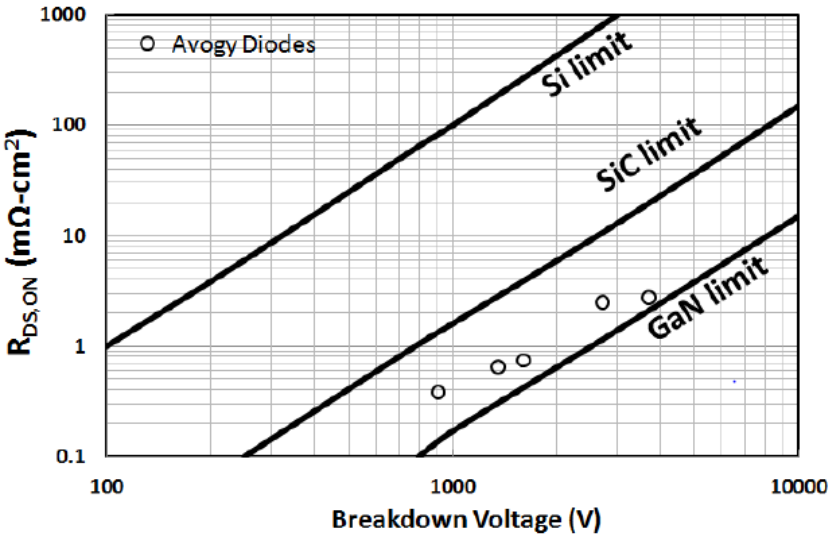

Figure 1.4. R_{on} vs. the breakdown voltage for Si, SiC, and GaN. (Ref 23)

Table 1.2. Physical properties comparison of Si, 4H-SiC, and GaN. (Adapted from Ref 24)

Materials Property	**Si**	**SiC-4H**	**GaN**
Band Gap (eV)	1.12	3.26	3.4
Critical Field 10^6 V/cm	0.3	3.0	3.3
Electron Mobility (cm^2 /V·s)	1350	700	1200
Electron Saturation Velocity (10^6 cm/s)	10	22	25
Thermal Conductivity (Watts/cm^2 K)	1.5	5	1.3

For many advanced power electronic device structures, such as junction barrier Schottky diode, floating field rings, filed effect transistors, and bipolar junction transistors, as shown in Fig. 1.5,[25] selective area doping is required, which means selectively doping regions into *n*-type or *p*-type. In the current Si and SiC industry, this is achieved using ion implantation and diffusion of dopants. However, doping of GaN using ion implantation and diffusion have been challenging. It was found that ion beam will cause considerable disordering in GaN, thus adversely affects its electronic properties.[26] Diffusion method is also problematic for GaN because the high dislocation density in GaN makes the control of dopants diffusion difficult. In addition, surface decomposition becomes significant during high temperature annealing required for the dopant diffusion.[27]

Currently, doping during epitaxial growth is still the most common method to get well-controlled doping in GaN. Therefore, an etch-and-epitaxial-regrowth process is a promising way to achieve selective-area doping in GaN. However, while most studies of Mg doping in GaN have been reported for films grown on flat *c*-plane substrates, questions arise when adding lateral structures requiring growth on surfaces etched away from the exact *c*-plane orientation. In advanced power devices, dopant distribution in doped regions is a critical issue that can impact the device performance. It is of high importance to

understand the nature of Mg doping in GaN on patterned and etched surfaces. It is in this historical context that the CL analysis of GaN:Mg will be done in this thesis.

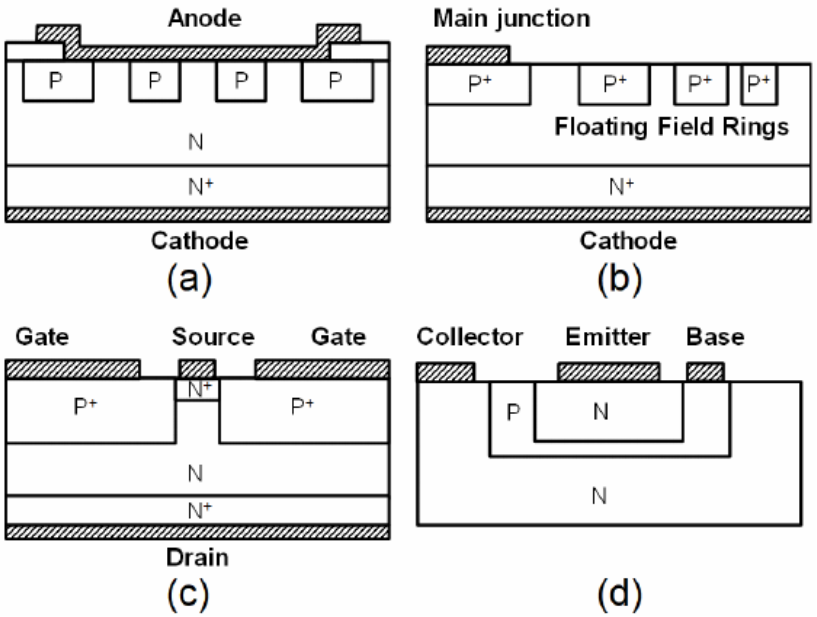

Figure 1.5. Schematics of possible applications of selective area doping of Mg in GaN for (a) junction barrier Schottky diode, (b) floating field rings, (c) field effect transistors, and (d) bipolar junction transistors. (Adapted from Ref. 27)

CHAPTER 2

EXPERIMENTAL METHODS

This chapter offers a brief description of the experimental techniques used in this thesis to investigate the material properties of semiconductors. The luminescence characteristics were studied using cathodoluminescence (CL) spectroscopy. The electrical properties such as charge carrier concentration and mobility, were measured using Hall effect measurement with the Van der Pauw method. Elemental analysis for the doping concentration and background impurity concentration, were done using the secondary ion mass spectroscopy (SIMS).

2.1 Cathodoluminescence

2.1.1 Introduction to cathodoluminescence

Cathodoluminescence spectroscopy is a powerful tool to study the luminescence properties of materials. A CL spectrometer is typically attached to a scanning electron microscope (SEM).[28] As the primary electron beam generated from the SEM cathode enters the sample, interaction of electrons with the solid can produce various signals as shown in Fig. 2.1.[29] Elastic scattering interaction with the specimen atoms produces back scattered electrons, which provide atomic number contrast. Inelastic scattering interaction produces secondary electrons, which give information of sample surface topography. High energy absorption of incident electrons leads to X-ray and Auger electron emission. Absorption also leads to generation of electron-hole (e^-/h^+) pairs. The recombination of e^-/h^+ pairs produces light. Cathodoluminescence refers to the generation of light as the results of electron beam interaction with a specimen.

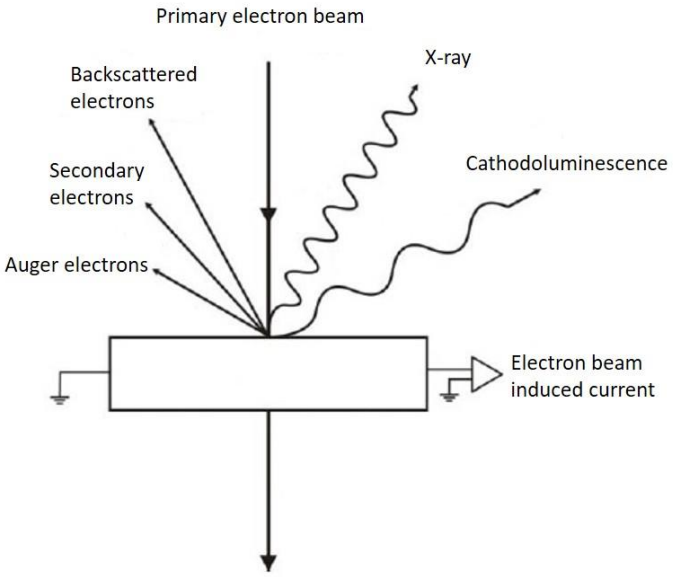

Figure 2.1. Schematic diagram showing different types of electron beam-specimen interactions.

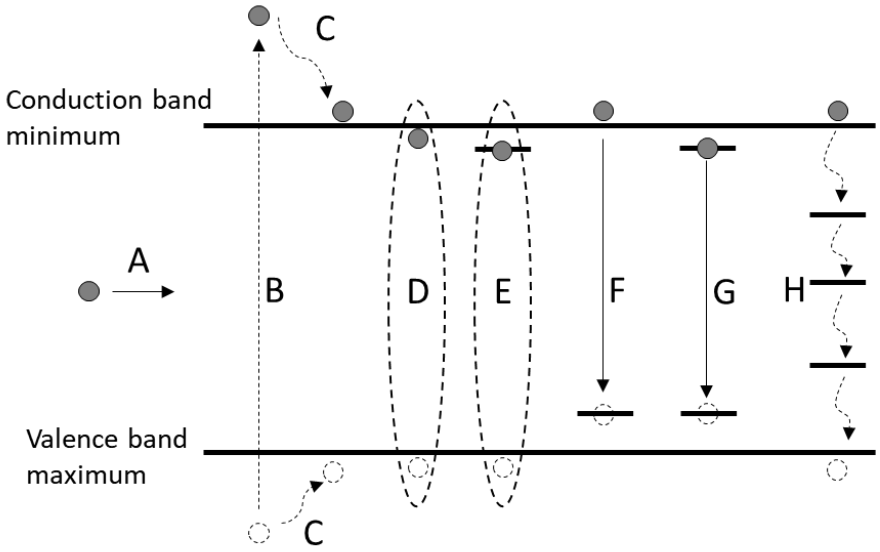

Figure 2.2. Electronic transitions during cathodoluminescence. (A) Primary electron, (B) e^-/h^+ pair generation, (C) thermalization. (D) free exciton, (E) bound exciton, (F) free-to bound transition, (G) donor-acceptor pair, (H) non-radiative recombination through traps.

After the generation of an e^-/h^+ pair, several electronic transitions can occur in a semiconductor material as shown in Fig. 2.2. The absorption of high energy primary electron promotes an electron from the valance band into the conduction band (process B). The electron and hole will quickly thermalize to the conduction band minimum and valance band maximum respectively (process C). They will then form an exciton, which is similar to a hydrogen atom, where two carriers of opposite charges are bound together by their Coulomb interactions (process D). Light emission due to recombination of excitons will have a photon energy of $E_{hv} = E_g - E_x$, where E_g is the bandgap and E_x is the binding energy of an exciton. If there are impurities in the semiconductor material, excitons can be bounded to an impurity site and become a donor-bound or acceptor-bound exciton (process E). Photon energy due to recombination of a bound exciton will be given by $E_{hv} = E_g - E_x - E_b$, where E_b is the binding energy of the exciton to the impurity site. Process F represents recombination between a free electron to a hole localized on an acceptor site. Process G represents donor-acceptor pair recombination where an electron localized on a donor site recombines with a hole localized on an acceptor site. Process F represents non-radiative recombination. This occurs when electron recombines through trap states within the bandgap without generating light, and energy is lost in this process by the generation of phonons.

Cathodoluminescence in a SEM is the combination of a spectroscopic and microscopic tool. It can be used to acquiring a CL spectrum, which is a plot of light emission intensity versus wavelength (or energy). In this case, it is similar to a photoluminescence (PL) spectroscopy. An average spectrum of the specimen can be obtained by scanning the electron beam over an area while recording the spectrum. The advantage of CL over PL

come from its high spatial resolution. For example, a spectrum can be obtained by changing the raster size of the electron beam, or even fixing the electron beam at a specific location when recording the spectrum. Since the electron beam probe size is very small (~ 5 nm), this can be used to investigate spatial variation of optical properties of a material. Moreover, user can fix the monochromator to a specific wavelength (energy) and record the spatial variation of light emission intensity over an area. This will give a virtual mapping of optical properties of the specimen. Sometimes when paired with SE image, correlation between structural and optical properties can be established.

2.1.2 Penetration depth of electron beam

The interaction volume of electron beam with the specimen is important for CL analysis. Although the primary electron beam probe size can be focused down to a few nanometers in an SEM, the spatial resolution of CL mapping is determined by the interaction volume of electron beam with the sample, which depends on the acceleration voltage of primary beam. The size of the interaction volume is measured from top of the surface to the depth where the electrons losses all energy and is usually characterized by what is called the electron beam penetration range. An illustration of the interaction volume is shown in Fig. 2.3.

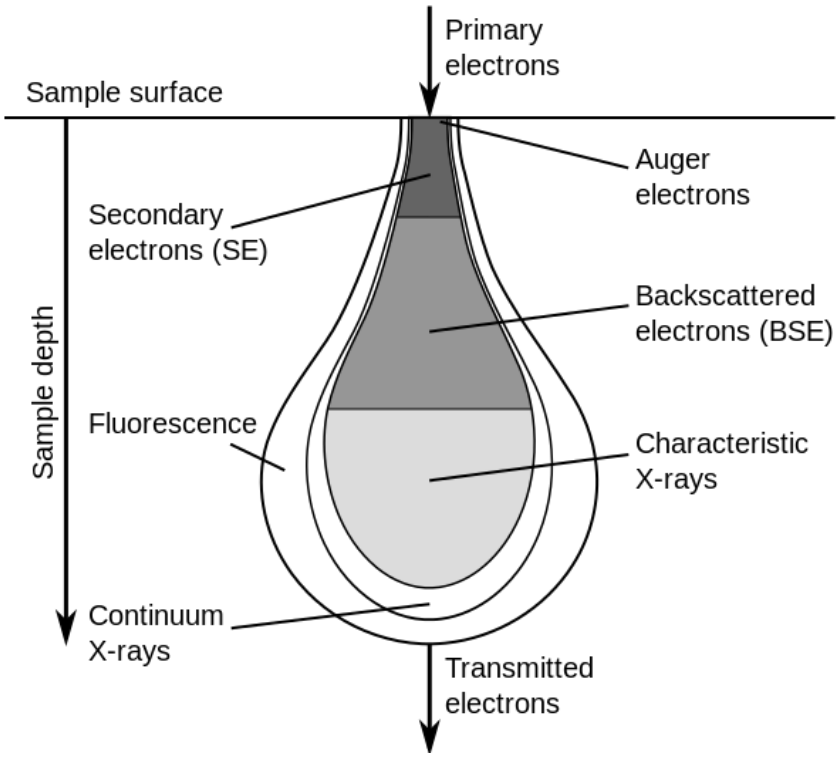

Figure 2.3. Interaction volume generated by electron bombardment. The approximate range of the secondary and backscattered electrons signals are indicated. (From Wikipedia)

An empirical expression for the electron beam penetration in solids was suggested by Kanaya and Okayama,[30]

$$R_e = \left(\frac{0.0276A}{\rho Z^{0.889}}\right) E_b^{1.67} (\mu m)$$

where A is the atomic weight in g/mol, ρ is in g/cm^3, Z is the atomic number, and E_b is primary beam voltage in keV.

A plot of maximum electron penetration depth versus electron beam acceleration voltage, calculated based on the Kanaya and Okayama model, is shown in Fig. 2.4 for GaN.

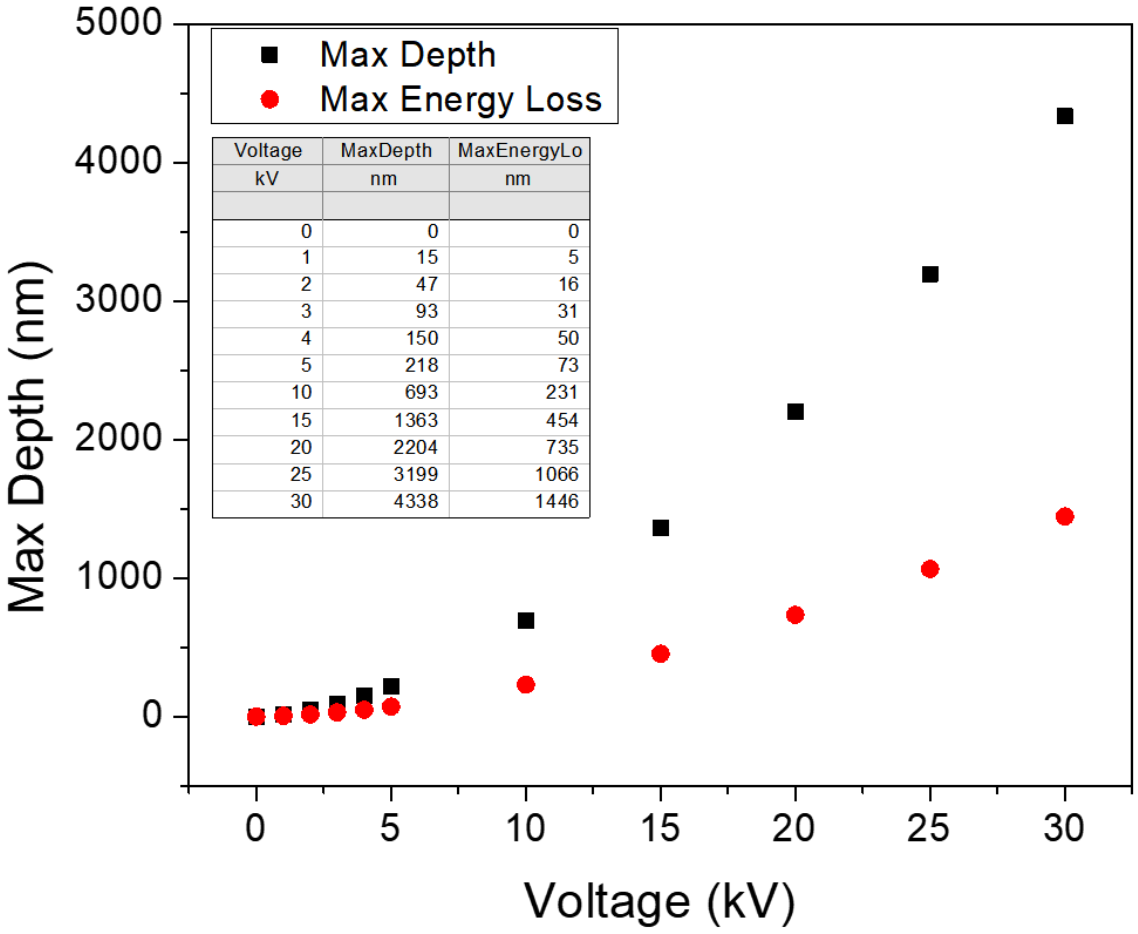

Voltage	MaxDepth	MaxEnergyLo
kV	nm	nm
0	0	0
1	15	5
2	47	16
3	93	31
4	150	50
5	218	73
10	693	231
15	1363	454
20	2204	735
25	3199	1066
30	4338	1446

Figure 2.4. Penetration depth for GaN calculated based on the Kanaya and Okayama model.

2.1.3 Time-resolved cathodoluminescence

The carrier recombination dynamics in a semiconductor can be studied using the time-resolved CL (TRCL). In a TRCL measurement, a pulsed electron beam that resembles a square wave is incident on semiconductor material to create luminescence. The electron beam pulses are produced by a beam blanker, which is essentially a capacitor of two parallel metal plates that can deflect the electron beam when applied with a voltage. The temporal behavior of the sample excitation and luminescence decay is measured. By setting the monochromator to a certain wavelength, one can measure the carrier lifetime associated to optical transitions of that specific energy.

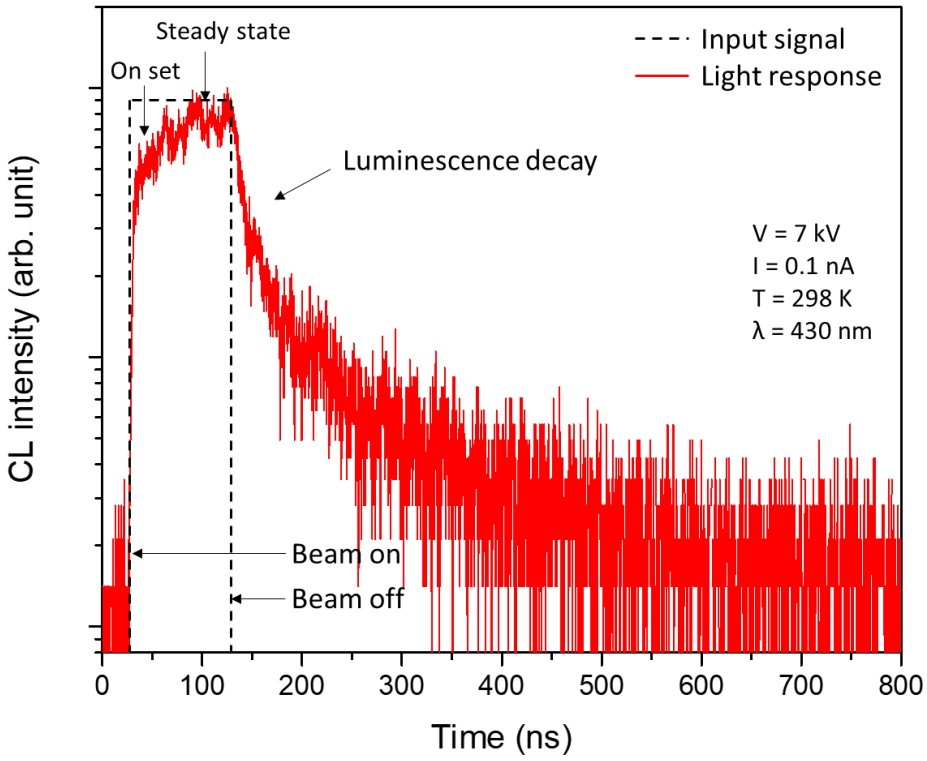

Figure 2.5. A room temperature time-resolved CL response recorded on the luminescence of a GaN:Mg epilayer, at wavelength of 430 nm.

Fig. 2.5 shows a room temperature time-resolved CL response for a GaN:Mg epilayer with Mg concentration of 6.3×10^{19} cm^{-3} at wavelength of 430 nm. The black dashed lines represent the electron beam square wave signal. After beam on at around ~50 ns, an increase of luminescence intensity is observed due to the increased generation and recombination of electron-hole-pairs. The luminescence intensity will reach a maximum when the generation and recombination rate of e^-/h^+ pairs is equal. After beam off, the luminescence intensity will decay. The decay can typically be fitted by the sum of one or more exponential decay functions to derive the carrier lifetimes:

$$I(t) = A_1 e^{-\frac{t}{\tau_1}} + A_2 e^{-\frac{t}{\tau_2}} + \cdots$$

Where A_1 and A_2 are the initial intensity values, and τ_1 and τ_2 are the carrier lifetimes.

2.1.4 Setup of a cathodoluminescence system

The CL system used in this thesis is shown in Fig. 2.6. It consists of a JEOL 6300 scanning electron microscope equipped with a LAB_6 thermionic electron gun, connected to an Oxford monoCL monochromator and a GaAs photomultiplier tube (PMT). The light emitted from the samples is collected by a movable parabolic mirror on top of the sample stage. The sample surface is adjusted to the focal point of the mirror for maximum light collection. The mirror contains a pinhole in the center, which allows the electron beam probe to pass through, scan, and excite the sample. The reflected light transmitting through a monochromator and will then be detected by a photomultiplier tube.

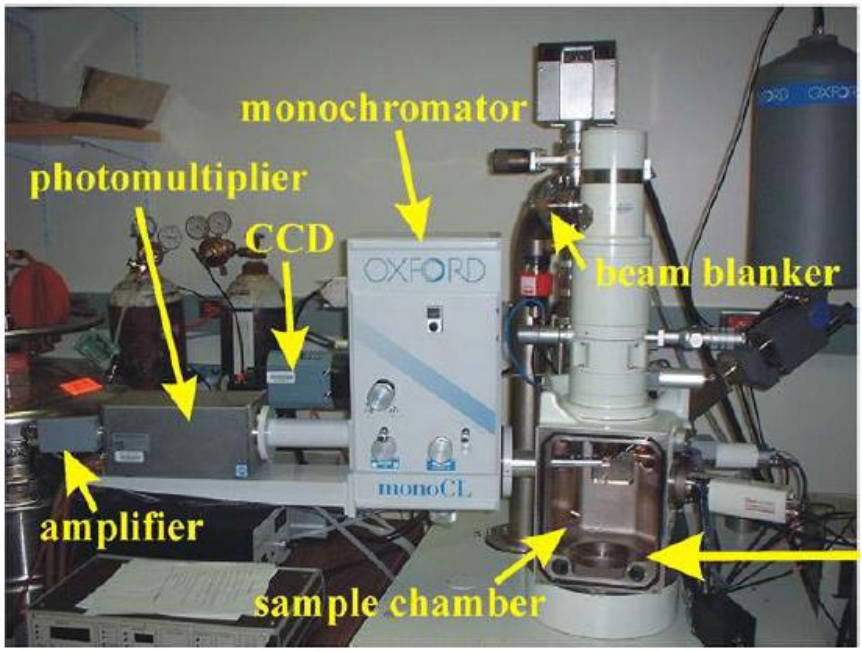

Figure 2.6. A photograph of the CL system used in this thesis.

2.2 Hall effect measurement

Hall effect measurement is a common and powerful method to measure the conductivity of a material. It can give the polarity, density, and the mobility of mobile charge carriers inside a sample. The underlying physical principle of Hall effect is the Lorenz force, which is the combination of electrical and magnetic force a mobile charge experiences when moving in the presence of a electromagnetic field. The force is given by:

$$\boldsymbol{F} = q(\boldsymbol{E} + \boldsymbol{v} \times \boldsymbol{B})$$

An illustration of Hall effect is shown in Fig. 2.7. A current is pass through a bar-shaped sample that has mobile electrons as charge carriers. When a magnetic field $\boldsymbol{B}$ is applied as shown in the figure, the electron trajectory will bend towards the left, causing an accumulation of negative charges on the left side and positive charges on the right side of the sample. This causes a potential difference across the two sides of the sample. This potential is called the Hall voltage (V_H). If the mobile charge carriers inside the sample are holes instead of electrons, the direction of the resulting field will be opposite. Therefore, by measuring the direction of electric field created by the accumulated charges, one can determine the polarity of mobile carriers.

The accumulated charges will create an electric potential $\boldsymbol{E}$ that exerts electrical force on the moving electrons to prevent further charging. An equilibrium is reached when the magnetic force equals to the electrical force produced by the accumulated charges:

$$q(\boldsymbol{E} + \boldsymbol{v} \times \boldsymbol{B}) = 0$$

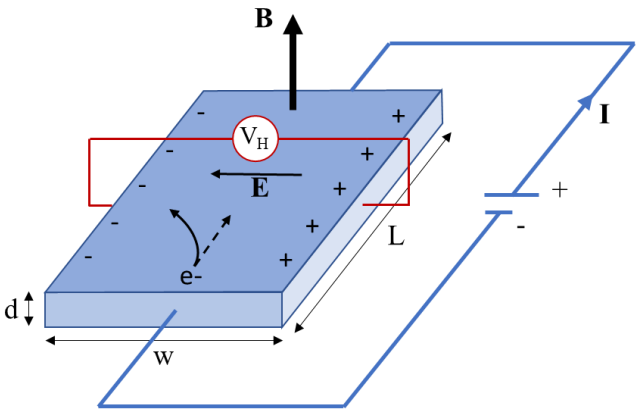

Figure 2.7. Illustration of Hall effect in a bar-shaped sample.

The current *I* in the material is given by:

$$\boldsymbol{I} = nq\boldsymbol{v}dw$$

where *n* is the bulk carrier concentration, *q* is the carrier charge, ***v*** is the carrier velocity, *d* is the sample thickness, and *w* is the sample width. Therefore:

$$\boldsymbol{v} = \frac{\boldsymbol{I}}{nqdw}$$

The electric field ***E*** resulted from the accumulating charges is given by:

$$E = \frac{V_H}{w}$$

Substituting ***E*** and ***v*** into the equilibrium condition equation, we obtain:

$$\frac{|V_H|}{w} = \frac{IB}{nqdw}$$

and the above equation can be rearranged to give the bulk carrier concentration as:

$$n = \frac{IB}{V_H qd}$$

Therefore, at a given current I, by measuring the Hall voltage V_H and sample thickness d, one can calculate the carrier concentration of the material.

In order to obtain the charge carrier mobility μ, a series of resistivity measurement and Hall measurement is needed. The most common and convenient technique to measure a uniform sample is the Van der Pauw method.[31,32] Fig. 2.8 shows an example of Van der Pauw configuration. A square sample is used, although any arbitrary shape is allowed. Electrical contacts are made at the four corners of the sample. It should be noted that the fundamental assumption of the Van der Pauw method is that the sample is uniform in thickness, with no voids or islands across the whole film, and the sample lateral dimension is much larger than the size of the contacts and the sample thickness.

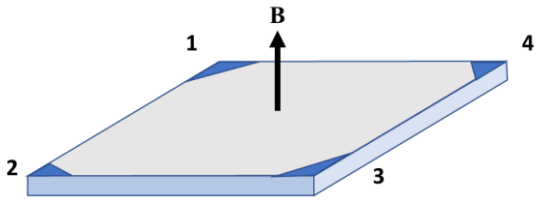

Figure 2.8. Example of the Van der Pauw configuration used in this thesis.

To measure the carrier concentration, a current is applied from contact 3 to contact 1 (I_{13}). The Hall voltage across contacts 4 and 2 is measured (V_{24}). Using the equation above, we can calculate the carrier concentration. One can also apply current through contacts 2 and 4, and measure voltage across 3 and 1, then flip the direction of the magnetic field and repeat the measurements. An average of the above measurements will provide a more accurate result of the final carrier concentration.

To obtain the carrier mobility μ of the sample, first we need to determine the sheet resistivity R_s. The sheet resistivity R_s is related to characteristic resistivity R_A and R_B by the Van der Pauw formula:

$$e^{-\frac{\pi R_A}{R_s}} + e^{-\frac{\pi R_B}{R_s}} = 1$$

R_A and R_B are calculated by the following expressions, measured under no magnetic field:

$$R_A = \frac{V_{43}}{I_{12}} \; and \; R_B = \frac{V_{14}}{I_{23}}$$

Generally, a reiterative method is used to solve the Van der Pauw formula numerically for R_s. A special scenario is when $R_A = R_B = R$. In this case, $R_s = \frac{\pi R}{ln2}$, and the quotient $\frac{\pi}{ln2}$ is known as the Van der Pauw constant and has a value of ~4.5326. The carrier mobility μ is related to the sheet resistivity by the following equation:

$$\mu = \frac{1}{nqR_s d}$$

2.3 Secondary ion mass spectroscopy

Secondary ion mass spectroscopy (SIMS) is a powerful tool to measure impurity concentrations in a solid. It uses an energetic ion beam to bombard the sample to release secondary ions or charged molecules, which are passed through a mass analyzer for mass separation. The selected ions with the specific mass to charge ratio are then projected onto a detector for quantitative analysis. The detection limit of SIMS is in the range of 10^{12} – 10^{20} cm^{-3} for thin film semiconductors. This makes it an ideal tool to measure the background impurity and doping concentration.[33] An illustration of a typical SIMS setup is shown in Fig. 2.9.

In this thesis, SIMS is used for impurity depth profiling. This is done by monitoring the intensity of the secondary ions as a function of sputtering time, which is converted into depth. For GaN, the most abundant background impurity elements are C, O, and H. Si and Mg are also common impurities since they are the dopant for *n*-type and *p*-type GaN, respectively. To monitor these elements, Cs^+ and O_2^+ ions are used. O and C concentrations are measured using the Cs^+ primary ion beam, which is efficient at generating negatively charged ions and molecules such as O^- or CN^-. Ga, N, Mg, and Si concentrations are measured using the O_2^+ primary ion beam, which is efficient at generating positively charged ions and molecules such as Ga^+, N^+, Mg^+, and Si^+.[34,35]

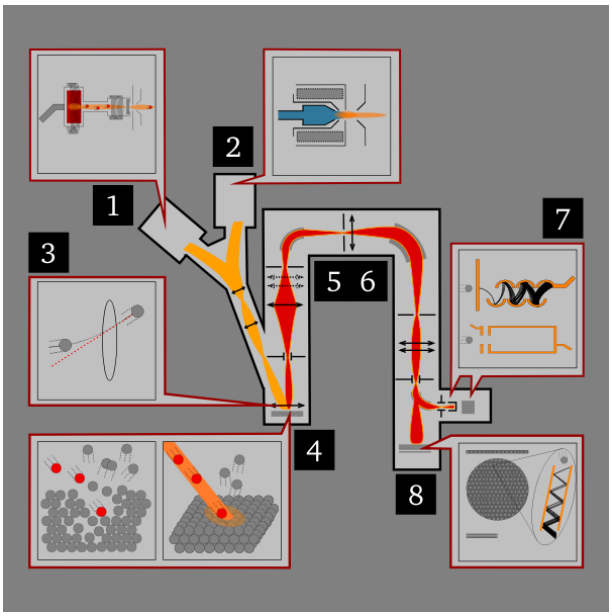

Figure 2.9. Illustration of a typical SIMS configuration, showing: (1) and (2) two different primary beam sources, (3) electrostatic lens to focus primary beam, (4) ionization and sputtering of sample surface, (5) electrostatic sector, (6) magnetic sector, (7) electron multiplier (top)/Faraday cup (bottom), and (8) CCD ion imaging detector. (Adapted from Wikipedia)

CHAPTER 3

OPTICAL PROPERTIES OF MG-DOPED GAN EPILAYERS STUDIED BY CATHODOLUMINESCENCE SPECTROSCOPY

The objective of this thesis is to study the optical properties of selectively doped GaN:Mg epilayers for power electronic applications. However, before studying the optical properties of GaN:Mg grown on mesa structures that involves growth on non-basal planes, it is important to have a solid understanding of GaN:Mg grown on a planar basal plane surface. The optical properties of GaN:Mg epilayers depend on a wide range of variables, including the Mg doping concentration, the acceptor activation level, and the background donor impurity concentration. When the optical properties are measured using cathodoluminescence spectroscopy, additional factors need to be taken into consideration, including the electron beam current and exposure time. In this chapter, the effects of these variables on the CL characteristics of GaN:Mg will be discussed.

3.1 Effect of low-energy electron-beam irradiation on the luminescence characteristic of GaN:Mg

The first *p*-type GaN was obtained by Amano and coworkers using low-energy electron-beam irradiation (LEEBI) treatment on MOCVD-grown GaN:Mg thin films. They found that e-beam irradiation induces changes in GaN:Mg films and lower its resistivity.[13] Since then, studies have shown that LEEBI will induce changes to the luminescence characteristics of both activated and un-activated GaN:Mg films.[36,37] In this thesis, cathodoluminescence (CL) spectroscopy was used as a tool to study the optical properties of GaN:Mg. CL utilizes an electron beam to excite the specimen causing it to luminesce.

The electron beam can be set to an acceleration voltage ranging from 1 to 30 kV, and a beam current ranging from 10^{-10} to 10^{-3} A. The highly energetic electrons may cause permanent changes to the luminescence properties of the specimen. Therefore, it is important to investigate how the specimen is affected by the electron beam, and whether a change in luminescence characteristics occurs during the CL measurement.

To study the effect of electron beam irradiation on the optical properties of GaN:Mg epilayers, three samples with the structure of GaN:Mg (1μm)/*n*-GaN (2 μm)/sapphire substrate have been grown using MOCVD. The Ga and N sources were trimethylgallium (TMGa) and ammonia (NH_3), respectively. The precursor for Si donors in the *n*-GaN layer was silane (SiH_4), and the precursor for Mg acceptors in the GaN:Mg layer is bis(cyclopentadienyl)magnesium (Cp_2Mg). The GaN:Mg layer was grown with a TMGa flow rate of 25 sccm, at a temperature of 950 °C. The Cp_2Mg flow rate during the GaN:Mg growth was changed to be 50, 100, and 200 sccm in Samples A, B, and C, respectively. This resulted in Mg concentrations of 1.3×10^{19}, 3.1×10^{19}, and 6.3×10^{19} cm^{-3}, as determined by SIMS. Post-growth thermal annealing was performed using rapid thermal annealing (RTA) at 800 °C for 10 minutes in a nitrogen environment in order to activate the Mg acceptors.

Photoluminescence (PL) spectra of the GaN:Mg layers in Samples A, B, and C were measured using a 325-nm HeCd laser with an excitation power of 6 mW at room temperature. Plan-view cathodoluminescence spectra of the same samples were measured at room temperature under an electron beam acceleration voltage of 7 kV, which corresponds to a maximum penetration depth of ~400 nm. The beam current was varied to 0.1, 1, and 8.5 nA to investigate the effect of electron beam current on the luminescence

characteristics of GaN:Mg. CL spectra were recorded in raster scan mode over a 50×50 μm^2 square region. The electron beam makes a rectangular raster that consist of 256 horizontal lines per frame and 60 frames per second. Three spectral scans were performed consecutively over the same region. The scan covers a wavelength ranging from 350 to 650 nm (1.9 - 3.54 eV) and takes 450 s to complete. When multiple spectral scans were recorded over the same area, the electron exposure time is added. The electron dose per scan is given by:

$$\delta = \frac{I_b t}{A}$$

where I_b is the beam current, t is the exposure time, and A is the scanning area. For beam currents of 0.1, 1, and 8.5 nA, the electron doses per spectral scan are 1.8, 18, and 153 mC/cm^2, respectively. Taking into consideration the electron beam interaction volume in the material, the diffusion of carriers, and drift in the precise location of the horizontal line scans for each frame, the irradiation over the raster area can be considered uniform, at least to a first approximation.

PL spectra of GaN:Mg epilayers in Samples A, B, and C with different Mg concentrations are shown in Fig. 3.1(a), the high frequency modulation in the spectra is caused by the Fabry-Pérot interference. CL spectra for the Samples A, B, and C, measured under beam current of 0.1 nA, are shown in Fig. 3.1(b). Three consecutive scans were performed over a same area on the sample to monitor if changes to luminescence characteristics occur under continuous electron beam irradiation. The first, second, and third scans are represented by the solid, dashed, and dotted lines, respectively. The total electron doses δ is added with each scan. The electron dose after the first scan is 0.18 mC/cm^2. After the second and third scan, the total electron dose is 0.36 and 0.54 mC/cm^2,

respectively. It can be seen that the CL and PL spectra look very similar. Three peaks located at 3.4, 3.25, and 2.85 eV were observed. These three peaks are commonly observed in GaN:Mg and have been reported in previous literatures.[38-43] The 3.4 eV peak is attributed to GaN band edge transition. The 3.25 eV peak is attributed to shallow donor to Mg acceptor transitions. The 2.85 eV peak is attributed to deep donor to Mg acceptor transitions. The deep donors have been speculated to be complexes formed by nitrogen vacancies with nearest neighboring Mg atom (V_N-Mg).[40-43]

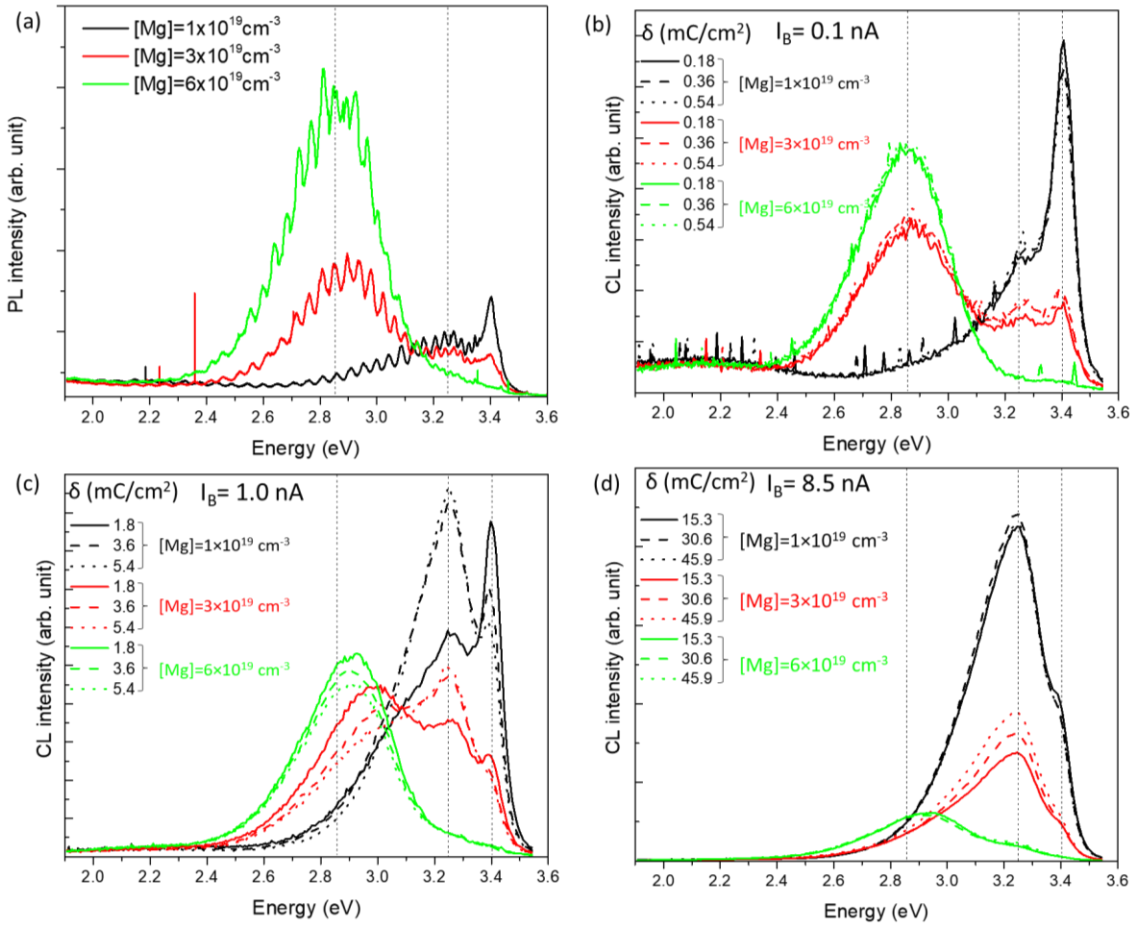

Figure 3.1. Optical characteristics of GaN:Mg epilayers in Samples A, B, and C, measured at room temperature. (a) PL spectra measured with a 6 mW 325 nm HeCd laser, and CL spectra measured using electron beam acceleration voltage of 7 kV and different beam currents of (b) 0.1, (c) 1.0, and (d) 8.5 nA, respectively.

The relative intensity of these emission peaks changes with Mg doping concentration. With increasing Mg concentration, the luminescence intensity for the 2.85 eV peak will increase, and that of the 3.4 and 3.25 eV peak will decrease.[38-41] The dependence of relative peak intensities with Mg concentration will be discussed in detail in section 3.3 as well as in chapter 4 of this thesis.

The similarity between the PL and CL spectra in Fig. 3.1(a) and (b) indicates that the CL spectra measured at 0.1 nA beam current represents the intrinsic luminescence characteristics of GaN:Mg, and is not affected by electron beam irradiation. In addition, under 0.1 nA, CL spectra for the GaN:Mg films remain unchanged after three consecutive scans. This means that under such electron dosage, the electron beam will not cause any change in the luminescence characteristics in the GaN:Mg films during the measurement.

In Fig. 3.1(c), we observed changes in spectral shape under e-beam irradiation when the electron beam current is increased to 1.0 nA. The intensity of the 2.85 eV peak decreases, and the intensity of 3.25 eV peak increases with each scan. For spectra recorded under electron beam current of 8.5 nA shown in Fig 3.1(d), it was observed that the intensity of the 3.25 eV peak has already increased significantly after the 1st scan. Subsequent 2nd and 3rd scans further increase the intensity of 3.25 eV peak. In addition, the position of the 2.85 eV peak is blue shifted under high beam currents. Therefore, CL spectra obtained under a beam current between 1.0 and 8.6 nA are affected by the electron beam irradiation, and do not represents the intrinsic luminescence properties of the material.

The quenching of 2.85 eV peak under electron beam irradiation may be due to saturation of deep donor states associated with the 2.85 eV transition. The blue shift of the

peak position under high beam current of 1.0 and 8.5 nA as seen in Figs. 3.1(c) and (d) also indicates saturation of states. The carrier lifetime for the 3.4, 3.25, and 2.85 eV transitions are measured and will be discussed in more details in section 3.2 of this chapter. It was found that the carrier lifetime for the 2.85 eV transition is much longer (~200-300 ns) than that of the 3.25 and 3.4 eV transitions (0.8 ns). This suggests that the 2.85 eV transition can be saturated under high excitation currents.

With the saturation of the deep donor states associated with the 2.85 eV transition under high excitation power, the excited electrons will thermalize to the shallow donor state and recombine with the Mg acceptors, producing the 3.25 eV emission. This leads to an increase of the 3.25 eV intensity. The carrier lifetime of the 3.25 eV transition is very short (0.8 ns), similar to the carrier lifetime of band edge transitions. So, it is less likely to be saturated.

In conclusion, PL and CL spectra of GaN:Mg films with different Mg concentrations were measured. It was found that when using an electron beam current of 0.1 nA in CL measurement, similar spectral signals were obtained with CL and PL. Electron dose under this condition is sufficiently low that it will not affect the luminescence properties of GaN:Mg. When the beam current is higher than 1.0 nA, we observed a quenching and blue shift of the 2.85 eV emission, and an intensity increase of the 3.25 eV peak under continuous electron beam irradiation. It is speculated that this change is due to the saturation of deep donor states associated with the 2.85 eV emission under high beam current.

Considering these results, all the remaining CL spectra on GaN:Mg thin films in this thesis were measured using an electron beam current of 0.1 nA.

3.2 Carrier lifetime studied by time-resolved cathodoluminescence

Carrier lifetime of GaN:Mg epilayers is studied using time-resolved CL at room temperature. The three samples studied are Samples A, B, and C, described in 3.1, with different [Mg] of 1.3×10^{19}, 3.1×10^{19}, and 6.3×10^{19} cm^{-3}, respectively.

The GaN:Mg epilayers were excited using pulsed electron beam, produced by a beam blanker. The electron beam pulses resemble square waves, with a pulse duration of 100 ns and a frequency of 1 MHz. The beam current is 0.1 nA and the acceleration voltage is 7 kV. Several transients were recorded at 3.4, 3.25 and 2.85 eV, to compare the carrier dynamics of optical transitions at these energies. The transients are plotted in Fig 3.2.

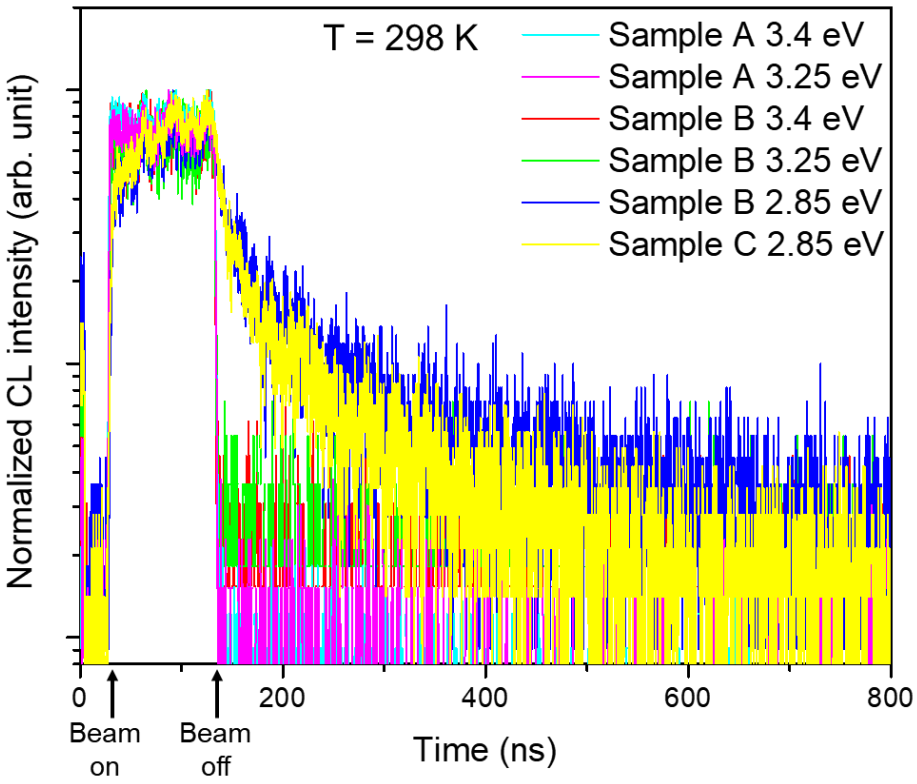

Figure 3.2. TRCL measurements of transients for Samples A, B, and C, measured for transitions at 3.4, 3.25 and 2.85 eV.

The decay of CL intensity after beam off is fitted with an exponential decay function:

$$I(t) = I_0 e^{-\frac{t}{\tau}}$$

where I_0 is the CL intensity at beam off, which is normalized to 1, and τ is the carrier lifetime.

Fig. 3.3 shows the carrier lifetimes for the 3.4 (band edge) and 3.25 eV (shallow donor to acceptor) transitions for Sample A. It was found that both transitions have a short lifetime of 0.8 ns. The transient for the 2.85 eV transition was not measured due to the low emission intensity.

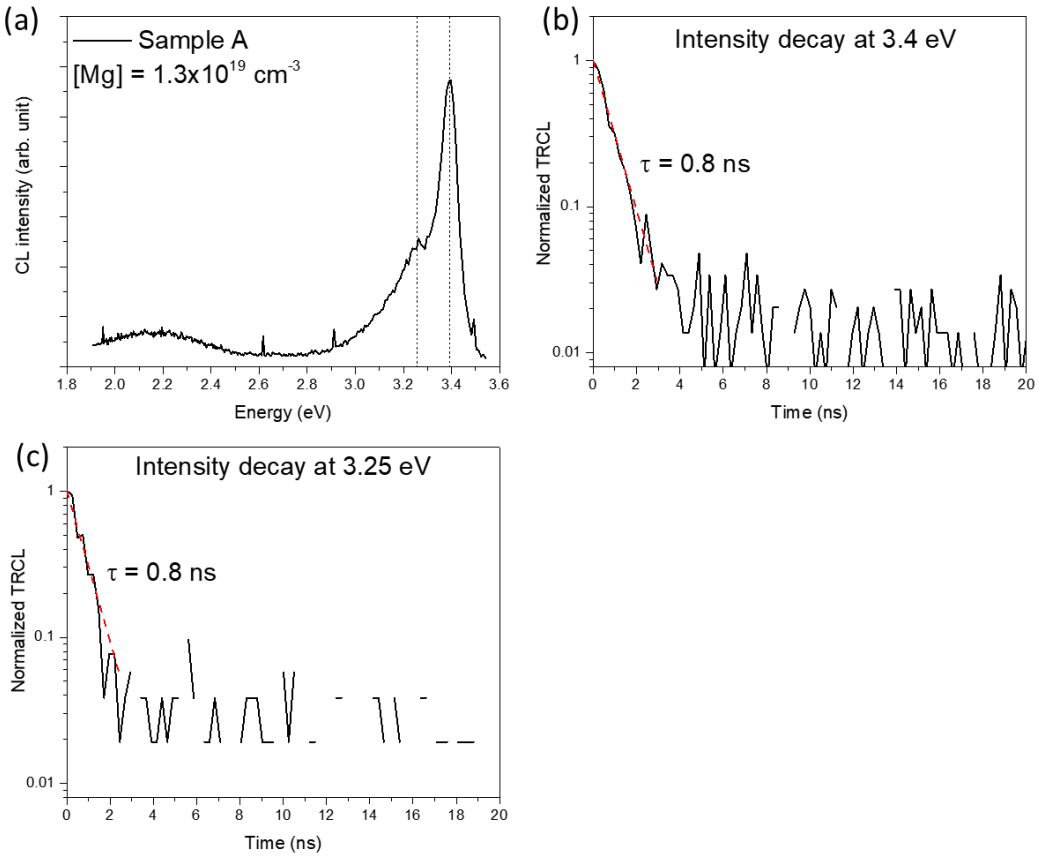

Figure 3.3. (a) CL spectra of Sample A. Normalized CL transients of the (b) 3.4 eV and (c) 3.25 eV transitions.

Fig. 3.4 shows the carrier lifetime for the 3.4 eV (band edge), 3.25 eV (shallow donor to acceptor), and 2.85 eV (deep donor to acceptor) transitions for Sample B. The 3.4 and 3.25 eV transitions have the same lifetime (~ 0.8 ns), same as those observed in Sample A. However, the lifetime for the 2.85 eV transition is much longer. The transient of the 2.85 eV decay cannot be fitted with a single exponential decay function. A double exponential decay function was used instead:

$$I(t) = A_1 e^{-\frac{t}{\tau_1}} + A_2 e^{-\frac{t}{\tau_2}}$$

This indicates there are two recombination processes associated with the 2.85 eV donor-acceptor-pair (DAP) transition. This has been observed in DAP transitions, where lifetime depends on the separation between donors and acceptors, which gets larger in time.[44] A_1 and A_2 are the recombination strength or probability of each recombination, τ_1 and τ_2 are the carrier lifetime associated with each recombination. The lifetime of τ_1 and τ_2 are 336.9 and 21.5 ns, respectively. This result is similar to a previous report, which shows the carrier lifetime of the 2.85 eV emission in GaN:Mg is around 300 ns at room temperature.[45]

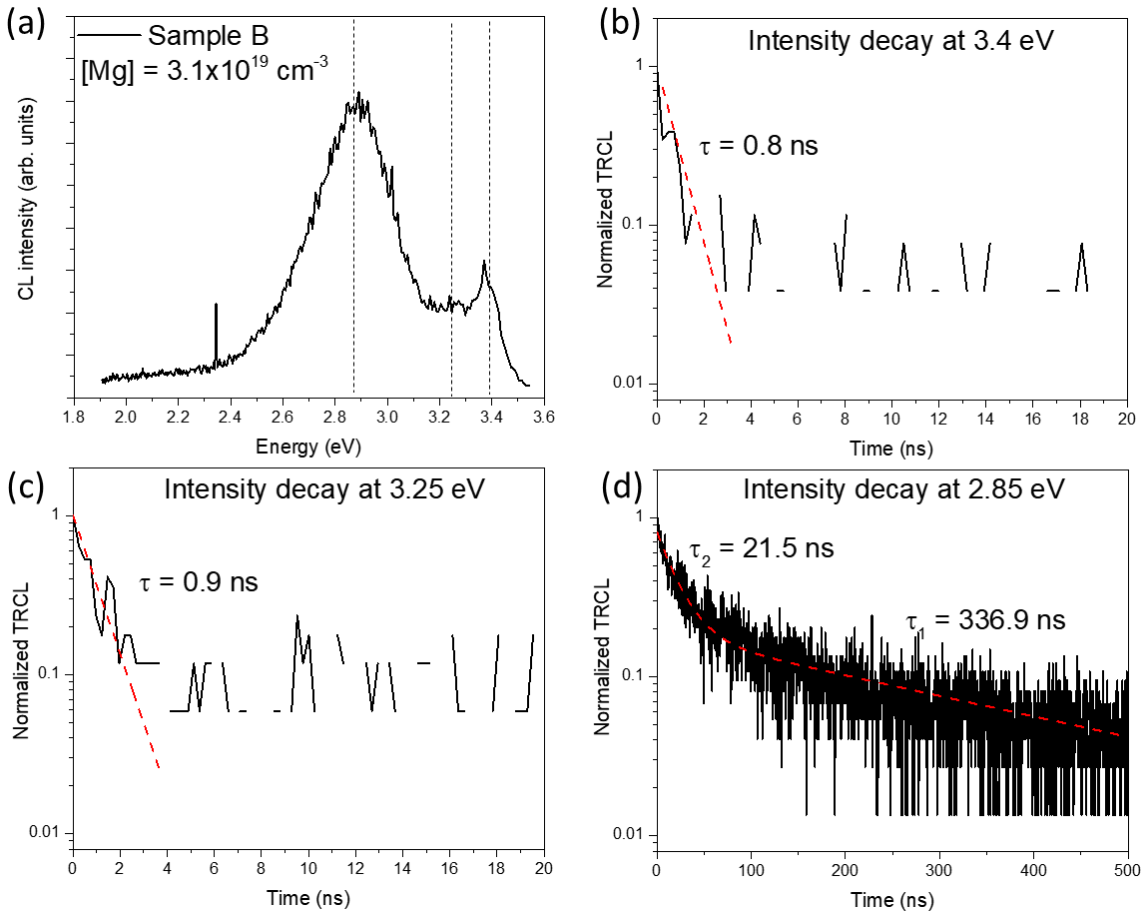

Figure 3.4. (a) CL spectra of Sample B. Normalized CL transients of the (b) 3.4 eV, (c) 3.25 eV, and (d) 2.85 eV transitions.

Recombination kinetics in Sample C is shown in Fig. 3.5. Since the luminescence intensities of the 3.4 and 3.25 eV peaks are very weak, only the transient of the 2.85 eV line can be reliably measured, which is shown in Fig. 3.5(b). The lifetime of τ_1 and τ_2 are 227.9 and 15.7 ns, respectively, both shorter than the τ_1 and τ_2 in Sample B. This is expected, since Sample C has a higher Mg acceptor concentration than Sample B. This leads to a higher recombination probability between deep donors and Mg acceptors, leading to a decrease in carrier lifetime.

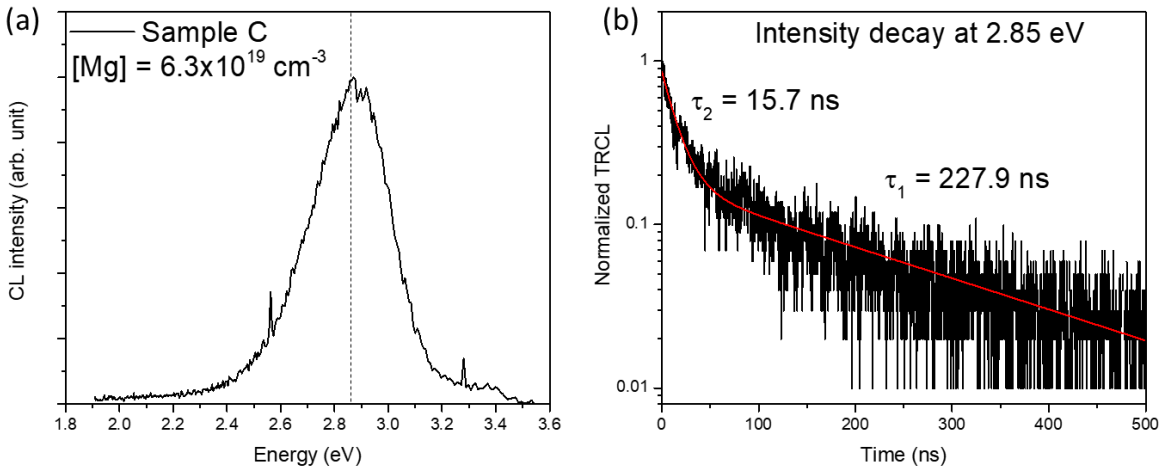

Figure 3.5. (a) CL spectra of Sample C. Normalized CL transient of the (b) 2.85 eV transition.

In conclusion, the recombination kinetics for the 3.4, 3.25, and 2.85 eV lines were measured at room temperature using time-resolved CL for GaN:Mg epilayers with different Mg concentrations. It was found that the 3.4 and 3.25 eV transitions both have a short carrier lifetime of ~0.8 ns, independent of Mg concentration. The 2.85 eV transition has a much longer carrier lifetime, which decreases with increasing Mg concentration in the GaN:Mg film.

3.3 Effect of Mg doping concentration and thermal activation on luminescence characteristic of GaN:Mg

In section 3.1, we observed that the luminescence properties of GaN:Mg depends on Mg doping concentration. A slight change of Mg concentration within an order of magnitude (from 1×10^{19} cm^{-3} to 6×10^{19} cm^{-3}) can have a significant impact on the luminescence characteristics of GaN:Mg epilayers (Fig. 3.1(a) and (b)). The spectra typically consist of three emission peaks at 3.4, 3.25, and 2.85 eV. As Mg doping

concentration increases, the intensities of the higher energy peaks will decrease, and the intensity of the lower energy peaks will increase.

It should be noted that the GaN:Mg spectra reported in 3.1 have been thermally annealed at 800°C for 10 minutes to activate Mg acceptors. During the experimental process of optimizing thermal activation temperature, we observed that the luminescence characteristics of GaN:Mg also depend on the thermal annealing temperature. GaN:Mg thin films with different Mg concentrations of 1.3×10^{19}, 3.1×10^{19}, and 1.6×10^{19} /cm^{-3}, as described in section 3.1, have been subjected to RTA at 700, 750, and 800 °C for 10 minutes in a nitrogen atmosphere. CL spectra were recorded for each sample after thermal annealing to investigate the effect of annealing temperature on the luminescence characteristics of GaN:Mg films. The spectra were recorded using raster scan mode over a 50×50 μm^2 area, with an acceleration voltage of 7 kV and a beam current of 0.1 nA.

Figure 3.6(a) and (b) show the spectra of the as-grown and thermal annealed GaN:Mg films with [Mg] = 1.3×10^{19} cm^{-3}. The luminescence from the as-grown sample is dominated by the 3.4 eV emission, with a shoulder peak at 3.25 eV. After thermal activation, the relative intensity of the 3.25 eV emission intensity increases. However, the spectrum is still dominated by the band edge transition at 3.4 eV. The spectra shape of samples annealed at 700, 750, and 800 °C are similar.

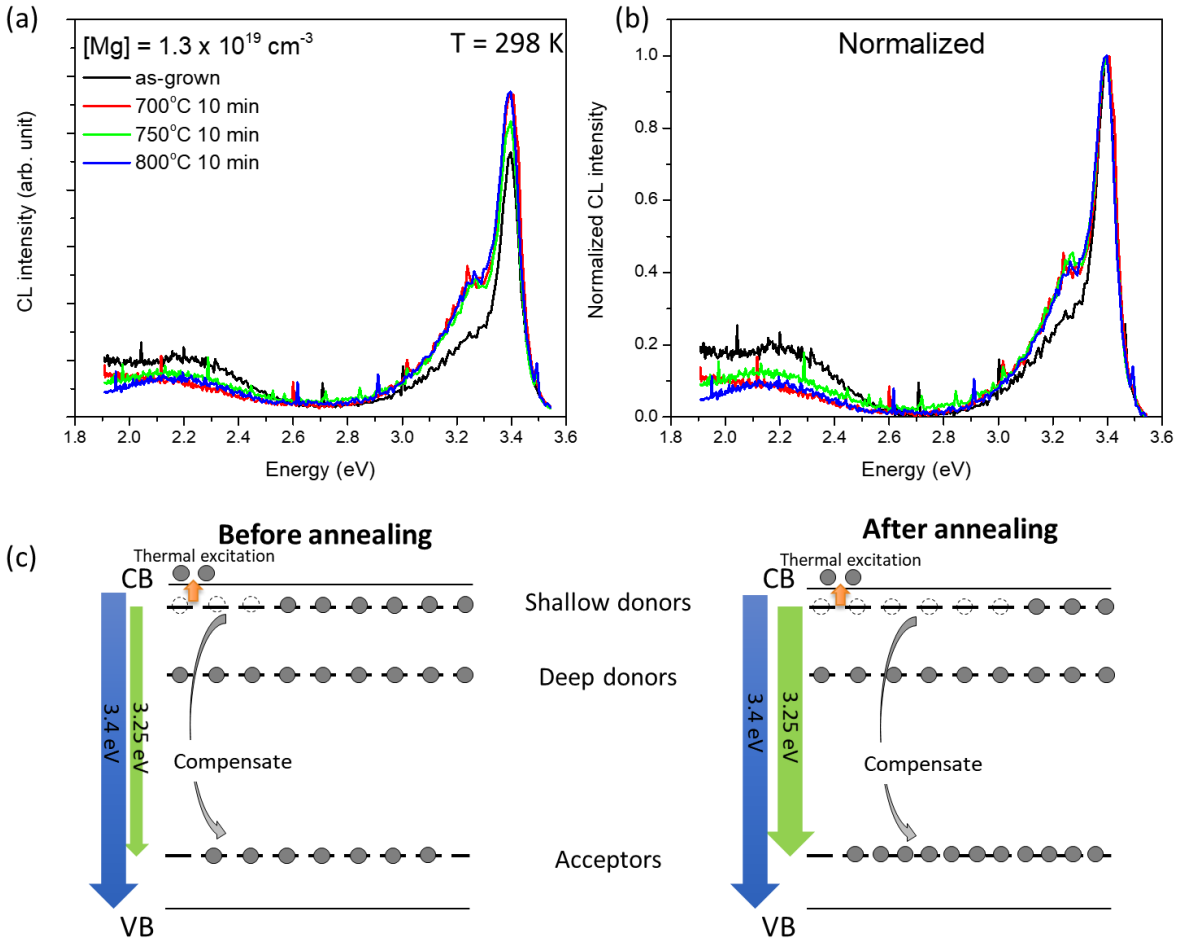

Figure 3.6. (a) not normalized, (b) normalized CL spectra of GaM:Mg films with [Mg] = 1.3×10^{19} cm^{-3}, as-grown and annealed at 700, 750, and 800°C for 10 minutes. (c) Illustration to explain changes in luminescence after thermal activation.

Here we propose a theoretical picture to explain the change in luminescence characteristics associated with Mg concentration and thermal activation. Figure 3.6(c) shows the band diagram of the GaN:Mg. Within the band gap are the shallow donor, deep donor, and Mg acceptor states. The donor states have extra electrons (illustrated as grey circles) that can be donated to Mg acceptor states or be thermally excited to the conduction band. When this happens, the donor states become ionized, and can participate in optical

transitions. Before activation, most of the Mg atoms do not behave as acceptors due to the Mg-H complex, leading to a very low acceptor concentration. Donor electrons cannot easily find acceptors to compensate. Therefore, most of the shallow donor states and all the deep donor states are neutral (occupied by electrons), as shown in Fig 3.6(c). An optical transition in this case will primarily come from the band edge transition at 3.4 eV, and a limited shallow donor to acceptor transition at 3.25 eV. After thermal activation, more acceptor states are produced due to the dissociation of Mg-H complexes. Therefore, an increased number of donors are ionized by the acceptors, leading to an increase of the shallow donor to acceptor transition at 3.25 eV. However, since the Mg doping concentration is low, most of the deep donor states are still neutral, and the spectrum is still dominated by the 3.4 eV emission.

Next, we study the CL characteristics of GaN:Mg layer with [Mg] = 3.1×10^{19} cm^{-3}. The as-grown sample has a dominant 3.4 eV peak, and a 3.25 eV shoulder peak, as shown in Figure 3.7(a) and (b). The intensity of the 3.25 eV peak in the as-grown sample is slightly increased compared to the previous sample with [Mg] = 1.3×10^{19} cm^{-3}. This is expected due to the higher Mg doping concentration. After thermal annealing, a significant increase in the 2.85 eV (deep donor to acceptor) emission intensity is observed, accompanied by a decrease of the 3.4 and 3.25 eV peak intensities. This is due to the increased number of ionized deep donors, as illustrated in Figure 3.7(c). Since the Mg doping concentration in Sample B is higher than that in Sample A, after thermal activation, the acceptors concentration is high enough to ionize all the shallow donor states and some of the deep donor states. This enables the transition between deep donor and acceptor states, producing the 2.85 eV emission.

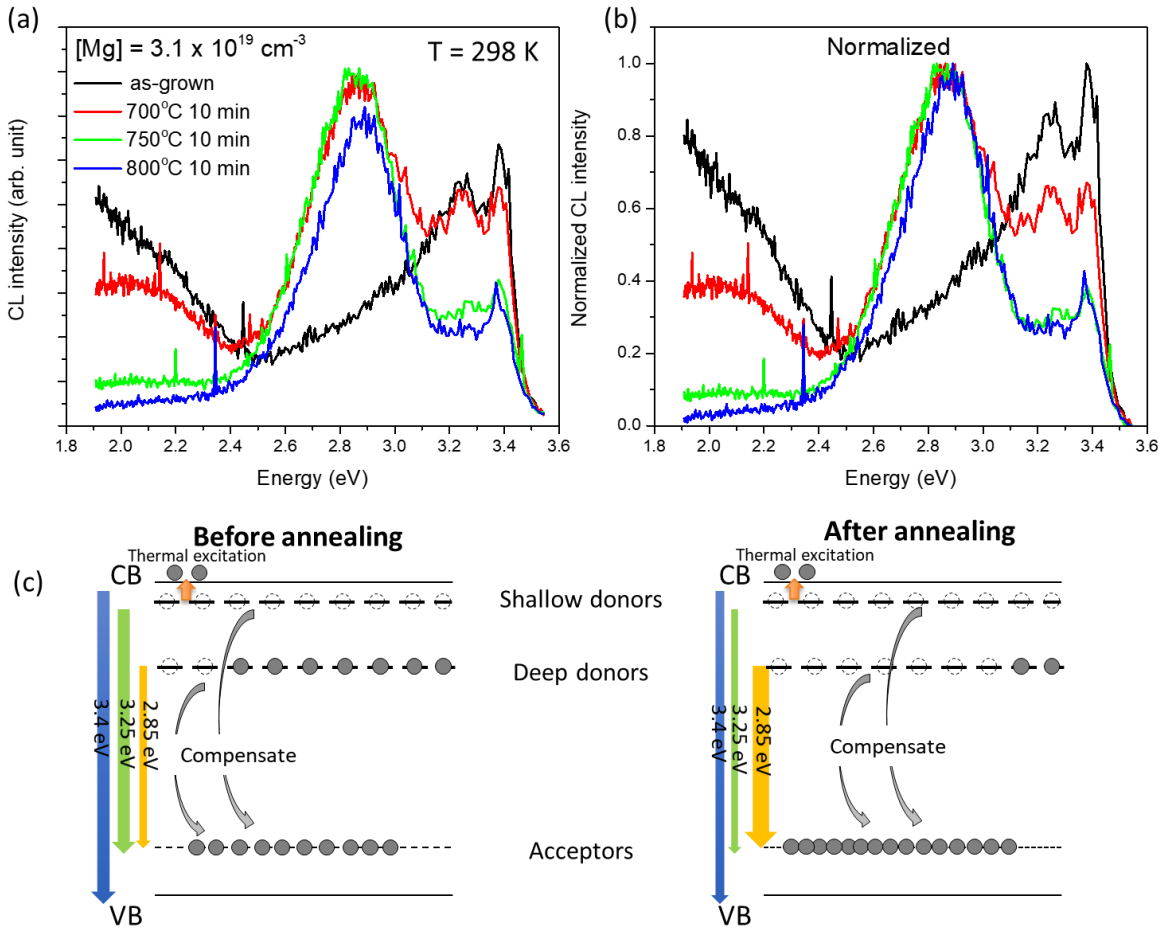

Figure 3.7. (a) not normalized, (b) normalized CL spectra of GaM:Mg film with [Mg] = 3.1×10^{19} cm^{-3}, as-grown and annealed at 700, 750, and 800 °C. (c) Illustration to explain changes in luminescence after thermal activation.

Finally, we study the CL characteristics of GaN:Mg layer with [Mg] = 6.3×10^{19} cm^{-3}, as shown in Fig. 3.8. It is observed that the luminescence spectrum from the as-grown sample is dominated by the 2.85 eV (deep donor to acceptor) transition. After thermal annealing, the intensity of the 2.85 eV peak increases. This agrees with our understanding that increasing the acceptor concentration will lead to an increase in the luminescence intensity of deep donor to acceptor transition. It is noted that the 2.85 eV emission intensity

reaches its maximum after annealing between 700 to 750 °C for 10 minutes. Annealing at higher temperature of 800 °C resulted in slightly lower intensity.

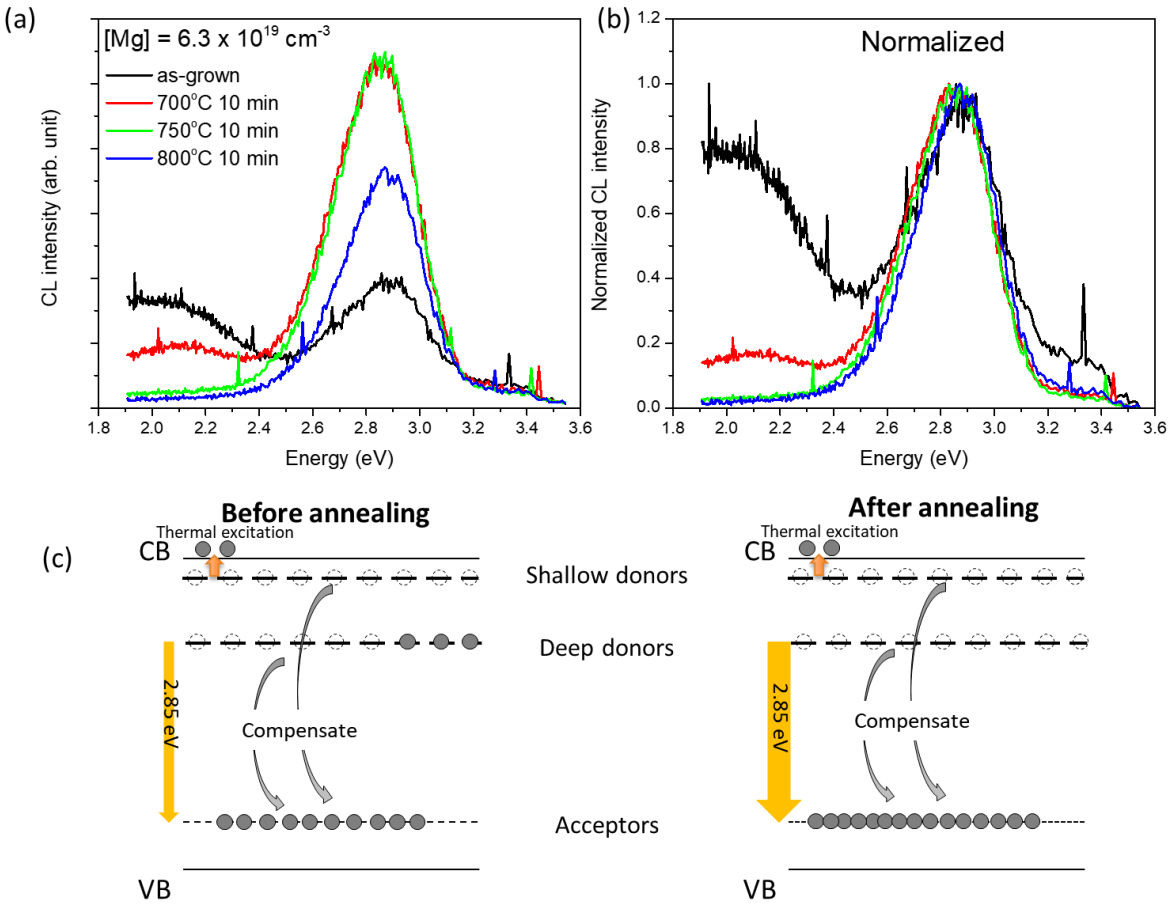

Figure 3.8. (a) not normalized, (b) normalized CL spectra of GaM:Mg film with [Mg] = 6.3×10^{19} cm^{-3}, as-grown and annealed at 700, 750, and 800 °C. (c) Illustration to explain changes in luminescence after thermal activation.

These results coincide with a report published by S. Nakamura *et al.*,[14] in which they performed thermal annealing on GaN:Mg at various temperatures in nitrogen environment and monitored the change in photoluminescence spectra and electrical resistivity of the film. It was found that a drop of GaN:Mg film resistivity is accompanied by the increase of 2.85 eV emission intensity. After annealing at 700°C for 20 minutes, the film resistivity

reached a minimum and the luminescence intensity of the 2.85 eV peak reached a maximum. Annealing at a higher temperature of 800°C will not further reduce the film resistivity, but the luminescence intensity of the 2.85 eV peak starts to decrease. It was not clear why the 2.85 eV intensity drops at higher annealing temperatures, but it was speculated that it is related to degradation of crystalline qualities or dissociation of GaN at high temperature annealing.[14]

In addition to the changes in band edge and donor-acceptor-pair transitions, we observed a significant drop in yellow (~ 2.2 eV) and deep level (< 1.8 eV) luminescence intensities resulted from thermal annealing for all samples. S. Nakamura *et al*. also reported a decrease in deep level transition intensities when GaN:Mg is annealed in temperature higher than or equal to 700°C. They observed that when the deep level luminescence intensity is very weak or not observed, the resistivity of GaN:Mg film becomes low.[14]

Room temperature Hall effect measurements were performed on samples with different [Mg] annealed at different temperatures. Results are shown in Table 3.1.

Table 3.1. Hole concentration and hole mobility for GaN:Mg thin films with different Mg concentrations, annealed at different temperatures, measure by Hall effect using Van de Pauw method at room temperature.

	700°C 10min	**750°C 10min**	**800°C 10min**
$[Mg]=1.3\times10^{19}\ cm^{-3}$	-	-	-
$[Mg]=3.1\times10^{19}\ cm^{-3}$	-	-	$[h]=1.3\times10^{17}\ cm^{-3}$ $\mu=9.5\ cm^2/(V\cdot s)$
$[Mg]=6.3\times10^{19}\ cm^{-3}$	-	$[h]=6.9\times10^{16}\ cm^{-3}$ $\mu=7.4\ cm^2/(V\cdot s)$	$[h]=2.0\times10^{17}\ cm^{-3}$ $\mu=6.0\ cm^2/(V\cdot s)$

For GaN:Mg film with 1.3×10^{19} cm^{-3}, no reliable Hall effect reading is available even when the film has been thermally annealed at up to 800°C for 10 minutes. This means the film conductivity is low. It is possible that the Mg doping concentration is too low, and are fully compensated by donor impurities, leaving no available acceptor states to produce holes in the valance band. This coincides with our CL measurement, which shows very weak 2.85 eV emission intensity for this sample, even after annealing at 800°C (Fig. 3.6).

For GaN:Mg film with 3.1×10^{19} cm^{-3}, no reliable Hall effect reading is available after annealing at 700 and 750 °C. *P*-type conductivity was observed when annealed at 800 °C for 10 minutes. Hole concentration was measured to be 1.3×10^{17} cm^{-3}, with a mobility of 9.5 $cm^2/(V\cdot s)$. The hole to Mg ratio is 0.42%, meaning an average of 0.48 hole is produced by every 100 Mg atoms.

For GaN:Mg film with 6.3×10^{19} cm^{-3}, *p*-type conductivity was observed after annealing at 750°C for 10 minutes. Hole concentration was measured to be 6.9×10^{16} cm^{-3}, with a mobility of 7.4 $cm^2/(V\cdot s)$. When annealing temperature was increased to 800 °C, hole concentration was increased to 2.0×10^{17} cm^{-3}, with a mobility of 6.0 $cm^2/(V\cdot s)$. The hole to Mg ratio is 0.30%, lower than that in Sample B. The decrease of doping efficiency can be explained by an increased degree of self-compensation. Kaufmann et.al observed that when Mg concentration exceeds 2×10^{19} cm^{-3}, doping efficiency in GaN:Mg starts to drop. They proposed that nitrogen vacancy related donors in highly Mg-doped GaN compensate the Mg acceptors, limiting the hole concentration.[46]

In conclusion, the luminescence characteristics of GaN:Mg epilayers with different Mg doping concentration and thermal activation history have been studied. It was found

that GaN:Mg epilayers typically have three emission peaks at 3.4, 3.25, and 2.85 eV. The relative intensities of these peaks are related to the doping concentration and thermal annealing history. With increasing doping concentration and annealing temperature, a shift of luminescence from high energy peaks towards low energy peaks was observed. A qualitative model is proposed to correlate the acceptor concentration with luminescence characteristics.

3.4 Effect of hydrogen plasma treatment on luminescence characteristics of GaN:Mg

During thermal annealing process, the Mg-H complexes are broken up to activate the Mg acceptors, leading to an increase in acceptor concentration. A reverse process of thermal activation, namely, the passivation of Mg acceptors, can be achieved by subjecting activated GaN:Mg films to H_2 plasma. The H atoms from the H_2 plasma will form Mg-H bond with Mg acceptors and render the *p*-type GaN:Mg layer insulating. This technique has been demonstrated as an etching-free process to form edge terminations in GaN *p*-*n* diode.[47,48] In this section, the effect of H_2 plasma treatment on the luminescence characteristics of activated GaN:Mg will be studied.

The sample structure studied was p^+-GaN:Mg (20 nm)/*p*-GaN:Mg(0.5 µm)/*u*-GaN(2 µm)/GaN substrate, as shown in Fig. 3.9(a). The Mg concentrations in the p^+-GaN and *p*-GaN are 2×10^{20} cm^{-3} and 2×10^{19} cm^{-3}, respectively. The sample was annealed at 800 °C for 10 minutes using RTA to activate the Mg acceptors. Metal contact was deposited on some regions of the sample surface to protect the underlying GaN:Mg layer from H_2 plasma. The sample was then treated with H_2 plasma generated by an inductively coupled plasma (ICP) system, with an ICP power of 300 W, an RF power of 10 W for 30 seconds. Finally,

the sample was thermally annealed using RTA at 400 °C to facilitate the formation of Mg-H complexes.[47,48]

A cross-section SE image of the sample is shown in Fig. 3.9(b). The GaN:Mg layer exhibit a bright contrast in the SE image, and the underlying *u*-GaN layer has a darker contrast. The right-hand portion of the GaN:Mg, which was covered by a metal contact that protect the layer from H_2 plasma, shows a uniform bright contrast. The left-hand of the GaN:Mg, which was exposed to H_2 plasma treatment, shows a reduction of SE contrast in the upper portion of the film.

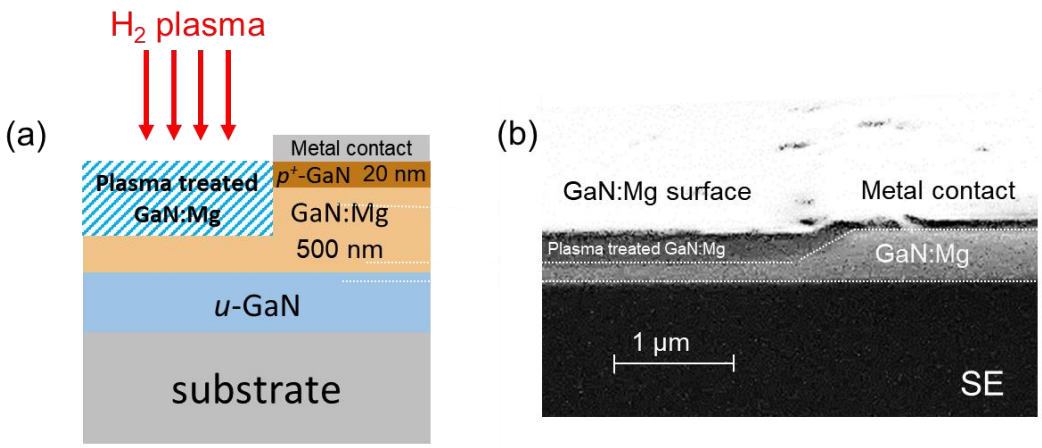

Figure 3.9. (a) schematic drawing of the sample structure treated with H_2 plasma. (b) Cross-section SE image of the sample after H_2 plasma treatment. The upper portion of the exposed GaN:Mg layer shows a reduced SE contrast, and the region protected by a metal contact shows a uniformly bright contrast.

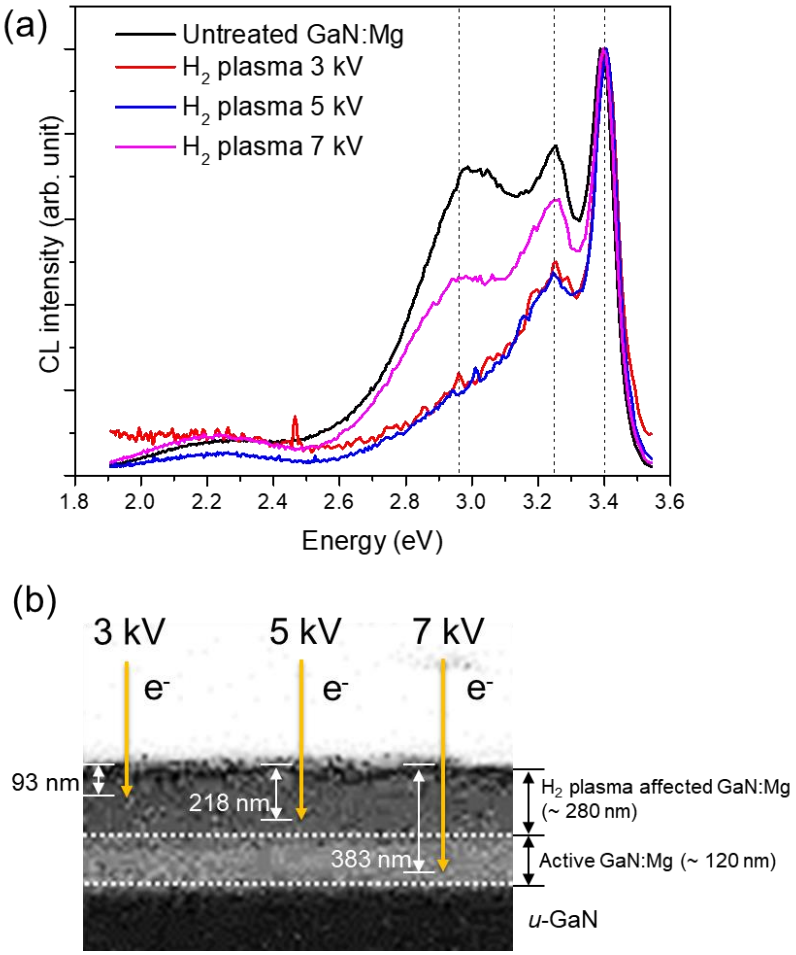

Figure 3.10. Influence of H_2 plasma treatment on the luminescence characteristics of GaN:Mg films. (a) CL spectra of untreated (activated) and H_2 plasma treated GaN:Mg films, measured under different electron beam acceleration voltages. (b) Cross-section SE image showing a H_2 plasma affected region, and the electron penetration depth for various acceleration voltages used in the CL measurements.

Fig. 3.10(a) shows the CL spectra of untreated (activated) and H_2 plasma treated GaN:Mg films. The spectrum of the untreated (activated) GaN:Mg layer shows a visible deep donor to Mg acceptor emission peak at 2.9 eV, suggesting good *p*-type conductivity. Three spectra of the H_2 plasma treated GaN:Mg have been measured at different electron

acceleration voltages of 3, 5, and 7 kV, corresponding to electron penetration depths of 93, 218, and 383 nm, respectively, as shown in Fig. 3.10(b).[30] The electron penetration depth under 3 and 5 kV are both within the H_2 plasma affected GaN:Mg region, which extends 280 nm deep under the surface, as determined by the SE contrast in Fig 3.10(b). The intensity of the 2.9 eV peak is decreased after H_2 plasma treatment. Spectra measured under 3 and 5 kV acceleration voltages show the most significant decrease in the 2.9 eV emission intensity, and the two spectra overlap. The spectra shape closely resembles the that of the GaN:Mg film in Fig. 3.6, which has been measured to be semi-insulating by Hall effect. This means H_2 plasma treatment has passivated the GaN:Mg. When electron acceleration voltage is increased to 7 kV, the penetration depth exceeds the H_2 plasma affected region. The reduction of the 2.9 eV emission intensity is less compared to that measured under 3 and 5 kV. This is because a portion of unaffected GaN:Mg is also measurement at the voltage of 7 kV.

These results further indicate that the deep donor to Mg acceptor transition located around 2.9 eV is closely related to the acceptor concentration in the GaN:Mg. The peak intensity increases with increasing acceptor concentration after thermal annealing and decreases with decreasing acceptor concentration after H_2 plasma treatment.

3.5 Effect of background impurity concentration on the luminescence characteristics of GaN:Mg

In the previous sections, we showed that the optical properties of GaN:Mg depend on the acceptor concentration in the film, which are affected by the Mg doping concentration, thermal annealing history, and H_2 plasma treatment. Another important factor that can affect the acceptor concentration in GaN:Mg films is the background impurity concentration. This is because some background impurities such as C and O can act as donors and compensate the Mg acceptors.[49] In this section, I report on the effect of background carbon concentration on the optical characteristics of GaN:Mg layers.

CL characteristics of GaN:Mg epilayers grown in two different MOCVD reactors were compared. Samples A and B, described in section 3.1, with Mg concentrations of 1.3×10^{19} cm^{-3} and 3.1×10^{19} cm^{-3}, respectively, were grown using MOCVD reactor I. Sample G, with the structure of GaN:Mg(0.12 μm)/*u*-GaN(2 μm)/GaN substrate, was grown in MOCVD reactor II. The GaN:Mg layer in Sample G has a Mg concentration of 1.2×10^{19} cm^{-3}, similar to Sample A. All samples have been thermally annealed to activate the Mg acceptors.

Plan view CL spectra of the GaN:Mg films in Samples A, B, and G are shown in Fig. 3.11. Mg concentrations in the GaN:Mg layers are measured by SIMS. For Sample A with a [Mg] of 1.3×10^{19} cm^{-3} grown by reactor I, the spectrum is dominated by the 3.4 eV emission. And the 2.85 eV emission intensity is very weak. When [Mg] is increased to 3.1×10^{19} cm^{-3} in Sample B, the 2.85 eV peak starts to emerge. For Sample G with a [Mg] of 1.2×10^{19} cm^{-3} grown by reactor II, the spectrum is dominated by the 2.85 eV emission peak.

In the previous sections, we have shown that for Samples A, B, and C grown in Reactor I, the 2.85 eV peak intensity increases with [Mg] and become dominant at [Mg] ~ 6.1×10^{19} cm^{-3} (Sample C in Fig. 3.1). We have also shown that the intensity of the 2.85 eV peak is proportional to the acceptor concentration in GaN:Mg. However, for Sample G grown in Reactor II, with only a [Mg] concentration of 1.2×10^{19} cm^{-3}, a dominant 2.85 eV peak is observed. This suggests a lower [Mg] is needed to achieve good *p*-type conductivity for GaN:Mg films grown in Reactor II.

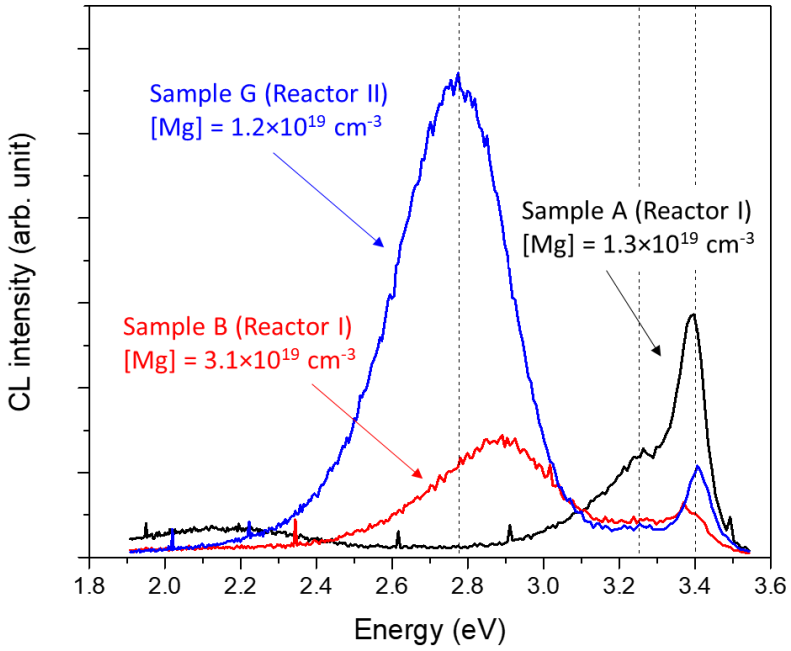

Figure 3.11. Plan-view CL spectra of GaN:Mg films grown in two different MOCVD reactors. CL characteristics varies significantly between Sample A and G, which have similar [Mg], but were grown in different reactors.

SIMS depth profiles were measured on GaN:Mg thin films grown using Reactor I and II as shown in Fig. 3.12. It was observed that the concentrations of background impurities such as O and Si are similarly low in the GaN:Mg layers grown in reactor I and II, ranging

from 5×10^{15} to 1×10^{16} cm^{-3}. However, the GaN:Mg layer grown in reactor I contains a significant higher amount of carbon compared to that grown in reactor II. The C concentration in the GaN:Mg layer grown in reactor I is 2×10^{17} cm^{-3}, about 30 times higher than that grown in reactor II, which is 6×10^{15} cm^{-3}.

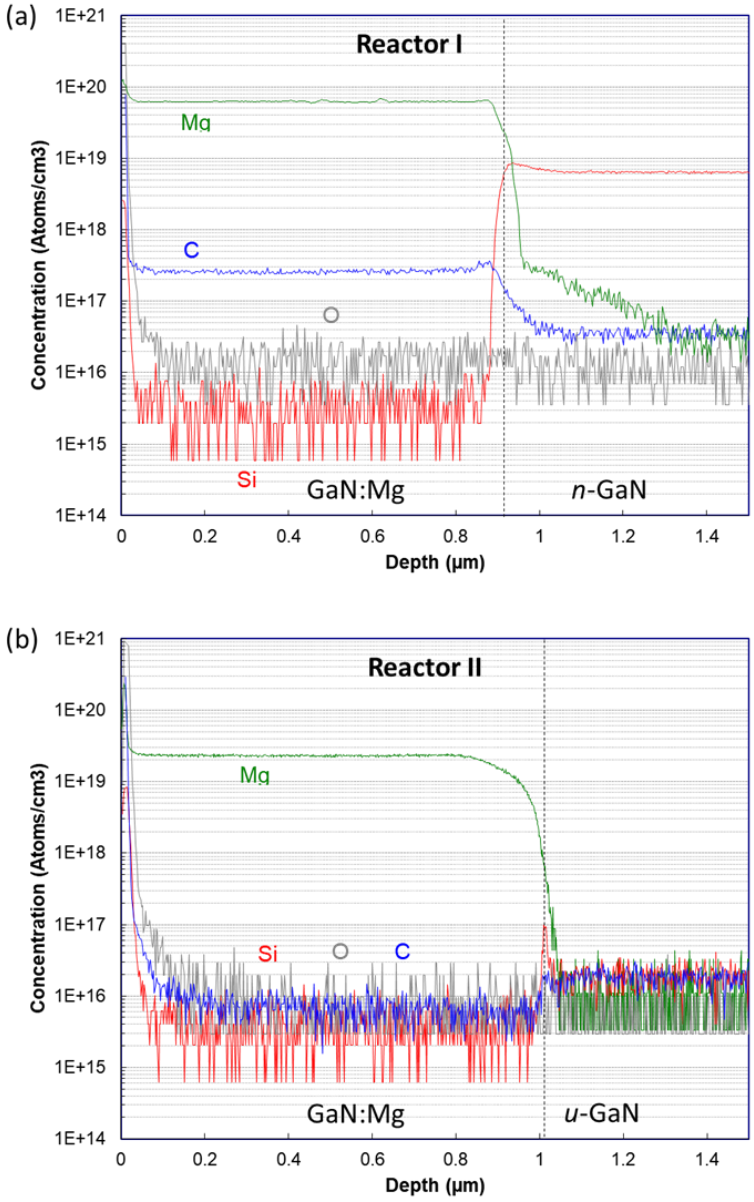

Figure 3.12. SIMS depth profile for samples grown in (a) reactor I, and (b) reactor II.

Carbon has been reported to act as deep donors in GaN and may compensate Mg-related acceptors.[49] Having a high C concentration in GaN:Mg layer means a higher amount of Mg is required to achieve *p*-type conductivity. However, increasing the Mg concentration will reduce the hole mobility due to impurity scattering. Putting too much Mg may also cause precipitation, which is detrimental to the film conductivity. Therefore, it is important to lower the C concentration in GaN:Mg films. It should be noticed that the C concentration is similar in the underlying *n*-GaN and *u*-GaN layers for samples grown in reactor I and II. Therefore, the high C concentration in the GaN:Mg layer grown in reactor I is not due to chamber contamination, but rather, should be related to the growth conditions of the GaN:Mg epilayer or contamination in the Mg source precursors.

In conclusion, the effect of C concentration on the optical properties of GaN:Mg is characterized. It is found that C impurity may compensate Mg acceptors, leading to a need of higher Mg doping concentration to achieve the target acceptor level.

3.6 Conclusion

In conclusion, Chapter 3 offers a broad overview of the room temperature CL characteristics of GaN:Mg. The electron beam current used for the CL measurement has been limited to 0.1 nA to avoid LEEBI affecting the optical properties of GaN:Mg. The effect of LEEBI, Mg doping concentration, thermal annealing, H_2 plasma treatment, and background impurity concentration on the optical properties of GaN:Mg has been studied. The findings in this chapter serves as a foundation for the further studies on optical properties of GaN:Mg epilayers grown on mesa structures and miscut substrates, reported in Chapter 4 and 5.

CHAPTER 4

NON-UNIFORM ACCEPTOR DISTRIBUTION IN GAN EPILAYERS GROWN ON MESA STRUCTURES FOR APPLICATIONS IN GAN POWER ELECTRONICS[*†]

4.1 Introduction

Gallium nitride (GaN) based power electronics has attracted much attention in recent years due to its advantages over traditional Si-based power devices in terms of energy conversion efficiency, switching frequency, operation temperature, and system volume.[23,50] Vertical architectures are usually preferred for high-voltage and high-power applications,[24,51,52,53] due to high voltage and current handling capability, good thermal management, and compact design. In the fabrication of advanced vertical power devices, such as normally-off vertical junction field effect transistors (VJFETs), junction barrier Schottky diodes, and superjunction diodes, it is important to produce laterally patterned *p-n* junctions and/or *p-uid* (unintentionally doped) junctions.

[*] Part of this chapter has been published as: H. Liu, H. Fu, K. Fu, S. R. Alugubelli, P.-Y. Su, Y. Zhao, and F. A. Ponce, Non-uniform Mg distribution in GaN epilayers grown on mesa structures for applications in GaN power electronics, Appl. Phys. Lett. **114**, 082102 (2019).

[†] Part of this chapter has been submitted to Appl. Phys. Lett. as: P.-Y. Su*, H. Liu*, C. Yang, K. Fu, H. Fu, Y. Zhao, and F. A. Ponce, *Lateral and vertical growth of Mg-doped GaN on trench-patterned GaN films.*

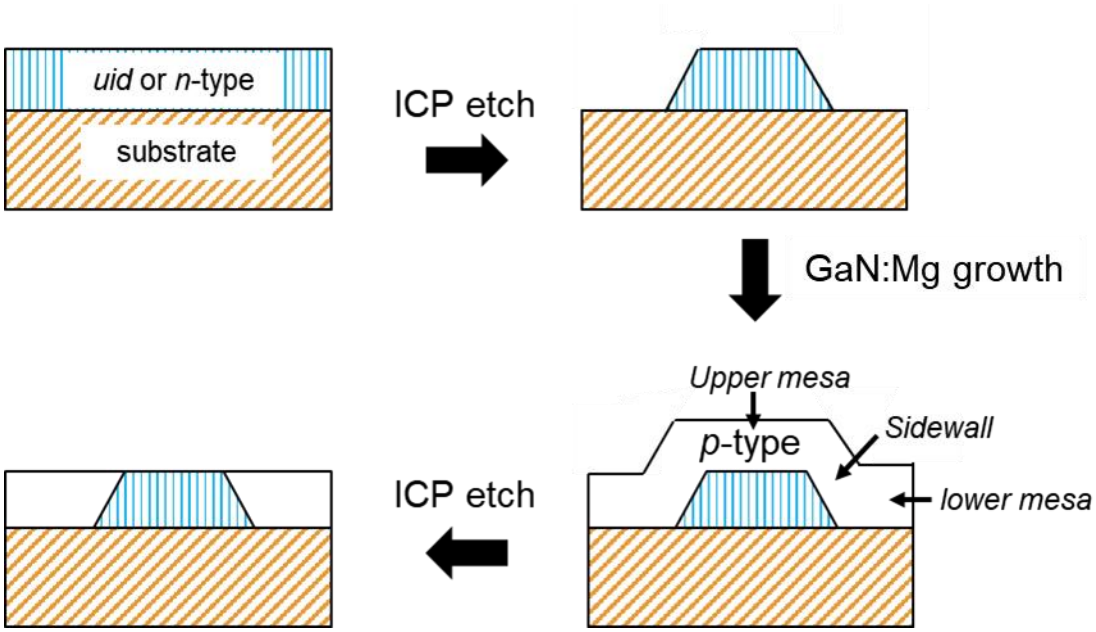

Figure 4.1. Growth sequence to produce a selective-area doped geometry in GaN, using the etch-and-regrowth procedure used in this work.

Selective-area doping using etch-and-regrowth procedures is one of the most effective ways to get controlled lateral junctions. Fig. 4.1 shows the growth steps to produce the selective-area doped geometry used in this work. In this case, a film of *uid*-GaN or *n*-type GaN will be grown on a GaN substrate, then etched in certain areas to create a patterned mesa structure. A Mg-doped *p*-type GaN layer will then be grown over the patterned mesa structures. Finally, the GaN:Mg on the upper mesa will be etched away to produce an alternating *p*-*uid* or *p*-*n* geometry.

During GaN:Mg regrowth, it is speculated that there could be two growth fronts, one being on the basal plane in the upper and lower mesa flat regions, and the other being on inclined crystal planes at the mesa sidewall. This difference in growth orientation may result in varied Mg doping efficiency.[54,55,56,57] The Mg doping efficiency in these regions is a critical issue that can impact the performance of vertical power devices. For example,

in VJFETs, the Mg doping level in GaN:Mg needs to be uniform and high enough to pinch off the channel without any bias, leading to a normally-off operation.[58] However, such variation in Mg concentration cannot be characterized by secondary ion mass spectroscopy (SIMS), due to its limited lateral spatial resolution. In this work, cathodoluminescence (CL) spectroscopy was used to investigate optical properties of GaN:Mg in a mesa structure. A correlation among Mg concentration, optical properties, and electronic properties of GaN:Mg has been established. This correlation has been used to extrapolate Mg distribution in regrown GaN:Mg over a mesa structure at sub-micron scale.

4.2 Experimental

The epitaxial structures were grown by metal-organic chemical vapor depositions (MOCVD) on free-standing *c*-plane GaN substrates, with hydrogen as the carrier gas, at a growth temperature of 1050 °C. The Ga and N sources were trimethylgallium (TMGa) and ammonia (NH_3), respectively. The precursor for Si donors was silane (SiH_4), and the precursor for Mg acceptors is bis(cyclopentadienyl)magnesium (Cp_2Mg). More details on the MOCVD growth can be found elsewhere.[59,60] We report on the properties of four thin film structures, labeled A to D. The initial layer of sample A consists of 4 µm of *uid*-GaN grown on *c*-plane GaN substrate. The *uid*-GaN layer was then selectively etched to produce periodic mesa structures. The etching was done by photolithography and chlorine-based inductively coupled plasma (ICP) dry etching (ICP/RF power of 400/70W, Cl_2/BCl_3/Ar flow rate of 30/8/5 sccm, pressure of 0.67 Pa). Following the etching, 0.3 µm of *uid*-GaN and 1.65 µm of GaN:Mg film were grown over the mesa structures. The GaN:Mg was grown with a TMGa flow rate of 25 sccm, and a Cp_2Mg flow rate of 100 sccm, at a temperature of 950 °C. The schematics drawing of one of the mesa structures is shown in

Fig. 4.2(a). Another series of samples (sample B, C, and D) were grown to investigate the effect of Cp_2Mg flow rate on the GaN:Mg optical and electronic properties. Their structure consists of 1 µm GaN:Mg on 2 µm *n*-GaN grown on sapphire substrates. The growth conditions of these 3 samples were identical, except three different Cp_2Mg flow rates of 50, 100 or 200 sccm were used during the growth of the GaN:Mg film to achieve different Mg doping concentrations. Post-growth thermal activation of GaN:Mg was performed on all samples using rapid thermal annealing at 800 °C for 10 mins in a nitrogen atmosphere. The Mg concentrations in the GaN:Mg layer of samples B, C, and D were determined by secondary ion mass spectroscopy (SIMS). Hole concentrations and hole mobility were measured at room temperature with Hall effect using the Van de Pauw method. Optical properties of all samples were studied using cathodoluminescence (CL) spectroscopy. The CL system consists of a JEOL 6300 scanning electron microscope (SEM) connected to an Oxford CL2 monochromator and a photomultiplier tube. Spot mode CL spectra were obtained by fixing the electron beam at a specific location on the sample and scanning the spectrum across the desired wavelength range. CL mappings were obtained by setting the monochromator to a certain wavelength and recording the spatial variation of luminescence intensity over an area. The electron beam current used in our CL studies was 0.1 nA, with an acceleration voltage of 7 kV.

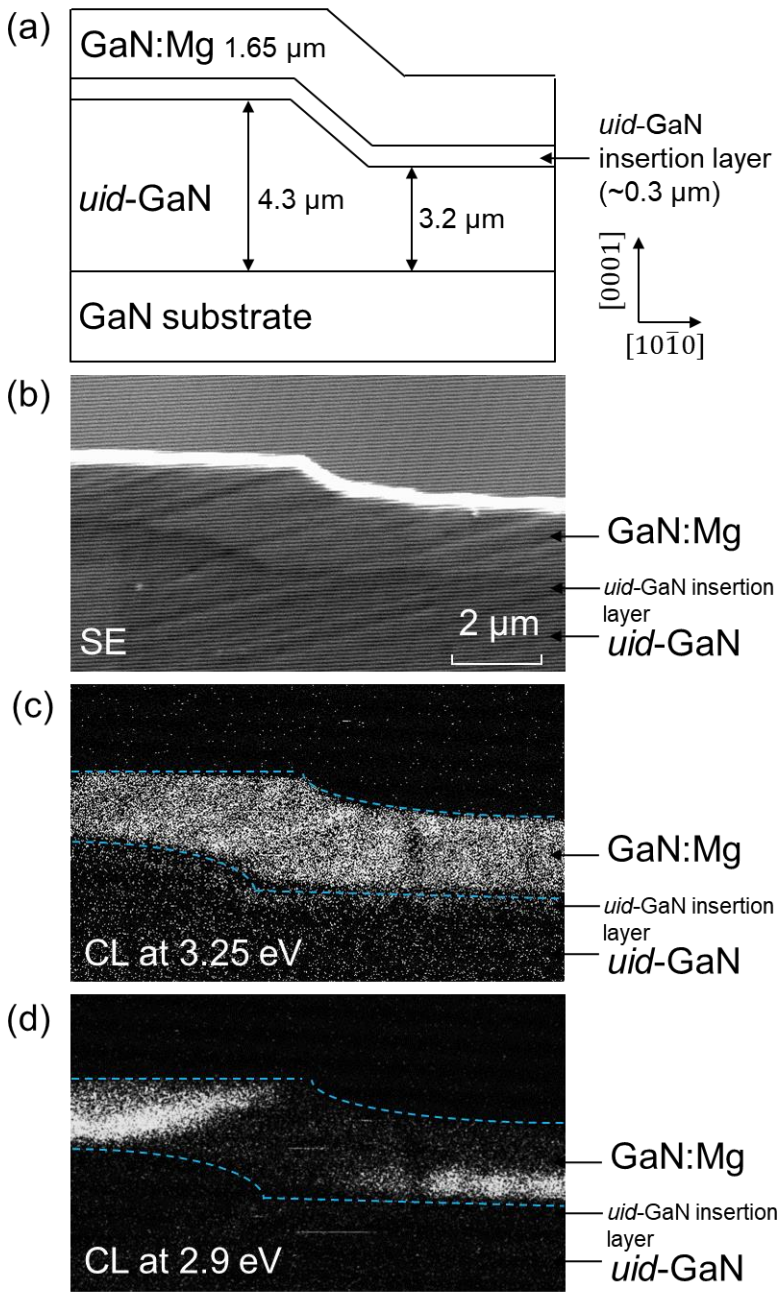

Figure 4.2. Cross-sectional view of the GaN:Mg/*uid*-GaN mesa structure in sample A. (a) Schematic drawing of the thin film structure, with the sidewall along *a*-directions (⟨11$\bar{2}$0⟩). (b) SE image using 7 kV primary beam. Monochromatic CL images at (c) 3.25 eV and (d) 2.9 eV. The dashed lines follow the differently-doped homojunctions as determined from (c).

4.3 Results

4.3.1 CL mapping and spot-mode CL on GaN:Mg grown on mesa structure

The optical properties of sample A, with the mesa structure, was studied in cross-section by CL imaging and spectroscopy. The cross-section samples were prepared by mechanical polishing. Fig. 4.2(a) shows a schematic diagram of the cross-sectional view of one of the mesa steps. Fig. 4.2(b) is a secondary electron (SE) image, (c) and (d) are CL mappings at 3.25 and 2.9 eV, respectively. A mesa step with 1.1 μm in height, resulting from the ICP etching, is observed in the SE image. The mesa has a hexagonal shape with the sides along a-directions ($\langle 11\bar{2}0 \rangle$), as indicated in Fig. 4.2(a). The sidewall initially makes approximately a 28° angle with respect to the basal plane, which corresponds to a $\{1\bar{1}02\}$ plane, and then approaches the basal plane. A GaN:Mg layer with a thickness of 1.65 μm was grown above the mesa structure. The CL mapping at 3.25 eV in Fig. 4.2(c) shows that the GaN:Mg layer exhibits a uniform emission at that energy. However, the CL mapping at 2.9 eV in Fig. 4.2(d) shows a lower emission in the vicinity of the sidewall. Fig. 4.3(a) is also a CL mapping at 2.9 eV, but at a lower magnification compared to Fig. 4.2(d). It is observed that the lower mesa, adjacent to the sidewall, also exhibits weak emission intensity at 2.9 eV. However, the area of low intensity portion in the lower mesa gradually recedes as the distance from the sidewall increases. When sufficiently far away (>10 μm) from the sidewall, the lower mesa has a uniform and strong emission at 2.9 eV, similar to that in the upper mesa. It should be noted that such non-uniform luminescence pattern is repeatedly observed near all the mesa steps.

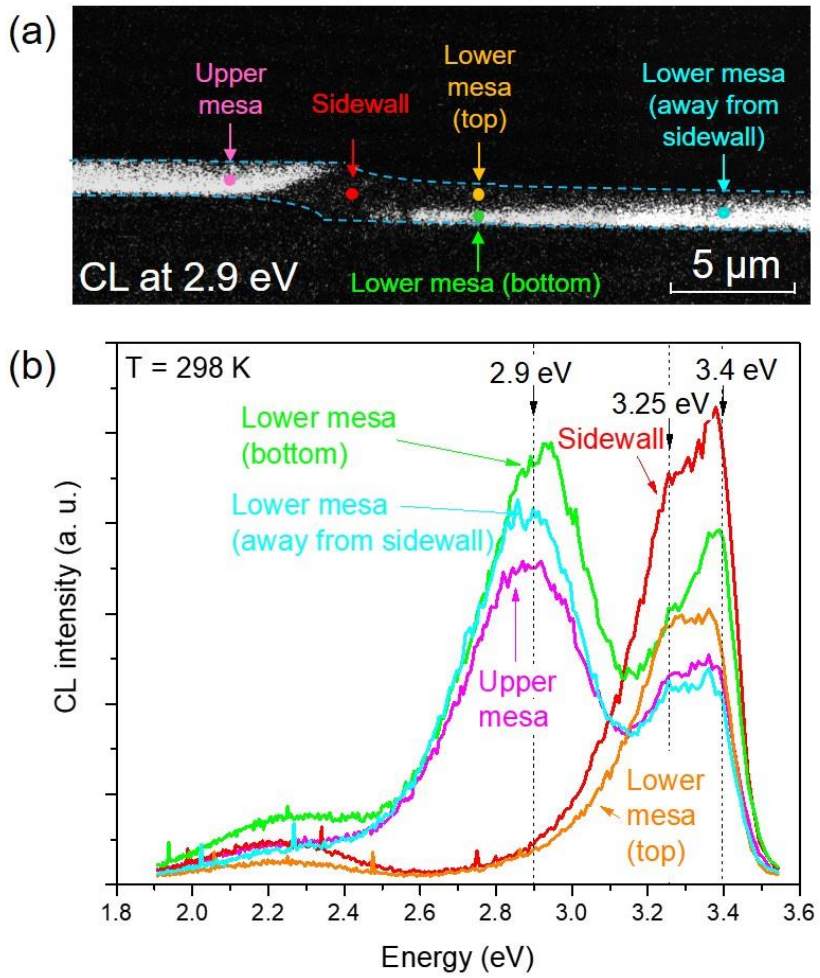

Figure 4.3. Cross-sectional optical properties of the GaN:Mg/*uid*-GaN mesa structure in sample A (a) Monochromatic CL mapping at 2.9 eV. (b) Spot-mode CL spectra at different regions in the GaN:Mg layer as indicated by arrows in (a).

Spot mode CL spectra were taken at five different locations within the GaN:Mg layer, as indicated in Fig. 4.3(a): upper mesa, sidewall, top of lower mesa, bottom of lower mesa, and center of lower mesa away from the sidewall. The interaction volume of the electron beam is estimated to be around 400 nm in diameter, which is smaller than the GaN:Mg layer thickness of 1.65 μm. Therefore, the CL signal should only originate from the GaN:Mg layer. The spot mode CL spectra are plotted in Fig. 4.3(b). Three common peaks

at 3.4, 3.25, and 2.9 eV are observed at all locations. The spectral shape is similar for upper mesa, bottom of lower mesa, and center of lower mesa away from sidewall, where emission is dominated by the 2.9 eV peak. The emission at the sidewall and the top of the lower mesa is dominated by the 3.4 and 3.25 eV peaks, while the 2.9 eV peak is very weak, as has been visualized in the CL mapping in Fig. 4.3(a).

4.3.2 CL characteristics of GaN:Mg films with different Mg concentrations

In order to establish a correlation between doping concentration and the optical and electronic properties of GaN:Mg films, we have studied samples B, C, and D, which have an epilayer structure of 1-μm GaN:Mg on 2-μm *n*-GaN on sapphire, a schematic diagram of which is shown in the inset of Fig. 4.4.

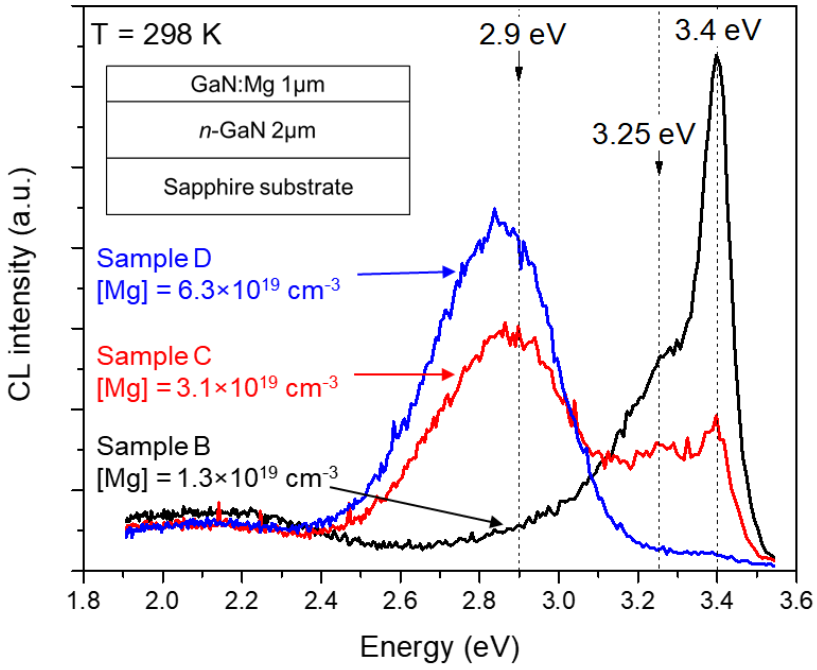

Figure 4.4. CL spectra of GaN:Mg layers with different Mg concentrations (sample B, C, and D). A schematic drawing of the sample structure of samples B, C, and D is shown in the inset.

The Cp_2Mg flow rates used for the GaN:Mg growth were 50, 100, and 200 sccm, for samples B, C, and D, corresponding to Mg concentrations of 1.3×10^{19}, 3.1×10^{19}, and 6.3×10^{19} cm^{-3}, as determined by SIMS. The CL spectra in Fig. 4.4 show three peaks at 3.4, 3.25, and 2.9 eV. The relative intensity of 2.9 eV peak as compared to 3.25eV peak increases with Mg concentration in the film.

Hole concentrations and mobilities of the GaN:Mg layer in samples B, C, and D are summarized in Table 4.1. Sample B is resistive with no reliable Hall effect reading available. Sample C with [Mg] = 3.1×10^{19} cm^{-3} presents a hole concentration of 1.3×10^{17} cm^{-3} and a mobility of 9.5 $cm^2/(V\cdot s)$. Sample D with [Mg] = 6.3×10^{19} cm^{-3} has a hole concentration of 2×10^{17} cm^{-3} and a mobility of 6.0 $cm^2/(V\cdot s)$.

Table 4.1. Summary of Mg concentration ([Mg]), hole concentration ($[h^+]$), and hole mobility of GaN:Mg layers with different Mg concentrations (sample B, C, and D).

	[Mg]	$[h^+]$	Hole mobility
Sample B	1.3×10^{19} cm^{-3}	Too resistive	Too resistive
Sample C	3.1×10^{19} cm^{-3}	1.3×10^{17} cm^{-3}	9.5 $cm^2/(V\cdot s)$
Sample D	6.3×10^{19} cm^{-3}	2.0×10^{17} cm^{-3}	6.0 $cm^2/(V\cdot s)$

4.4 Discussion

The transitions observed in the CL spectra have been previously reported for Mg-doped GaN.[38-43] The 3.4 eV peak has been attributed to near-band-edge excitonic transitions at room temperature, the 3.25 eV peak to shallow-donor to Mg-acceptor transitions, and the 2.9 eV peak to deep-donor to Mg-acceptor transitions. The origin of

deep donor states is of much debate, but the commonly accepted view is that they are complexes formed by nitrogen vacancies with nearest neighbor Mg atoms (V_N-Mg_{Ga}).[40-43] The relative intensities of these peaks change with [Mg], as shown in Fig. 4.4. When [Mg] is increased, the intensities of the high-energy peaks (3.4 eV and 3.25 eV) decrease and the intensity of low energy peak (2.9 eV) increases.[38-41]

To explain the change in light emission characteristics of GaN:Mg with increasing Mg concentrations, we propose a model, depicted in Fig. 4.5.

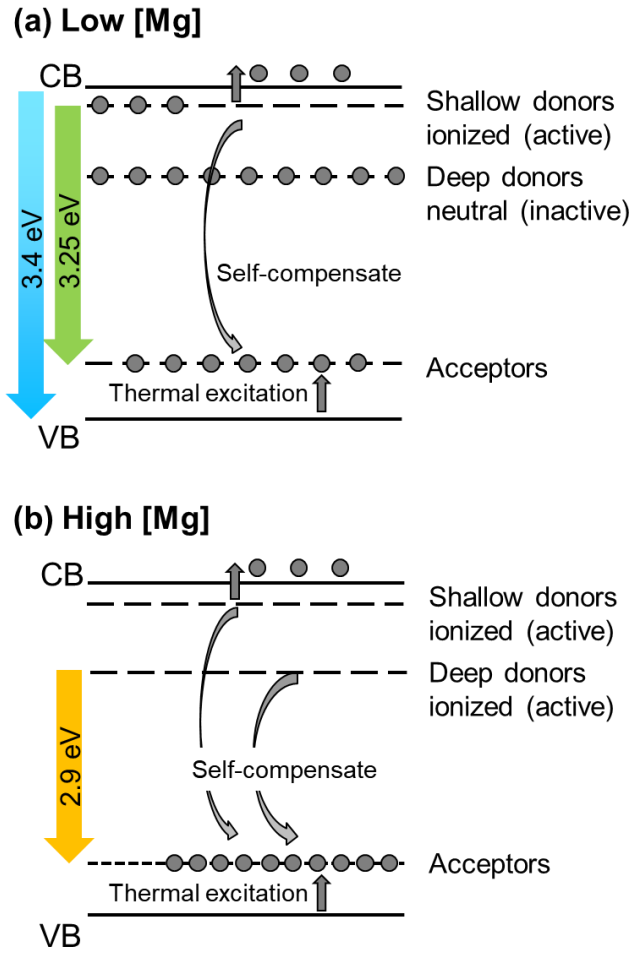

Figure 4.5. Illustration to explain the different luminescence characteristics of GaN:Mg with (a) low, and (b) high Mg concentrations.

The shallow and deep donor states are initially neutral (occupied by electrons). They are ionized by transferring electrons to the acceptors (compensation) or thermally exciting electrons to the conduction band. When the shallow or deep donors are ionized, their states are available for radiative recombination, and can contribute to light emission at 3.25 or 2.9 eV respectively. For GaN:Mg with low [Mg] in Fig. 4.5(a), there are not enough acceptors to accept the electrons from both shallow and deep donors. In this case, only part of the shallow donors is ionized, and the deep donors are neutral. Therefore, light emission will originate from band edge transitions (3.4 eV) and shallow donor to acceptor transitions (3.25 eV), as observed in Fig. 4.4 for sample B with [Mg] = 1.3×10^{19} cm^{-3}. For GaN:Mg with high [Mg] in Fig. 4.5(b), there are sufficient acceptor states to accept electrons from both shallow and deep donors, leading to complete ionization (unoccupied electron states). An electron excited to the conduction band in this sample will relax to the lowest energy state (deep donor state) and then via a radiative transition to the acceptor states causing luminescence at 2.9 eV, as observed in Fig. 4.4 for sample D with [Mg] = 6.3×10^{19} cm^{-3}. At medium [Mg], deep donor states are partially ionized, and optical transition happens at 2.9 eV. Depending on the excitation power, some electrons will also recombine from shallow-donor states or from the conduction band edge, producing 3.25 eV, and 3.4 eV emissions, as in Fig. 4.4 for sample C with [Mg] = 3.1×10^{19} cm^{-3}.

We use spot mode CL to probe local variations of acceptor concentration in the GaN:Mg films with sub-micron resolution. By comparing the CL spectra taken at various location of the mesa structure (Fig 4.3(b)) to the CL spectra of GaN:Mg with different [Mg] (Fig. 4.4), we can see some similarities. The spectra from upper mesa, bottom of lower mesa, and center of lower mesa away from sidewall in Fig. 4.3(b) closely resembles the

spectrum of sample C with [Mg] = 3.1×10^{19} cm^{-3} in Fig. 4.4. This is expected, because the GaN:Mg layer growth condition in these two samples (sample A and C) are identical with the same Cp_2Mg flow rate of 100 sccm. On the other hand, the spectra from the sidewall and the top of lower mesa closely resembles the spectrum of sample B with [Mg] = 1.3×10^{19} cm^{-3} in Fig. 4.4. This implies the acceptor concentration in the sidewall and top of lower mesa are lower.

We attribute the non-uniform acceptor concentration in the mesa structure to Mg doping efficiency during growth on different crystal planes. The bright and dark regions in GaN:Mg in Fig. 4.3(a) represent higher and lower acceptor concentrations, respectively. This is due to vertical growth (perpendicular to the basal plane) at the flat surfaces in the upper and lower sections of the mesa and growth on inclined crystal planes near the sidewall. This finding suggests that CL spectroscopy can also be utilized as a tool to visualize the vertical vs. lateral growth regions of Mg-doped GaN on uneven structures.

The doping nonuniformity in the GaN:Mg layer on mesa structures can cause unintended and detrimental effects on device performance, since it alters the electric potential profile of the device from the original design. Therefore, visualizing the doping nonuniformity is important.

The doping uniformity of the GaN:Mg layer on mesa structures with different trench width, height, and sidewall orientations has been investigated using CL spectroscopy. Fig. 4.6 (a) and (b) shows GaN:Mg grown on etched *u*-GaN with different trench widths of 5 and 9 μm, respectively. In the SE images, the regrown GaN:Mg layer appears in bright contrast, compared to the underlying *u*-GaN layer, which appears in a darker contrast. For

the 5 μm case (Fig. 4.6(a)), monochromatic CL mapping at 2.9 eV shows GaN:Mg grown near the sidewalls have low emission intensity, indicating low acceptor concentration due to lateral growth. Regions near the bottom of the trench show brighter emission intensity at 2.9 eV, indicating higher acceptor concentration from vertical growth on the basal plane. The red dashed lines mark the boundary between the lateral and vertical growth regions and makes a 32° angle with the basal plane. In Fig. 4.6(b), the width of the trench is increased to 9 μm. Since the sidewalls are further apart, more regions can adopt vertical growth from the bottom basal plane of the trench, leading to increased portion of GaN:Mg with bright 2.9 eV emission. The boundary between the lateral and vertical growth region makes 32° with the basal plane, same as the 5 μm case, indicating that the lateral vs. vertical growth rate is not affected by the width of the trench.

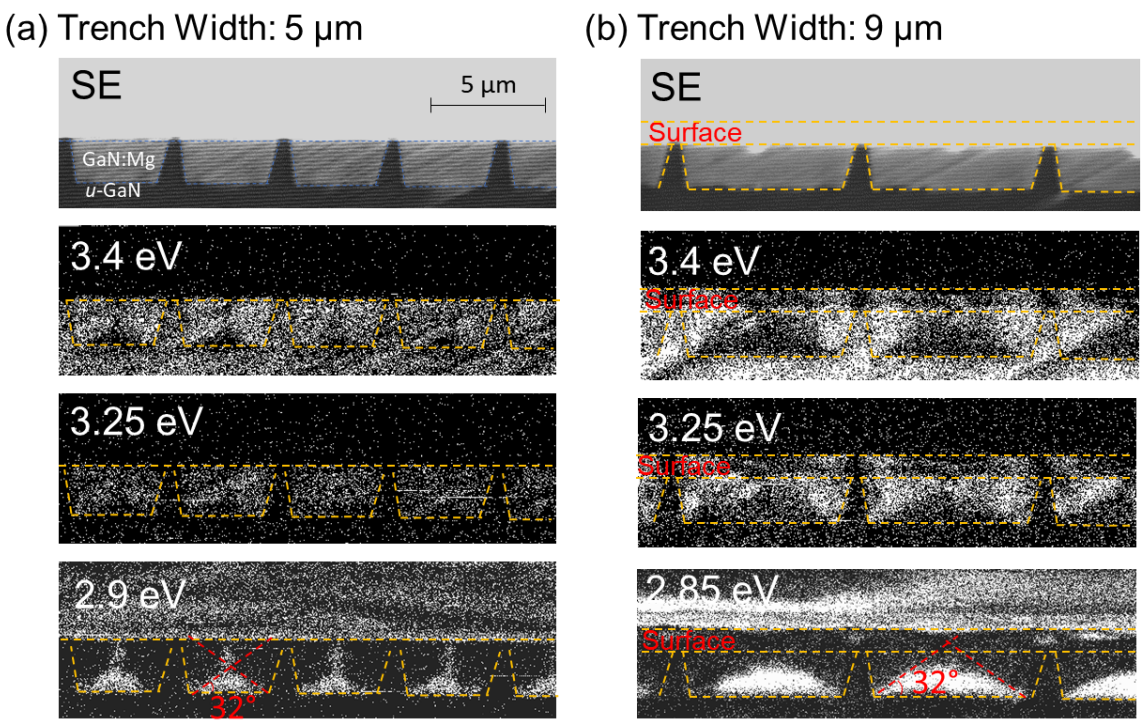

Figure 4.6. Cross-sectional SE and monochromatic CL mapping at 3.4, 3.25, and 2.9 eV for selective-area regrowth on mesa structures with different trench widths of (a) 5 μm and (b) 9 μm. The sample in (b) is slightly tilted such that part of the top surface is also in view.

Fig. 4.7 shows a comparison of GaN:Mg regrown on mesa structures with different heights. For mesa with a sidewall height of 0.3 μm, the lateral growth from the sidewall is minimum. As the mesa height increases, the area of the sidewall also increases, allowing an increased portion of the epilayer to adopt lateral growth, as observed in the 2.9 eV CL monochromatic mappings. The red dashed lines, marking the lateral vs. vertical growth regions boundaries, make a 32° angle with the basal plane for samples with different mesa heights. This indicate the lateral growth rate is not affected by the height of the mesa.

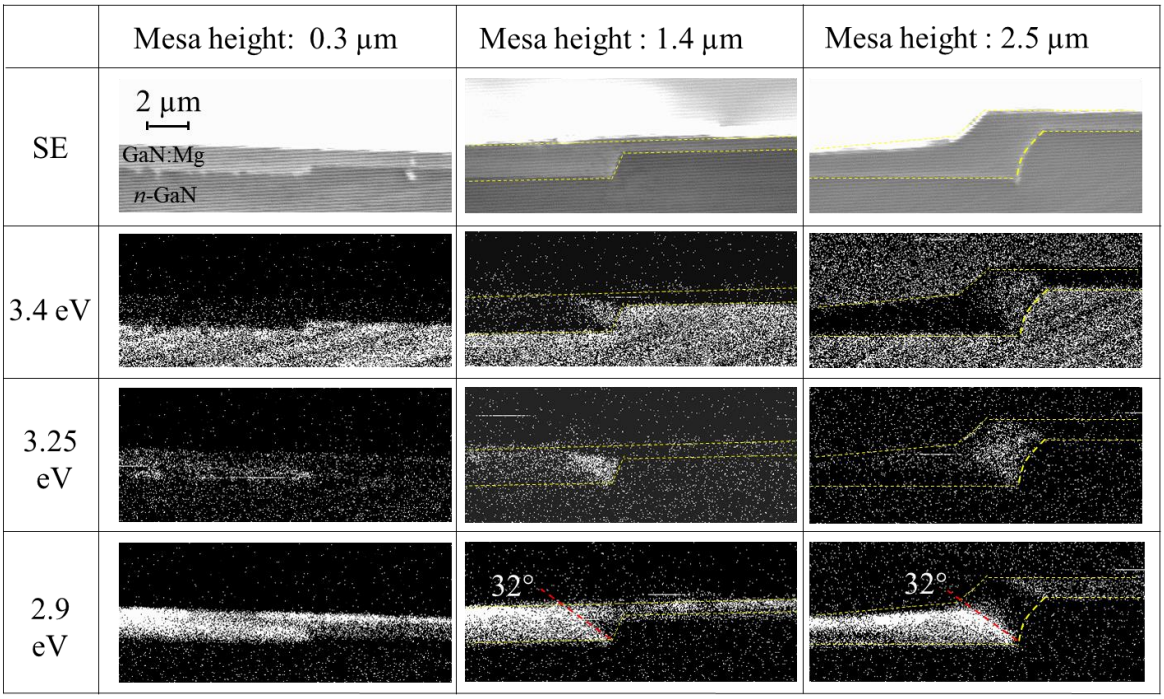

Figure 4.7. Cross-sectional SE and monochromatic CL mapping at 3.4, 3.25, and 2.9 eV for GaN:Mg grown on mesa with different heights of 0.3, 1.4, and 2.5 μm. Red dashed lines mark the boundary between the lateral and vertical growth regions.

Finally, the effect of mesa sidewall orientation on the acceptor distribution in regrown GaN:Mg has been studied. Fig. 4.8 (a) and (b) shows GaN:Mg grown on mesa sidewall aligned parallel to the $[1\bar{1}00]$ and $[11\bar{2}0]$ direction, respectively. The sidewalls were produced by ICP dry-etching followed by Tetramethylammonium hydroxide (TMAH) wet-etching processes. It is observed in the SE images that the sidewall angle is affected by the crystalline orientation. When the sidewall is along $[1\bar{1}00]$ direction in Fig 4.8(a), the sidewall makes 76° with the basal plane. When the sidewall is along $[11\bar{2}0]$ direction in Fig. 4.8(b), the angle is 83.4°. This is due to the difference etching characteristics of GaN on different crystal planes. In the 2.9 eV CL mappings, the boundary between the lateral vs. vertical growth regions still makes a 32° angle with the basal plane. This suggests

the lateral growth rate is not affected by the sidewall angle and the crystalline orientation of sidewall.

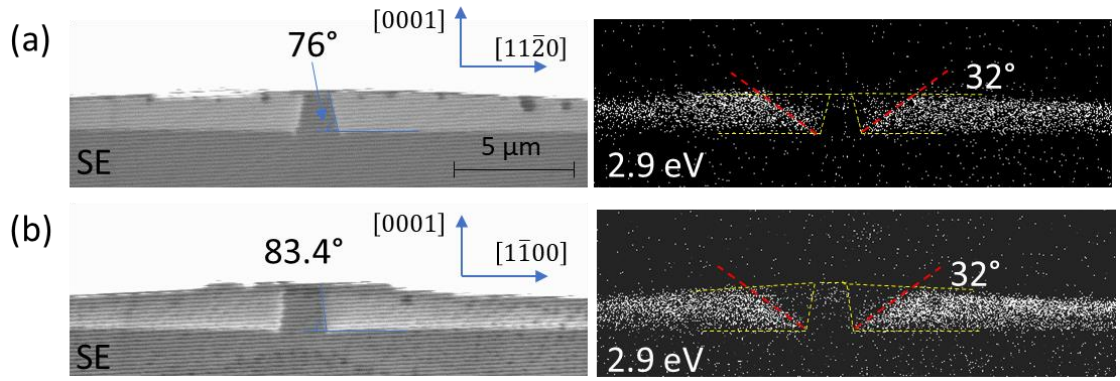

Figure 4.8. Cross-sectional SE and monochromatic CL mapping at 2.9 eV for GaN:Mg grown in mesa with different sidewall orientations. Mesa sidewalls are aligned paralleled to the $[1\bar{1}00]$ direction in (a) and paralleled to the $[11\bar{2}0]$ direction in (b). Red dashed lines mark the boundary between lateral and vertical growth regions.

The lateral growth rate in GaN has been reported to depend on parameters such as growth temperature, pressure, and III/V ratio.[61] In addition, Mg doping is also reported to enhance the lateral growth rate of GaN.[62] Therefore, these parameters need to be optimized carefully in order to control the lateral growth of GaN:Mg on mesa structures.

4.5 Conclusion

In conclusion, selective area doping of Mg in GaN has been achieved by etch-and-regrowth processes. Spot mode CL spectroscopy and CL mapping have been used to reveal that the sidewall of Mg-doped GaN grown over a mesa structure is acceptor deficient. The lower acceptor concentration at sidewall is attributed to inefficient Mg doping at non-basal crystal planes. CL mapping was used to illustrate the growth mechanism in mesa structures where vertical growth and tilted growth take place simultaneously in close vicinity.

CHAPTER 5

INFLUENCE OF SUBSTRATE MISORIENTATION ON THE OPTICAL PROPERTIES OF MG-DOPED GAN[*]

5.1. Introduction

Development of high-performance Mg-doped *p*-type GaN thin films is important for many applications, in particular for light emitting devices in optoelectronics and for junction gate field-effect transistors in power electronics.[1,4,23,58] While silicon in GaN is an effective *n*-type dopant, Mg-doped GaN (GaN:Mg) is characterized by low carrier concentrations and poor hole mobility. This is due to a relatively high activation energy of about 170 meV for Mg acceptors in GaN,[19,63] which results in a low fraction of ionized acceptors at room temperature. Another important limitation is the solubility limit of Mg in GaN (~ 1×10^{20} cm^{-3}) beyond which Mg forms precipitates that drastically reduce *p*-type conductivity.[20,21] Additionally, self-compensation with intrinsic donor defects has been observed in heavily doped films, further limiting the hole density.[43,46] While most reports of GaN:Mg have been for films grown on *c*-plane, questions arise when adding lateral structures requiring growth on surfaces etched away from the exact *c*-plane orientation. In such cases, basal plane steps play an important role, particularly due to the effect of Mg doping towards high lateral growth rates over basal planes in GaN.[62]

Numerous efforts have been made to improve *p*-type conductivity. Epitaxy of GaN:Mg on GaN substrates, with miscut angles between 0.2° and 1.7° away from the *c*-plane, reportedly result in a significant increase in hole concentration.[64,65,66] This is attributed to

[*] Part of this chapter has been published as: H. Liu, P.-Y. Su, Z. Wu, R. Liu, and F. A. Ponce, "*Influence of substrate miscut angle on the optical properties of Mg-doped GaN*," J. Appl. Phys. **127**, 195701 (2020).

a decrease in the unintentional donor density with miscut angle with no change in the Mg incorporation.[64,65] However, it is not clear how substrate miscut affects *p*-type doping in GaN at a microscopic scale. We report here on a study on the optical properties of GaN:Mg epitaxial layers grown on GaN substrates with miscut angles of 0.3° and 4° performed using high-spatial-resolution cathodoluminescence (CL). A correlation has been established between nanoscale optical properties, growth surface morphology, and Mg composition variations.

5.2 Experimental

Epitaxial films were grown by metal-organic chemical vapor deposition (MOCVD), on *c*-plane GaN substrates with nominal miscut angles of 0.3° and 4° towards the $[1\bar{1}00]$ direction, as illustrated in Fig. 5.1.

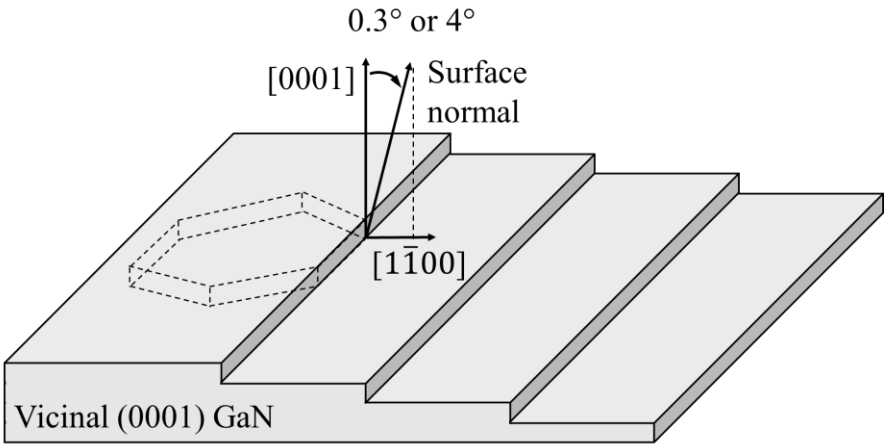

Figure 5.1. Schematic diagrams showing vicinal GaN substrates with miscut angle of 0.3° or 4° towards $[1\bar{1}00]$. Periodic straight step edges on basal plane are related to the miscut angle.

A 2-μm thick unintentionally-doped GaN (*u*-GaN) was grown on the GaN substrates, which acted as a buffer between the substrate and the following layers, in order to eliminate

substrate surface preparation involving mechanical and chemical polishing. A GaN:Mg layer was grown next. For 0.3° miscut substrates, two different films were grown with thickness of 0.12 μm and of 1.0 μm. For 4° miscut substrates, we studied films with 1.0 μm thickness. The Ga and N sources were trimethylgallium (TMGa) and ammonia (NH_3). The carrier gas was hydrogen, and the precursor for Mg was bis(cyclopentadienyl)magnesium (Cp_2Mg). The GaN:Mg layers were grown with a TMGa flow rate of 90 sccm, and a Cp_2Mg flow rate of 1430 sccm, at a temperature of 920 °C. Post-growth thermal activation of GaN:Mg was performed using rapid thermal annealing at 700 °C for 20 mins in a nitrogen atmosphere. Cross-section samples were produced by mechanical polishing using diamond lapping films. The optical properties were studied using cathodoluminescence (CL) spectroscopy, with an electron beam current of 100 pA in a JEOL 6300 scanning electron microscope equipped with an Oxford CL2 monochromator and a photomultiplier tube. The electron beam acceleration voltage was 7 kV for cross-section measurements and ranged between 3 to 14 kV for plan-view measurements. The surface morphology of the GaN:Mg layers was studied using a Bruker MultiMode atomic force microscope (AFM) operating in tapping mode. Transmission electron microscopy (TEM) was performed in a Philips CM 200 instrument to search for structural defects such as dislocations and Mg-induced precipitates.

5.3. Growth on 0.3° miscut GaN substrates

Plan-view CL spectra of the 1.0 μm GaN:Mg layer on 0.3° miscut substrate is shown in Fig. 5.2. The electron beam acceleration voltage was varied from 3 to 14 kV for a depth probe of the film's optical properties. The maximum penetration depth (where injected electrons come to a rest) is given by the following equation:[28,29,30]

$$R = \left(\frac{0.0276A}{Z^{0.89}\rho}\right) E_b^{1.67} \text{ (μm)}$$

where A is the atomic weight in g/mol, Z is the atomic number, ρ is the material density in g/cm^3, and E_b is the electron acceleration voltage in KeV. The acceleration voltages were 3, 7, 10, and 14 kV, corresponding to maximum penetration depths of about 0.09, 0.38, 0.70, and 1.22 μm, respectively. A schematic drawing illustrating the electron penetration depths under different acceleration voltages is in the inset of Fig. 5.2. The luminescence signal is generated within a tear-shaped interaction volume above the maximum penetration depth, with maximum photon generation happening at ~1/3 of the maximum penetration depth.

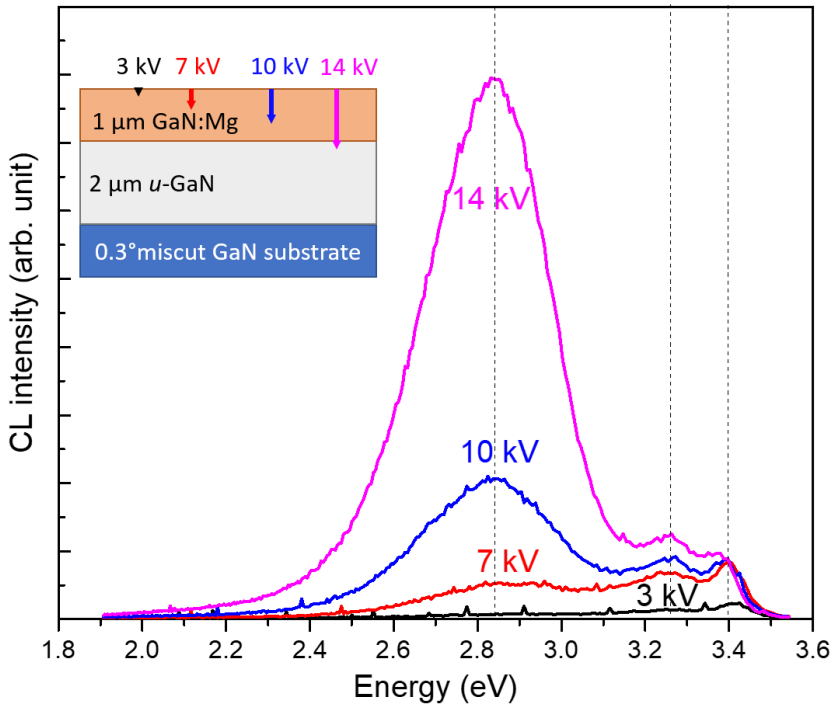

Figure 5.2. Plan-view CL spectra of the 0.3° miscut, 1.0 μm thick GaN:Mg sample, measured under different electron beam acceleration voltages. The intensity of 2.85 eV peak increases with the acceleration voltage. Inset: schematic drawing illustrating the probing depth of electron beam for various acceleration voltages.

The CL emission peaks at 3.4, 3.25, and 2.85 eV correspond to near band-edge, shallow donor to acceptor, and deep donor to acceptor transitions, respectively.[38-43] The acceptors have been assigned to Mg substituting for Ga, and the shallow donors responsible for the 3.25 eV emission could be Si, O, or C. Regarding the deep donor responsible for the 2.85 eV peak, a widely accepted theory is that it is a complex formed by nitrogen vacancies with nearest neighboring Mg atoms (V_N-Mg_{Ga}).[40-43] It is observed in Fig. 5.2 that the relative peak intensity varies with probing depth. The intensity of the 2.85 eV peak is very weak near the surface (at V_{acc} = 3 kV), and gradually increases with the probing depth, and becomes dominant (at V_{acc} = 14 kV).

Further information about the variation of luminescence with depth is obtained in cross-section in Fig. 5.3. GaN:Mg is brighter than *u*-GaN in the secondary electron (SE) image,[67] with the yellow dashed lines marking the boundaries between the layers. It is noted that both the *u*-GaN and GaN:Mg thin films exhibit a uniform flat surface morphology. The 3.25 eV emission (shallow donor to acceptor) in Fig. 5.3(b) is spatially uniform inside the GaN:Mg layer. On the other hand, the 2.85 eV emission (deep donor to acceptor) in Fig. 5.3(c) is laterally uniform, but the intensity is stronger in the lower portion of the GaN:Mg film and gradually decreases towards the top surface.

CL spectra on spot mode from two locations, marked as Area 1 and Area 2 in Fig. 5.3(c), near the bottom and top of the GaN:Mg layer, respectively, are plotted in Fig. 5.3(d). The characteristics of the 3.4 and 3.25 eV peaks remain the same. But the intensity of the 2.85 eV peak decreases significantly in the growth direction (from Area 1 to Area 2).

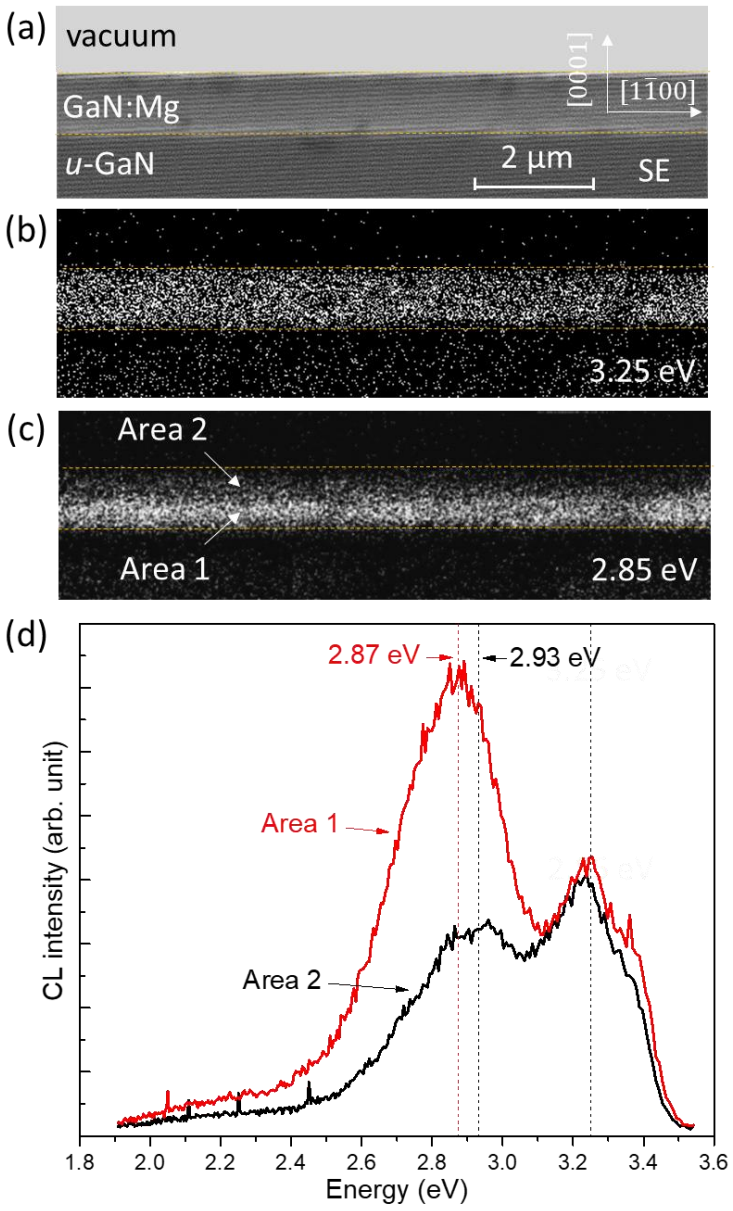

Figure 5.3. Cross-section characteristics of the 1.0 µm thick GaN:Mg film on 0.3° miscut substrate, showing flat *u*-GaN and GaN:Mg films. (a) Secondary electron image. Monochromatic CL images at (b) 3.25 eV showing spatially uniform 3.25 eV emission, and (c) 2.85 eV showing a decrease of the 2.85 eV emission intensity from the bottom (Area 1) to the top portion (Area 2) of the GaN:Mg film. (d) Spot mode CL spectra of Areas 1 and 2.

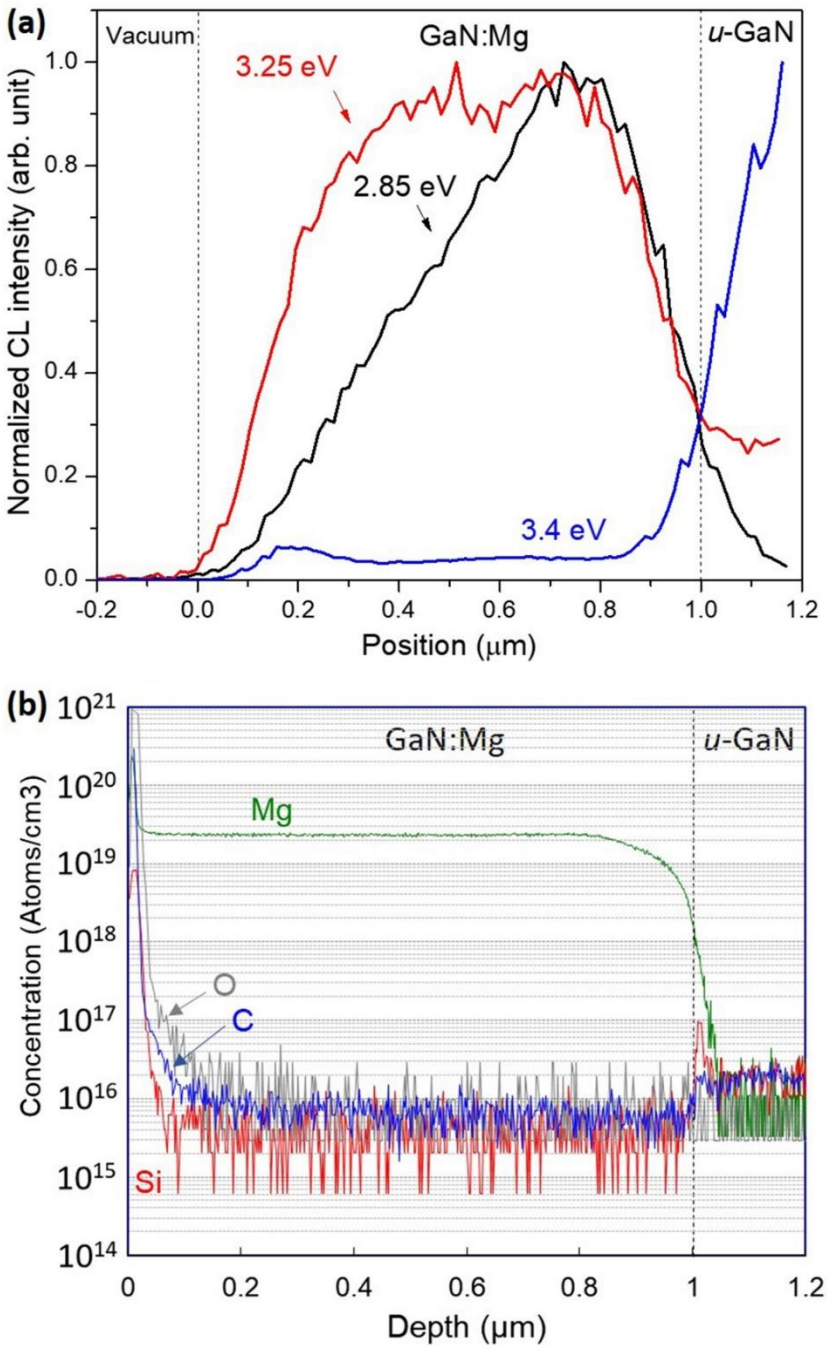

Figure 5.4. (a) Line scan profile of the luminescence intensity at 3.4, 3.25, and 2.85 eV across the GaN:Mg film for the 0.3° miscut, 1.0 μm thick GaN:Mg sample (b) SIMS depth profiles showing uniform concentrations of Mg, Si, O, and C across the GaN:Mg layer.

Line-scan CL profiles in Fig. 5.4(a), obtained by scanning the electron beam across the GaN:Mg film, show the intensity variation of the 3.4, 3.25, and 2.85 eV emissions. The 3.25 and 3.4 eV emission profiles remain relatively constant in the bulk of the GaN:Mg film. The slopes of the intensity in the vicinity of the GaN:Mg/*u*-GaN interface and of the top surface are quite similar and result from the minority carrier diffusion and the interaction volume produced by the electron beam inside the sample. On the other hand, the 2.85 eV emission profile exhibit a gradual decrease along the growth direction.

It has been reported that the relative intensities of the 3.4, 3.25, and 2.85 eV peaks are related to the acceptor concentration in GaN:Mg epilayers. When the Mg doping level increases, the luminescence intensity of the 2.85 eV peak increases.[38-41] Results from Chapter 3 and 4 in this thesis indicate a correlation between luminescence properties and *p*-type conductivity in GaN:Mg, with the presence of 2.85 eV emission at room temperature as a signature of *p*-type conductivity in GaN.[68] Therefore, the variation of the 2.85 eV luminescence intensity in the GaN:Mg film in Fig. 5.3 represents a reduction of acceptor concentration with increasing film thickness.

We used secondary ion mass spectroscopy (SIMS) and TEM[*] to determine whether the observed variations are associated with changes in Mg concentration or with the presence of crystal defects. The SIMS data in Fig. 5.4(b) shows depth profiles of Mg, Si, C, and O, indicating no noticeable variations in their concentrations, and a constant Mg concentration of 2.2×10^{19} cm^{-3}. TEM images, shown in Fig. 5.5, indicate that the GaN:Mg layers are free of precipitates and dislocations. We conclude that the depth variation of the

[*] TEM measurements were performed by Dr. Po-Yi Su from Arizona State University, Tempe AZ, USA

2.85 eV emission is not associated with doping concentrations, nor with the presence of crystal defects.

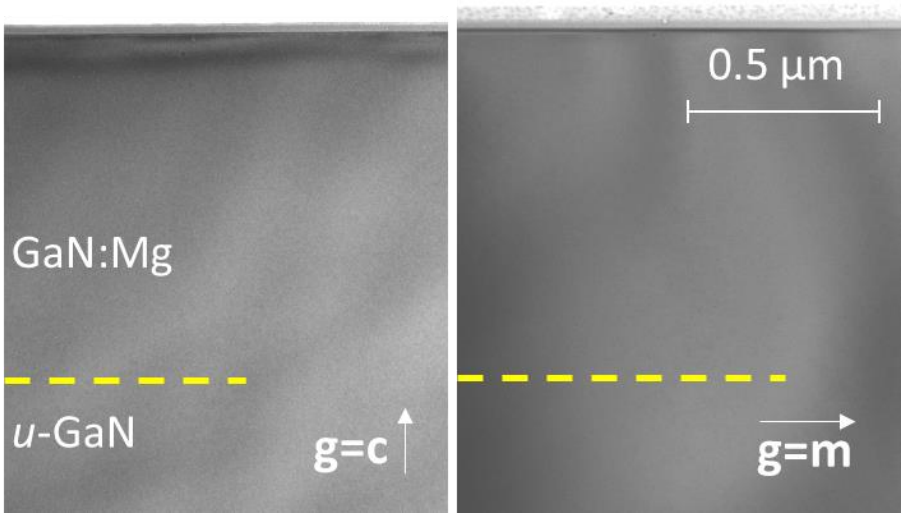

Figure 5.5. Cross-sectional two-beam bright field TEM images taken with Philips CM-200 instrument operated at 200 keV, with $\boldsymbol{g} = \boldsymbol{c}$ (left) and $\boldsymbol{g} = \boldsymbol{m}$ (right) conditions, for the 1-µm GaN:Mg layer grown on *u*-GaN/0.3° miscut GaN substrate. No dislocations and precipitates have been observed within the GaN:Mg layer.

A possible explanation was found by observation of the characteristics of thin and thick GaN:Mg films. Plan-view CL spectra of thin (0.12 µm) and thick (1.0 µm) films are shown in Fig. 5.6. The electron beam acceleration voltage was 3 kV, which corresponds to a maximum penetration depth of around 0.1 µm. Thus, the spectra represent the properties of the top (< 0.1 µm) of each layer. The large drop in the 2.85 eV emission in the thick sample is clearly observed. Plan-view secondary electron (SE) and monochromatic CL images taken at 3.4, 3.25, and 2.85 eV, shown in the Figure 5.7, indicate smooth surfaces and spatially uniform luminescence for 1.0 µm GaN:Mg on 0.3° miscut substrate.

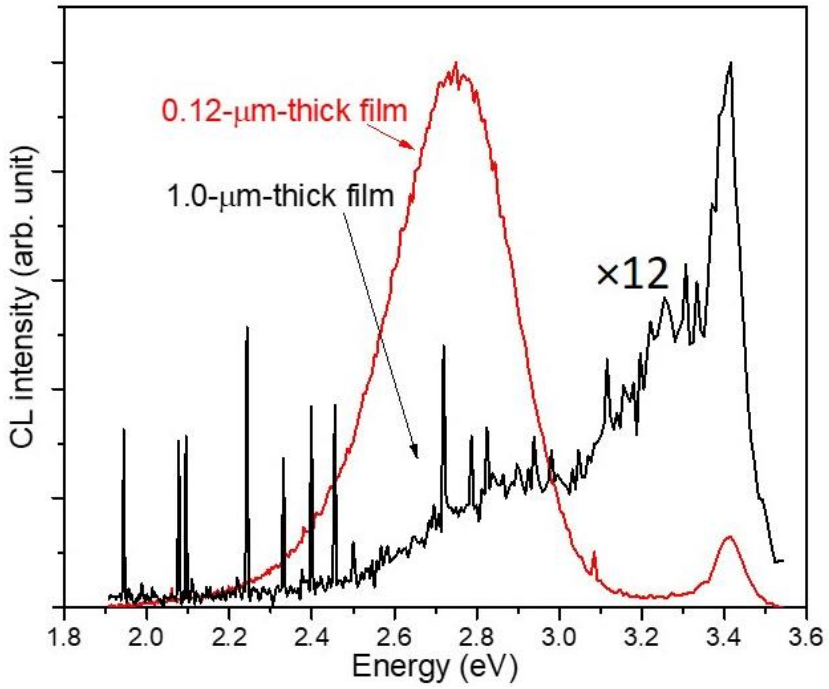

Figure 5.6. Film thickness effect on the optical properties at the top surface of GaN:Mg epilayers on 0.3° miscut GaN substrates. Plan-view CL spectra of 0.12 and 1.0 μm thick films, taken under the same conditions with a 50 μm × 50 μm^2 electron beam raster, and with an electron beam acceleration voltage of 3 kV that corresponds to a penetration depth of ~0.1 μm.

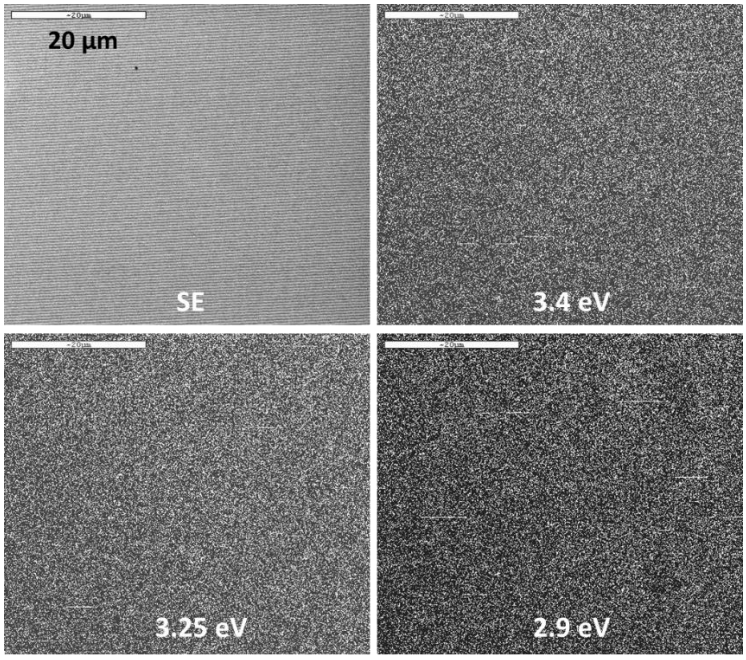

Figure 5.7. Plan-view SE and monochromatic CL images at 3.4, 3.25, and 2.85 eV, taken at an acceleration voltage of 7 kV, and a beam current of 0.1 nA, for the 1-µm GaN:Mg grown on 0.3° miscut substrate. The surface has a smooth appearance in the SE image. No lateral variations in the luminescence distribution is observed in plan-view CL images.

A correlation is found between the optical properties and the surface morphology of films with different thickness, observed using AFM (see Fig. 5.8). In our GaN:Mg films, periodic surface steps are observed aligned along the $[11\bar{2}0]$ direction, perpendicular to substrate tilt towards $[1\bar{1}00]$. In the case of the 0.12-µm-thick film in Fig. 5.8(a), the step period is ~ 121 nm, and the step height is ~ 0.5 nm. For the 1.0-µm-thick film in Fig. 5.8(b), the steps have a period of ~ 354 nm, and a height of ~ 1 nm. The AFM surface roughness from a 10 µm × 10 µm area was 0.69 and 1.18 nm for the thin and thick films, respectively, indicating that the surface becomes rougher with increasing film thickness.

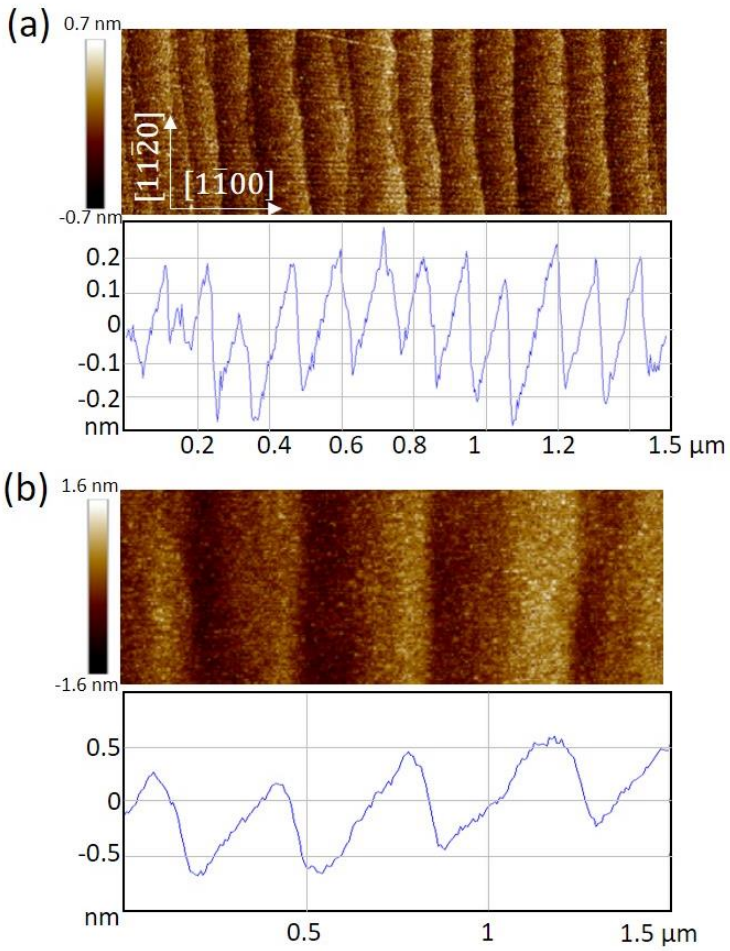

Figure 5.8. Effect of film thickness on surface morphology in GaN:Mg epilayers grown on 0.3° miscut GaN substrates. AFM image and line scan of the surface steps for (a) 0.12 µm thick, and (b) 1.0 µm thick GaN:Mg films. A step height evolution is observed from 1 *c* into 2 *c*.

We attribute the variation of 2.85 eV luminescence to an increase of surface roughness with film thickness. From the AFM images in Fig. 5.8, we observe that as the layer grows thicker, single steps coalesce to form macrosteps, with an increase in surface roughness. We speculate that the presence of macrosteps may change the incorporation mechanism of impurities, causing Mg atoms to accumulate at the steps and form Mg atomic clusters. For

Mg atoms to act as acceptors, they need to be incorporated as a single Mg atom substituting for a Ga atom in the GaN lattice. When Mg atoms incorporate as clusters (with Mg bonded to Mg), their ability to act as acceptors is reduced. Such atomic clusters cannot be detected using TEM or CL, because TEM is a projection imaging technique without single atom resolution, and CL is limited by the interaction volume of electrons and the diffusion of carriers, which is in the order of 10 to 100 nm under most favorable conditions. Step bunching gradually increases with thickness, causing more Mg atoms to incorporate as atomic clusters. Therefore, even though the overall Mg concentration is unchanged, the effective acceptor concentration decreases, leading to a decrease of the 2.85 eV emission intensity. Another less likely possibility, following the contrast observed in Fig. 5.3(b), is that a decrease in nitrogen vacancy concentration with increasing thickness would reduce the concentration of deep donors associated to V_N-Mg complexes.[46]

5.4. Growth on 4° miscut GaN substrates

It has been reported that the epilayer surface grown on miscut substrates has a tendency to form macrosteps.[69] In the preceding discussion, we observed in the 0.3° miscut case that the optical properties of GaN:Mg films are affected by the presence of macrosteps. We now extend our discussion to the 4°miscut case, in order to explore the effect of macrosteps at a higher misorientation on the optical properties of GaN:Mg.

A 1.0 μm GaN:Mg layer was grown on 4°miscut GaN substrates, using the same growth parameters as for the samples previously discussed. Cross-section SE and CL images are shown in Fig. 5.9.

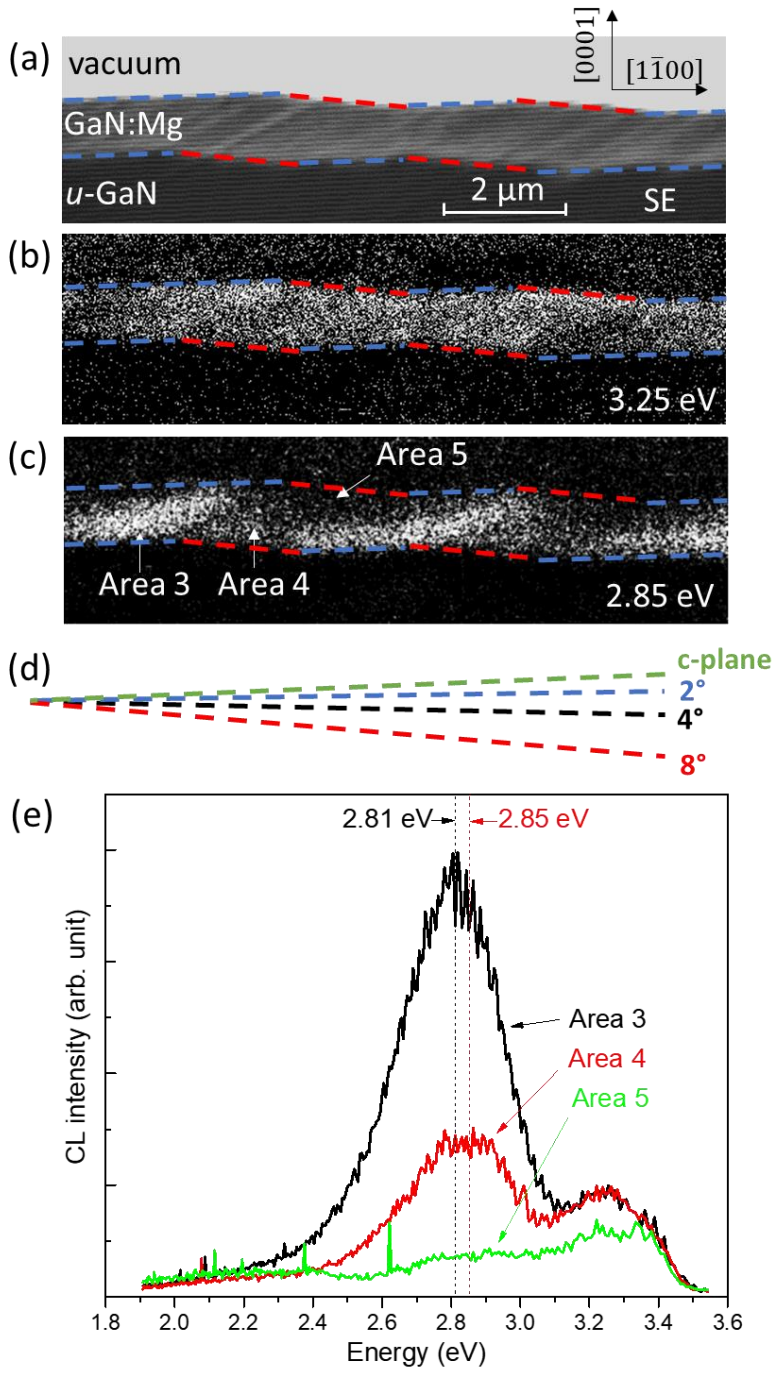

Figure 5.9. Surface morphology and luminescence for the 1.0 µm thick GaN:Mg epilayer on 4° miscut GaN substrate. (a) Cross-section SE image shows variation in the surface orientation of 2° and 8° that follows the underlying *u*-GaN layer, with a lateral displacement of about 2 µm. Monochromatic CL images at (b) 3.25 eV and (c) 2.85 eV.

(d) Relative orientation of surface regions, including the *c*-plane, the 4° nominal miscut, and the 2° (blue) and 8° (red) tilted regions. (e) Spot mode CL spectra taken from Areas 3, 4, and 5 in (c).

The GaN:Mg layer boundaries are marked by dashed lines. We observed surface regions with two main orientations: one with a 2° tilt from the basal plane (blue dashed line) followed by a region with a high tilt of 8° (red dashed line), which alternate to produce the 4° average miscut. As observed in Fig. 5.9(a), the wavy morphology already existed in the original *u*-GaN surface and is preserved during the GaN:Mg growth, with a lateral displacement to the right by ~2 μm. We attribute the lateral displacement of the surface morphology to a lateral/normal growth rate ratio of about 2. The 3.25 eV emission in Fig. 5.9(b) is relatively uniform inside the layer. However, strong variation in the 2.85 eV luminescence intensity following the wavy morphology is observed in Fig 5.9(c). Bright bands with strong 2.85 eV luminescence intensity are observed originating from 2° tilted regions (blue dash lines), marked as Area 3. However, near the top portion of the film, the 2º tilted region shows reduced 2.85 eV intensity. This suggests that step bunching occurs in a similar fashion as in the 0.3º miscut case (Fig. 5.3(c)). Darker bands are observed originating from the 8° tilted regions (red), marked as Area 4. The darkest 2.85 eV emission region is marked as Area 5. The dashed lines in Fig. 5.9(d) serve as guidelines for the various surface orientations. The black dashed line follows the average sample surface of 4° from the *c*-plane (green dashed line). Spot mode CL spectra from Area 3, 4, and 5 are plotted in Fig. 5.9(e). It is observed that the intensity of the 2.85 eV peak is highest in area 3 and decreases in areas 4 and 5. The intensities of the 3.25 eV and 3.4 eV peaks are relatively unchanged.

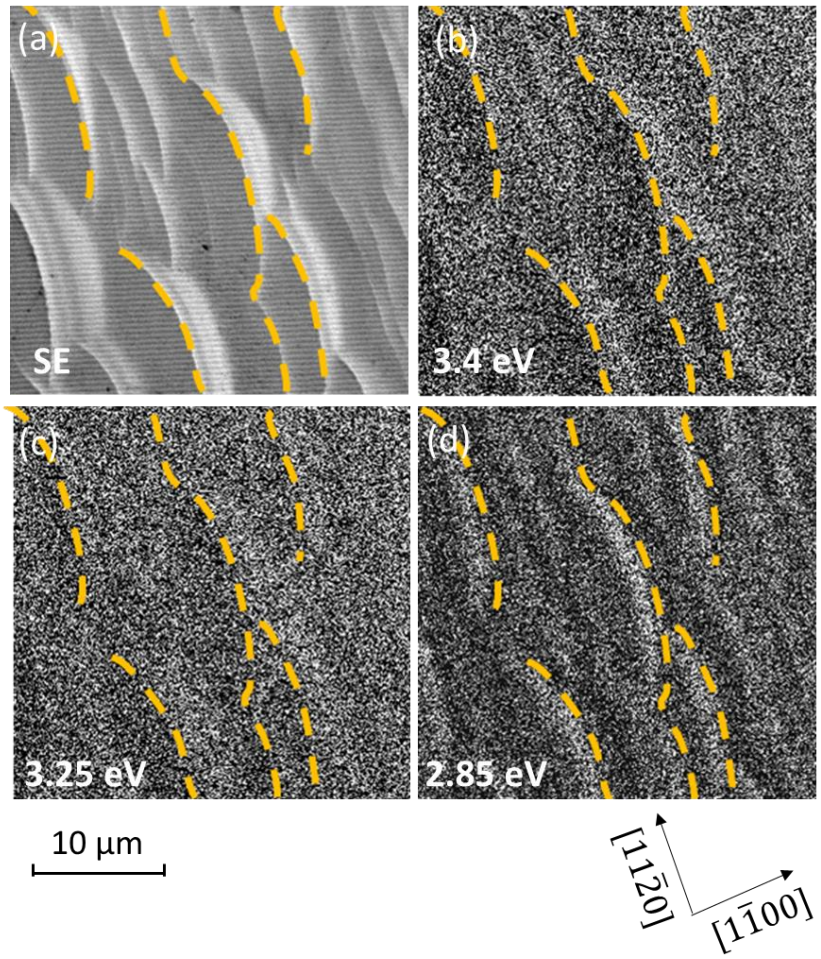

Figure 5.10. Surface morphology and luminescence for the 1.0 µm thick GaN:Mg epilayer on 4° miscut GaN substrate. (a) Plan-view SE image, and monochromatic CL images at (b) 3.4 eV, (c) 3.25 eV, and (d) 2.85 eV. Wavy features on film surface indicate severe step bunching.

A correlation between surface morphology and luminescence is shown in Fig. 5.10. The SE image in Fig. 5.10(a) shows the wavy features of the surface, highlighted by the position of the detector, which is located to the right side. The crest of some of the waves are marked with yellow dashed lines, which represent ridgelines closely perpendicular to the [1$\bar{1}$00] direction. Bright crest lines separated by about 4 µm can be observed, similar

to Fig. 5.9. Nonuniform luminescence can be observed in the CL mappings in Fig. 5.10(b-d). For the 3.4 eV emission, regions to the right of the ridgelines (yellow dashed lines) are brighter, while regions to the left are darker. For the 2.85 eV emission, the reverse is true, where stronger luminescence intensities are observed to the left of the ridgelines. This agrees with the cross-sectional CL image in Fig. 5.9(c), which shows the bright 2.85 eV bands stretch towards the surface and terminate to the left of ridgelines, with period of about 4 μm.

The nonuniform emission intensity at 2.85 eV is clearly associated with the presence of the high tilt regions. This is very similar to the nonuniformity in luminescence properties in GaN:Mg reported in Chapter 4, where GaN:Mg grown laterally from a mesa sidewall showed low 2.85 eV luminescence intensity compared to GaN:Mg grown vertically on the *c*-plane surface.[68] It has also been observed in Chapter 4 that a slight drop in the Mg concentration can have a severe effect on the 2.85 eV emission.[68] This agrees with our observation that the surface on the left side crest (Area 3) is a near-*c*-plane surface with a low density of surface steps. On the other hand, the surface on the right side of the crest (Area 4) contains a high density of macrosteps, similar to a mesa sidewall. The high density of surface steps may affect the incorporation of Mg and reduce the 2.85 eV luminescence intensity, as described in section 5.3, for the 0.3° miscut growth.

5.5. Conclusions

Non-uniform luminescence distribution in GaN:Mg films grown on miscut GaN substrates has been shown to be associated with the presence of atomic step clusters introduced by substrate miscut. In the case of GaN substrates with a miscut angle of 0.3°, the GaN:Mg films are flat with uniform luminescence in the lateral directions. For a

GaN:Mg film thickness of 0.12 μm, the film exhibits strong 2.85 eV emission, indicating good *p*-type conductivity. However, the intensity of the 2.85 eV peak gradually decreases with thickness, indicating a decrease in hole concentration. SIMS and TEM measurements show the decrease in 2.85 eV emission intensity is not related to change in dopant or impurity concentrations, nor to the presence of dislocations or precipitates. Coalescence of single steps into macrosteps was observed for the 0.3° miscut case as the film thickness increases from 0.12 to 1.0 μm, resulting in an increase in surface roughness. We proposed that the decrease of 2.85 eV peak intensity is due in some degree to Mg clustering at surface steps. Mg incorporated as atomic clusters would decrease the acceptor density, leading to a reduction of acceptor concentration, and a reduced 2.85 eV emission intensity. For GaN:Mg film grown on a 4° miscut GaN substrate, wavy features due to step bunching were observed on the film surface. Lower 2.85 eV peak intensity has been observed in regions grown on highly tilted surfaces, where the density of macrosteps is high. The low acceptor concentration regions should introduce a gap in the lateral *p*-type conductivity in the GaN:Mg film.

The variation in the properties of the thick GaN:Mg films reported here have also been observed by us in other similar epilayers grown by other labs. It seems to us it is an intrinsic property of GaN:Mg, independent of the reactor and growth conditions.

CHAPTER 6

EFFECT OF THERMAL ANNEALING AND LOW-ENERGY ELECTRON-BEAM IRRADIATION ON OPTICAL PROPERTIES OF INGAN

6.1 Introduction

In the past two decades, considerable progress has been made in the research of InGaN alloys, which has enabled the development and commercialization of blue-green light-emitting diodes (LEDs) and laser diodes (LDs).[1] Since the bandgap of this ternary alloy ranges over most of the solar spectrum, this material is also of much interest for applications in photovoltaic solar cells.[70,71] Due to the robustness of nitride bonds, a potential application for these materials is in concentrated solar cells, where operating temperature above 600 °C is desirable.[72] The stability of InGaN at high temperature thus becomes an important issue, leading to significant amount of research on this topic. A previous study has shown that the crystalline quality of an $In_{0.16}GaN$ multi-quantum-well (MQW)-based solar cell does not degrade under thermal stress of 500 °C for 5 hours in a nitrogen atmosphere. The decreased performance of the solar cell after thermal stress has been attributed to degradation of metal contacts.[73] Instability of InGaN at higher annealing temperatures has been demonstrated. For example, a decrease in luminescence intensity has been reported for 200nm $In_{0.14}GaN$ films annealed at temperatures above 600 °C in nitrogen for 15 minutes, with formation of indium metal droplets when the annealing temperature was increased to 1000 °C.[74] Phase separation was reported in $In_{0.27}GaN$ MQWs after annealing at 950 °C for 40 hours.[75] On the other hand, significant increases in luminescence intensity has been reported following thermal annealing of InGaN MQW

at 900 °C in nitrogen for 10-15 minutes,[76,77] and of InGaN single-quantum-well at 990 °C for 20 s.[78] It has also been reported that low-energy electron-beam irradiation (LEEBI) improves luminescence intensity of InGaN multiple quantum wells (MQWs).[79,80,81,82] In this work, we have studied the effect of thermal annealing and LEEBI on the optical properties of InGaN, with the objective to understand the thermal stability for application in solar cells operating under solar concentration conditions.

6.2 Experimental

The samples consisted of 60-nm-thick $In_{0.14}Ga_{0.86}N$ epitaxial layers grown on a 3-μm thick unintentionally-doped GaN on a (0001) sapphire substrate. The InGaN films were grown nominally at 735 °C by metalorganic chemical vapor deposition (MOCVD). Samples were cut into 1.5 mm×1.5 mm square pieces from a single wafer for annealing at various temperatures. Sample pieces were picked near the center of the wafer to ensure they were of similar optical quality. Thermal annealing was carried out in a quartz tube furnace under a N_2 gas flow environment. The optical properties were measured using cathodoluminescence (CL) spectroscopy at room temperature, in a scanning electron microscope equipped with a spectrometer with a 1200 lines/mm grating and a GaAs photomultiplier tube. An acceleration voltage of 3 kV was used, corresponding to a maximum electron beam penetration depth of ~100 nm, and a maximum energy dissipation at a depth of ~33 nm. The beam current was 500 pA. Average spectra were obtained using a raster scan at 60 Hz over a square region with dimensions of 14 μm per side. Monochromatic CL images were obtained by setting the monochromator to a specific wavelength and recording the spatial variations of the light emission intensity. The effect

of prolonged electron beam exposure was studied over a square area of 14 μm per side, with an acceleration voltage of 3 kV and with beam currents of either 500 pA or 2.0 nA.

6.3 Effect of thermal annealing on luminescence of InGaN films

Samples were annealed at temperatures ranging from 400 to 700 °C for 1 hour. Little or no variations in the CL spectra were observed as shown in Fig. 6.1. The average spectrum for five as-grown samples is plotted and the variations from sample to sample are represented by error bars. It can be seen the intensity variation is small (~10%) for the as-grown samples. After annealing at temperature between 400 to 700 °C for 1 hour, the spectra of the annealed samples lay within the range of the as-grown sample. There is no change in the CL intensity and spectrum line shape and FWHM (95 meV) after annealing. Secondary-electron (SE) images and monochromatic CL images at peak wavelength (431 nm) (not shown here) taken before and after annealing show no change in the spatial distribution of luminescence. Thus, it is concluded that $In_{0.14}Ga_{0.86}N$ is thermally stable up to 700 °C for thermal anneals of one hour.

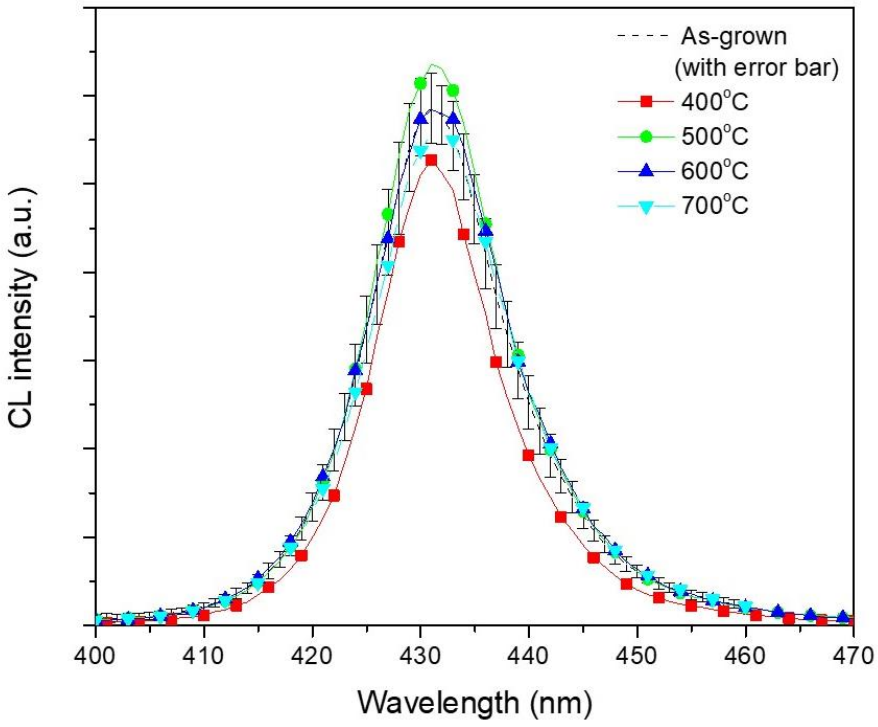

Figure 6.1. CL spectra of $In_{0.14}GaN$ thin films as-grown and after annealing at 400, 500, 600, and 700 °C for 1 hour.

When the annealing temperature is raised to 800 °C, it was observed that the CL intensity increased by ~ 3 times after annealing for 5 minutes as shown in Fig. 6.2(a). The spectrum line shape does not change, implying no noticeable change in the band structure of the material resulting from annealing. No significant changes are observed in surface morphology and light emission distribution after annealing. Therefore, the luminescence intensity improvement after annealing at 800 °C for 5 minutes is not due to change in surface morphology. Longer annealing times of 10 and 20 minutes also result in CL intensity increase as shown in Fig 6.2(b) and (c). But the amount of increase is smaller compared to the 5 minutes annealed sample. The spectrum line shape does not change after

annealed in 800 °C for up to 20 minutes. 40 minutes annealing causes a slight decrease in CL intensity and a 3nm red shift, shown in Fig 6.2(d).

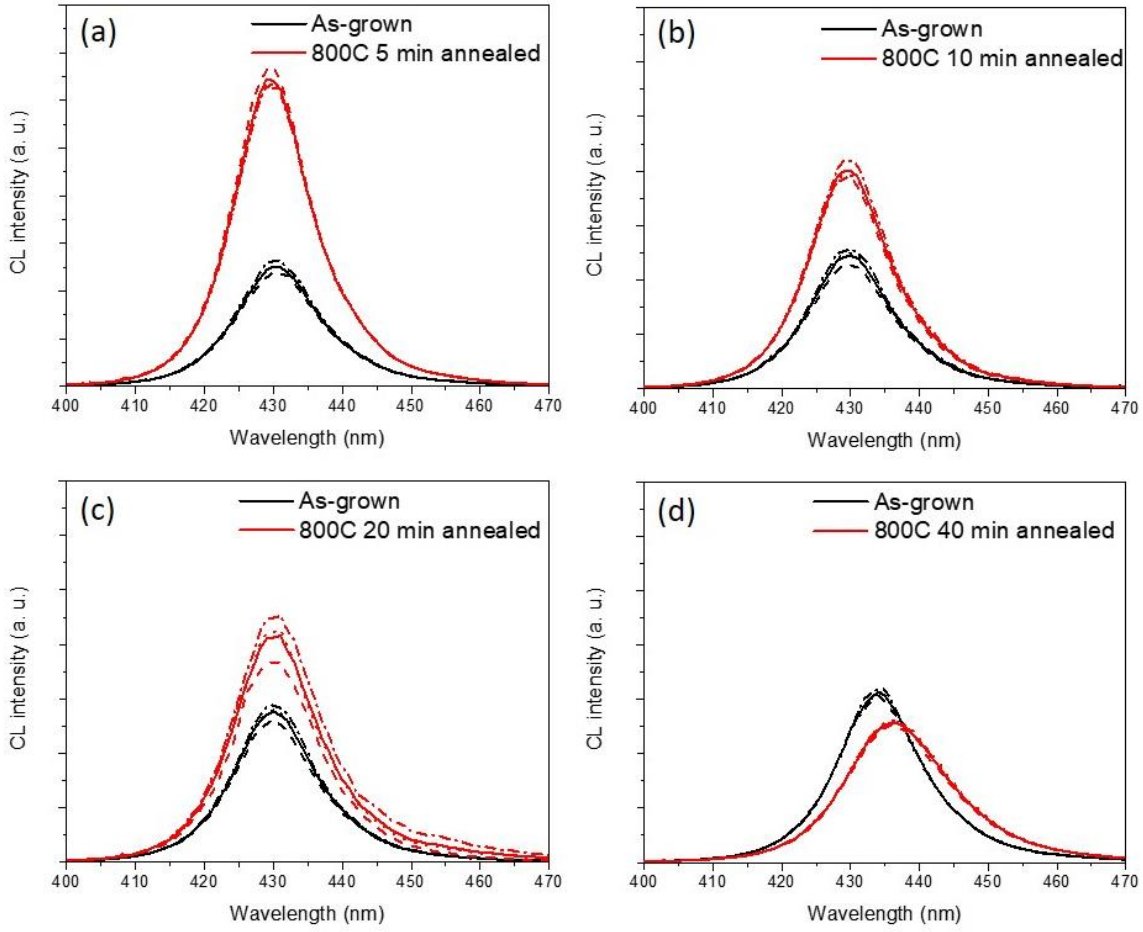

Figure 6.2. CL spectra of $In_{0.14}GaN$ thin films as-grown and after annealing at 800 °C for (a) 5 minutes, (b) 10 minutes, (c) 20 minutes, and (d) 40 minutes. Three spectra were taken at different locations across the sample for each case to show homogeneity in the emission.

The increase in CL intensity after annealing at 800 °C for 5 minutes is stable. As observed in Figure 6.3, further anneal at 600 °C for 1 hour is not detrimental to the improved CL intensity.

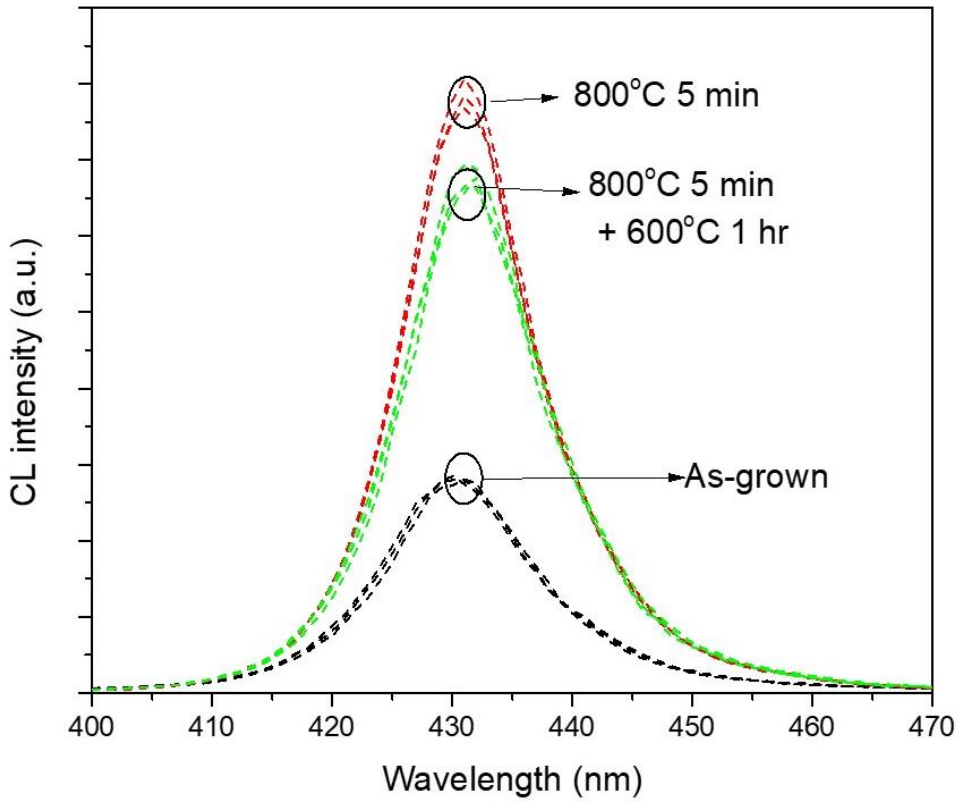

Figure 6.3. CL spectra of $In_{0.14}GaN$ thin films as-grown, after annealing at 800 °C for 5 minutes; and after annealing at 800 °C for 5 minutes followed by annealing at 600 °C for 1-hour. Annealing at 800 °C for 5 minutes increases the luminescence by 3 times. Improved luminescence is retained after annealing at 600 °C for 1-hour.

Annealing at higher temperatures of 900 °C and 1000 °C leads to surface degradation and a decrease in CL intensity as shown in Figure 6.4. After annealing at 900 °C for 6 hours, the intensity of the 431 nm InGaN emission is decreased and red-shifted. Also, a broad peak ranging from 350 nm to 500 nm appears. After annealing at 1000 °C for 1 hour, the intensity of the 431 nm InGaN emission further decreases. Intensity of the broad peak increases, with a maximum appearing at 380 nm. We speculate that at such elevated temperatures, indium will evaporate from the film. This will accelerate the oxidation of

GaN by providing larger surface area and more volume for gallium oxide growth. Oxidation of GaN by thermal annealing in oxygen at temperatures above 800 °C has been previously reported.[83] The bandgap of GaON ternary alloy was reported to range from 4.8 eV to 2.05 eV, depending on the crystal structure and oxygen composition.[84] This is similar to the spectra we observe in our annealed samples.

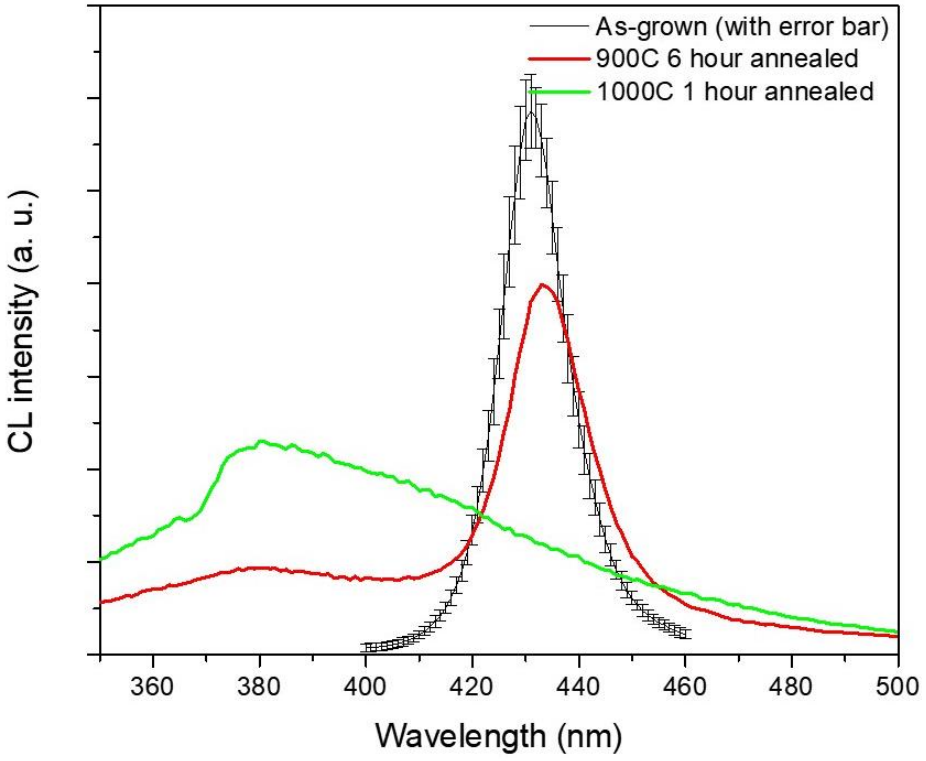

Figure 6.4. CL spectra of $In_{0.14}GaN$ thin films as-grown and after annealing at 900 °C for 6 hours, and after annealing at 1000 °C for 1hour.

Fig. 6.5 and Fig. 6.6 show the SE and CL images of samples before and after 900 °C 6-hours and 1000 °C 1hour annealing processes, respectively. Grains were observed to form on the surface of the InGaN film. CL images at 380 nm, 431 nm and 445 nm show that these grains have a broad emission range. They are responsible for the broad emission

observed in the spectrum. We suspect they are GaON crystals with a continuous variation in N and O composition.

Energy dispersive spectroscopy (EDS) measurements were performed on as-grown, 900C 6-hour annealed and 1000 °C 1-hour annealed samples as shown in Fig. 6.7. The insets are SE images taken at location of EDS measurement. It can be seen the as-grown sample has a smooth surface, EDS spectrum shows a noticeable indium L*a* peak and a very weak oxygen K*a* peak. After annealing at 900 °C for 6 hours, grains were observed to have formed on the surface. EDS spectrum shows a decrease in the intensity of indium L*a* peak and an increase in the oxygen K*a* peak. After annealed at 1000 °C for 1 hour, the surface looks very grainy and many voids were formed. EDS spectrum shows a strong oxygen K*a* peak and no detectable indium L*a* peak. It is speculated that the grains are gallium oxides or GaON alloy. The voids are caused by the indium loss of the InGaN film.

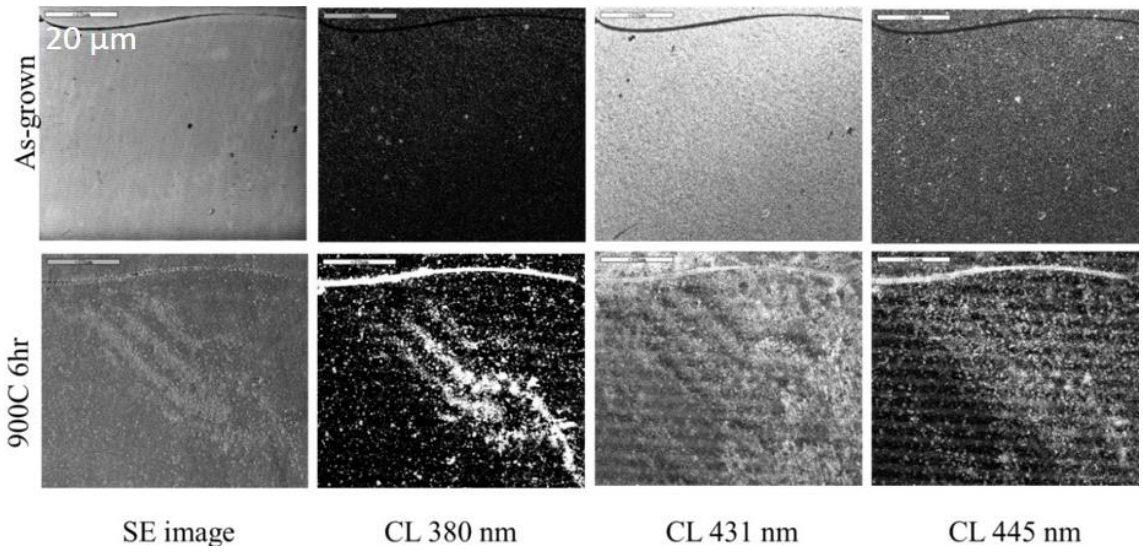

Figure 6.5. SE images and CL mappings of InGaN films as-grown and after annealing at 900 °C for 6 hours.

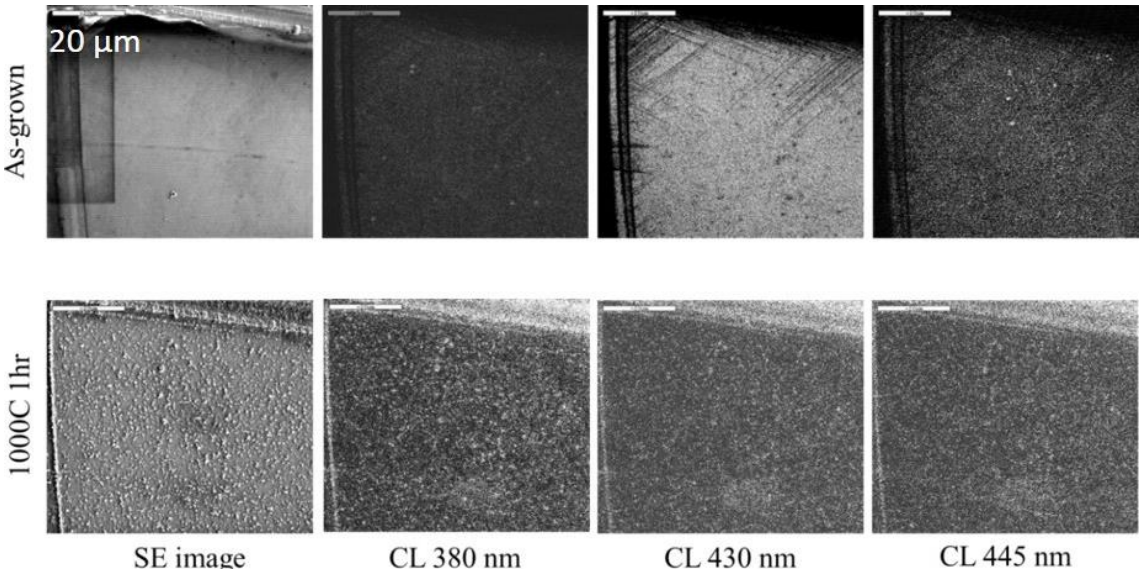

Figure 6.6. SE images and CL mappings of InGaN films as-grown and after annealing at 1000 °C for 1 hour.

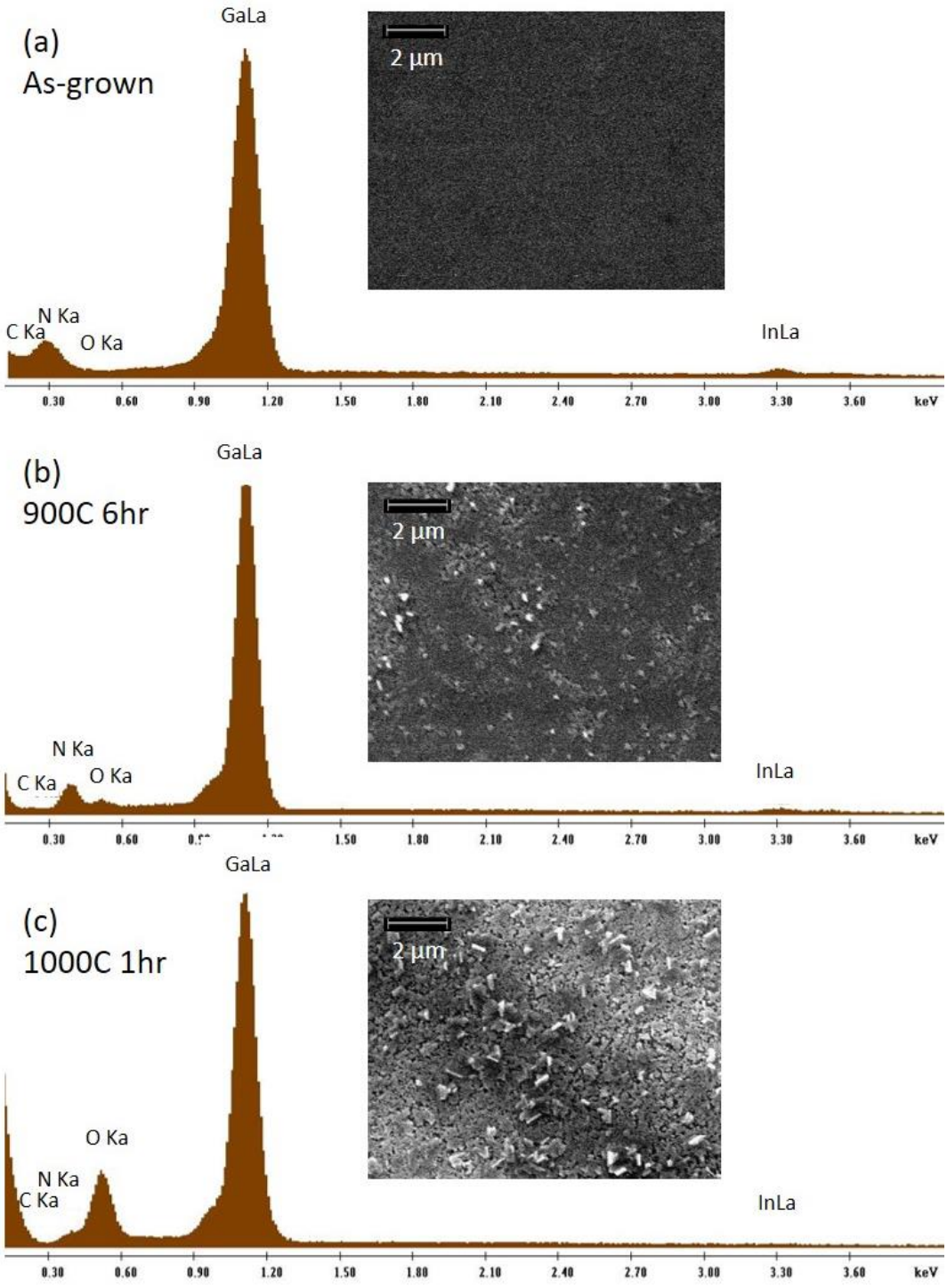

Figure 6.7. EDS spectra of InGaN films (a) as-gown, after annealing at (b) 900 °C for 6 hours, (c) 1000 °C for 1 hour. Insets are SE images taken at an acceleration voltage of 10 kV.

6.4 Effect of low-energy electron-beam irradiation on luminescence properties of InGaN films

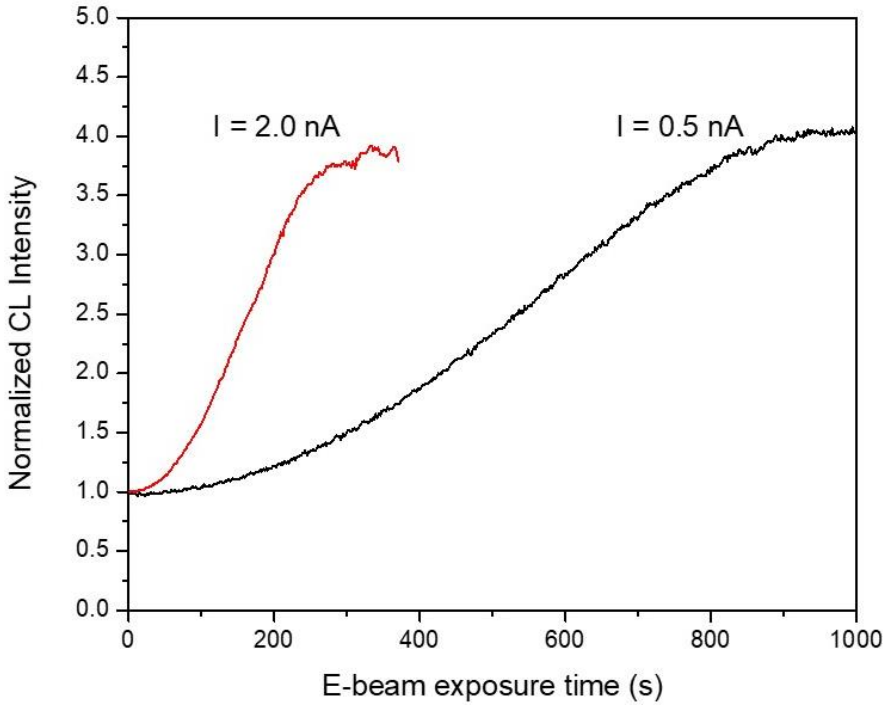

Figure 6.8. Normalized CL peak intensity at 431 nm versus e-beam exposure time when the InGaN film is irradiated with 3 kV and at beam currents of 0.5 or 2.0 nA. A four-fold improvement in the luminescence is observed for both beam currents. The rate of improvement is related to the dose of electrons from the e-beam.

We found that low-energy electron-beam irradiation also increases the CL intensity of $In_{0.14}Ga_{0.86}N$ films grown by MOCVD. The CL intensity increases by a factor of ~ 4 after exposure to the electron beam, and eventually saturates. The rate of intensity increase depends on the e-beam current used during irradiation. Fig. 6.8 shows the peak intensity at 431 nm versus e-beam irradiation time under beam currents of 500 pA or 2.0 nA. The higher current leads to more rapid increase and earlier saturation of the CL intensity. Fig.

6.9 shows spectra (a) before and (b) after e-beam irradiation. A slight 1-nm red shift happens after e-beam exposure. But the overall spectrum line shape remains the same. Fig. 6.10(b) and (b') shows the SE image and monochromatic CL mappings at 431 nm after e-beam irradiation, respectively. It can be seen that the emission intensity at the e-beam irradiated area are uniform and significantly higher than the surrounding area.

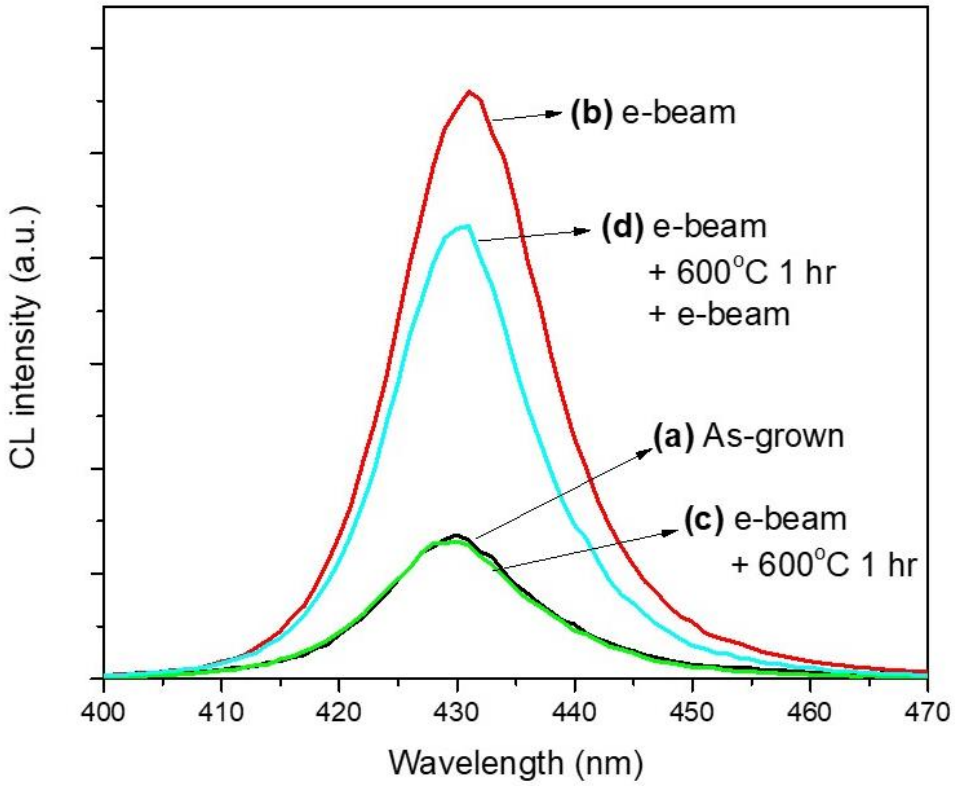

Figure 6.9. CL spectra for InGaN films following e-beam irradiation, and further thermal annealing at 600°C for 1-hour plus a second e-beam irradiation. The luminescence intensity increased 4-fold after e-beam irradiation, but the effect is reversed after annealing at 600°C for 1 hour. Further e-beam irradiation still improves luminescence.

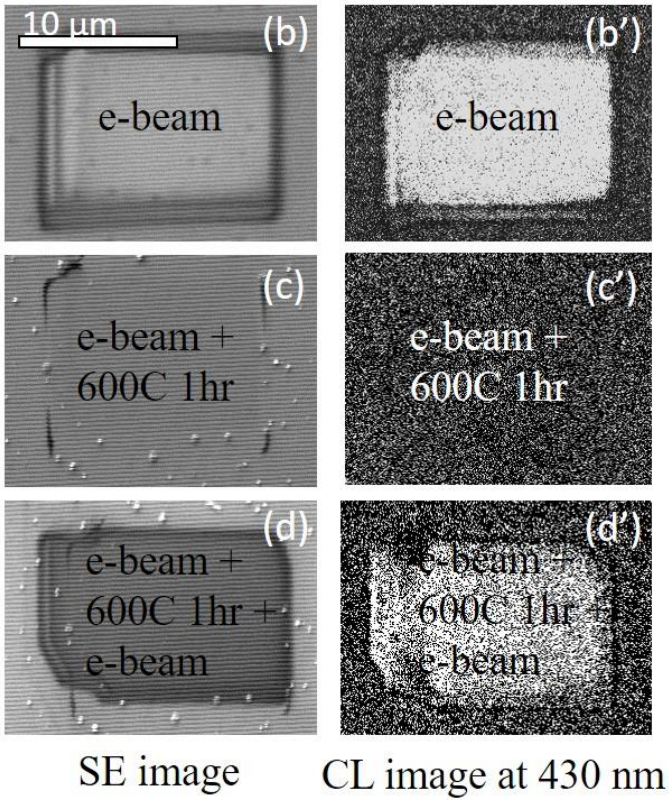

Figure 6.10. SE images (b), (c), (d), and CL mapping at 430 nm (b'), (c'), (d') of InGaN films after subsequent treatments of e-beam irradiation, e-beam irradiation + 600°C 1 hour annealing, and e-beam irradiation + 600°C 1 hour annealing + e-beam irradiation.

The stability of the LEEBI effect on luminescence intensity is discussed next. We found that the LEEBI effect can be reversed after annealing the sample at nitrogen at 600 °C for 1 hour. As observed in Fig 6.9(c), the CL intensity drops back to the as-grown level after such annealing step. The 1-nm red-shift caused by the LEEBI is also recovered. CL image in Figure 10(c') also show that the intensity of the e-beam irradiated area falls back to as-grown level. An additional subsequent LEEBI step increases the CL intensity and causes a red-shift again, as shown in Fig. 6.9(d) and Fig. 6.10(d'). This shows that while

the LEEBI effect can be reversed when the sample is heated to higher temperatures, it can be restored again by a second irradiation step.

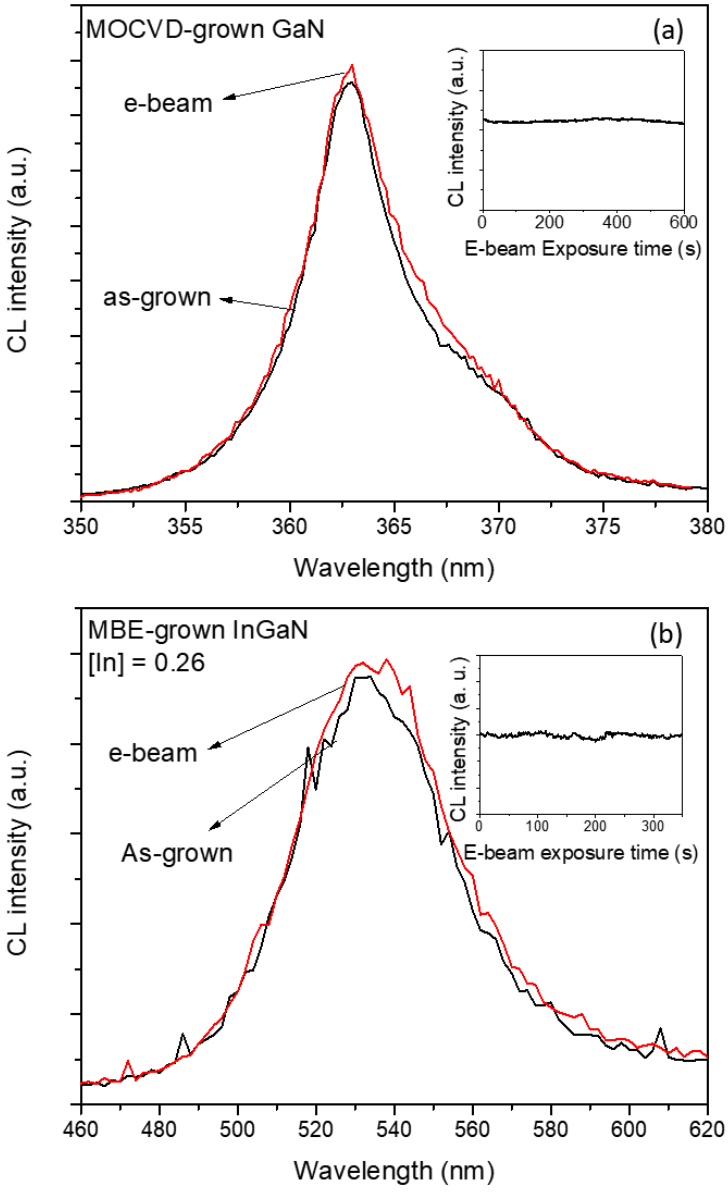

Figure 6.11. Comparison of (a) GaN grown by MOCVD and (b) InGaN film grown by MBE before and after LEEBI. Insets: Peak CL intensity versus e-beam irradiation time. No change is observed in CL characteristics under LEEBI for both samples.

We also studied the e-beam irradiation effect on an GaN film grown by MOCVD and on an InGaN thin film grown by molecular beam epitaxy (MBE). The CL spectra in Fig. 6.11(a) corresponds to MOCVD-grown GaN before and after e-beam irradiation, with no significant change observed. The inset shows the CL peak intensity vs exposure time of GaN under 5 nA electron beam exposure for 10 minutes. CL spectra in Fig. 6.11(b) corresponds to MBE-grown $In_{0.26}GaN$ thin film before and after the same e-beam irradiation process. It was found that CL intensity does not change under electron beam irradiation for MBE-grown InGaN.

6.5 Discussion

Our interpretation for the improved CL intensity after thermal annealing at 800 °C for 5 minutes is that high temperature promotes dissociation of the un-reacted NH_3 present in the film due to the MOCVD low growth temperature. Full dissociation of NH_3 has been reported to occur at temperatures around 1050 °C.[85,86] For that reason, growth of GaN by MOCVD is performed at that or higher temperatures (1050 °C and above) for significant dissociation of the nitrogen source.[87,88] At such high temperatures, indium has difficulty in incorporating into the growth surface. Epitaxy with high indium content requires significantly lower growth temperatures. For our films with 14% indium content, the growth temperature was lowered to around 735 °C. There should be NH_3 that fails to dissociate into nitrogen and hydrogen. The unreacted NH_3 will become unstable when sample is heated up to temperature exceeding the growth temperature. This explains why the optical property remains unchanged when annealing up to 700 °C, but changes start to occur when annealing at 800 °C and higher temperatures. It is speculated that the un-reacted NH_3 serves as non-radiative recombination centers, which reduce the luminescence

intensity of InGaN. After annealing at temperatures higher than growth temperature (i.e. 735 °C), they dissociate into hydrogen and nitrogen. With the assistance of thermal energy, hydrogen atoms may diffuse out of the film. This is similar to the dissociation of Mg-H bonds in GaN:Mg, where high temperature annealing removes the H atoms prevalent in MOCVD growth and activate the Mg acceptors. With the dissociation and removal of H atoms in InGaN films, the InGaN crystal quality is improved after annealing at temperatures above the growth temperature. However, annealing at 800 °C or higher temperatures for extended amount of time will cause surface deterioration of InGaN film, leading to a decrease in CL intensity.

It is possible that during the LEEBI treatment, the electrons break the existing N-H bonds in un-reacted NH_3, thus deactivating the corresponding non-radiative recombination centers. An electron beam with higher current density offers more electrons to break the N-H bonds faster, leading to the observed more rapid increase in intensity. However, the hydrogen atoms released in the process will remain in the vicinity.

When annealing at 600 °C after e-beam irradiation, the thermal energy causes the N-H bond to form again, re-activating the non-radiative recombination centers and causing the CL intensity to drop back to as-grown level. Any subsequent annealing at 600 °C is not sufficient to effectively dissociate the NH_3, and no improvement in the luminescence is observed (Figure 6.9(c)). Further e-beam exposure on the 600 °C 1-hour annealed sample again caused the CL intensity to increase (Figure 6.9(d)), suggesting the N-H bonds are still present and are once again passivated by the electrons.

To obtain corroboration that the CL intensity increase is related to dissociation of un-reacted NH_3, we studied the LEEBI effect on an GaN film grown by MOCVD and on an InGaN thin film grown by molecular beam epitaxy (MBE). GaN growth by MOCVD is at a temperature of ~ 1050°C, at which we expect NH_3 to be fully dissociated with no N-H related non-radiative recombination centers. Therefore, LEEBI has no effect on CL intensity of GaN as shown in Fig. 6.11(a). For the second case, $In_{0.26}GaN$ grown by MBE uses indium, gallium and nitrogen gas as source. This method does not involve use of NH_3 and trimethyl-metal precursor that contains H atoms. Therefore, it should not introduce N-H groups in the InGaN film. It was found that CL intensity does not change under LEEBI for MBE-grown InGaN as shown in Fig. 6.11(b).

Finally, we studied the effect of LEEBI on a MOCVD-grown InGaN film which has already been thermally annealed at 800°C for 5 minutes. Fig. 6.12 shows the CL intensity versus e-beam irradiation time. For an as-grown film, the luminescence intensity is increased under the e-beam irradiation. However, for the 800°C 5 minutes annealed sample, with improved luminescence intensity compared to as-grown sample, does not show further improvements in luminescence intensity under LEEBI. This agrees with our speculation that 800 °C 5 minutes annealing helps breakup the NH_3 left in the sample and assist with the out-diffusion of hydrogen atoms. Therefore, further e-beam irradiation will not improve the luminescence intensity.

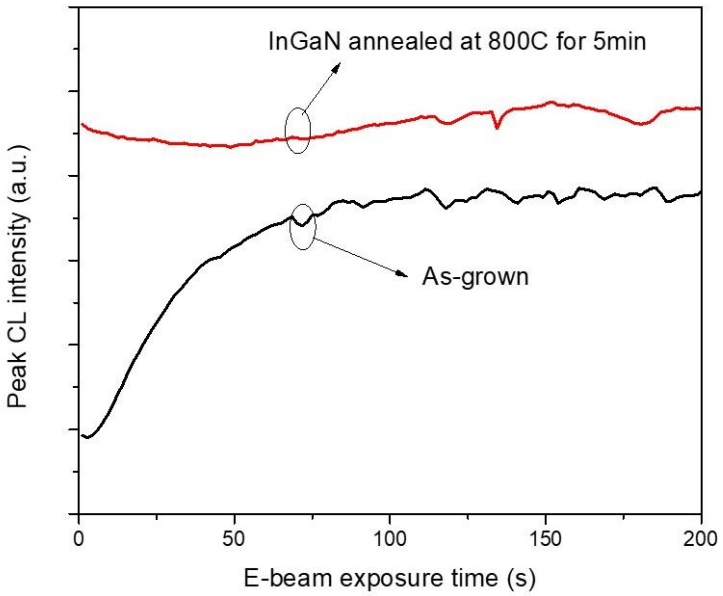

Figure 6.12. Peak CL intensity versus irradiation time of as-grown and 800 °C 5 minutes annealed InGaN films under e-beam irradiation.

6.6 Conclusion

The effects of thermal annealing and electron beam irradiation on the optical properties of $In_{0.14}Ga_{0.86}N$ films grown by MOCVD have been studied. No changes to cathodoluminescence (CL) intensity and spectrum line shape have been observed for annealing at temperatures up to 700 °C for 1 hour in nitrogen atmosphere. A 3-fold increase in CL intensity was observed for annealing at 800 °C for 5 minutes. The improved luminescence intensity was found to be stable even after subsequent annealing at lower temperature of 600 °C for 1 hour. We attribute the improvement to the dissociation of N-H bond and out diffusion of H atoms. We also observed a 4-fold increase in CL intensity of InGaN under low energy electron beam irradiation. The improvement in CL intensity by LEEBI is reversed back to the as-grown level after subsequent annealing at 600 °C for 1 hour. MOCVD-grown GaN and MBE-grown InGaN do not show changes under LEEBI.

Sample with increased CL intensity after 800 °C thermal annealing does not show further intensity improvement under e-beam irradiation, suggesting non-recombination centers related to N-H sites are eliminated during 800 °C thermal annealing.

CHAPTER 7

SUMMARY AND FUTURE WORK

7.1 Luminescence properties of Mg-doped GaN epilayers

The luminescence properties of GaN:Mg epilayers have been studied comprehensively using cathodoluminescence spectroscopy. CL is a powerful tool to study the luminescence characteristics of GaN:Mg, by providing spectral measurements with sub-micron spatial resolution. However, the electron dose incident on the specimen during the CL measurements need to be carefully controlled to prevent changes in luminescence characteristics induced by electron beam irradiation.

In Chapter 3, the relationship among luminescence characteristics and acceptor concentration and *p*-type conductivity in GaN:Mg epilayers has been studied. It was found the that the intensity of the 2.85 eV emission peak, produced by deep donor to Mg acceptor transitions, is positively proportional to the acceptor concentration in the GaN:Mg film. The acceptor concentration is determined by a convolution of factors including the Mg doping concentration, direction of growth front, thermal annealing history, and background impurity concentration. The effects of these parameters on the luminescence characteristic of GaN:Mg have been shown. The use of CL to probe local acceptor concentration variation at sub-micron scale enabled the correlation between luminescence properties and acceptor concentration. This capability has served as a basis for the studies in Chapters 4 and 5.

Chapter 4 is a report on the optical properties of GaN:Mg epilayers grown on mesa structures. It was found that the luminescence in GaN:Mg grown on a mesa structure is not

spatially uniform. The correlation between luminescence characteristics and acceptor concentration was used to reveal that lateral growth of GaN:Mg from the mesa sidewall results in a lower acceptor concentration when compared with the vertical growth from the basal plane surface. CL mapping was used to visualize the lateral vs. vertical growth in GaN:Mg films on mesa structures.

In many power electronic device designs, selective area *p*-type doping involves growth of thick (> 1μm) GaN:Mg epilayers on mesa structures. The reduction of acceptor concentration near the sidewall by lateral growth will likely affect device performance. It will be important to establish the correlation between device performance and the non-uniformity in acceptor distribution. Growth parameters such as growth temperature, pressure, III/V ratio, and doping concentration have been reported to affect the lateral growth rate in GaN. A possible future study would be to change these growth parameters to tune the lateral growth in GaN:Mg on mesa structures and correlate them with device performances.

Chapter 5 investigated the influence of GaN substrate miscut angle on the luminescence properties of GaN:Mg. For optimum misorientations of 0.3°, Mg-doping gradually introduces roughness that decreases the doping efficiency, eventually rendering the film semi-insulating. This explains the difficulty in producing thick (> 1μm) Mg-doped GaN reported by many organizations. For a high misorientation of 4°, step bunching leads to faceting, and inhomogeneous doping profiles, like what we reported from mesa sidewalls. It is speculated that with increasing surface roughness, Mg atoms are incorporated in forms of atomic clusters or defect complexes that no longer act as acceptors.

A future work would be to measure the drop in Mg_{Ga} acceptors using C-V, deep level transient spectroscopy (DLTS) or electron paramagnetic resonance (EPR).

The Mg doping efficiency was observed to decrease with increasing surface roughness. However, only the 0.12 μm and 1.0 μm thick films have been studied. It would be interesting to study a few intermediate thicknesses, to better understand the mechanism of surface roughening as film thickness increases. The depth profile will provide an idea about a critical thickness for roughening. This may enable a deeper understanding of the Mg atom incorporation mechanism on atomic step edges.

7.2 Effect of thermal annealing and electron beam irradiation on the optical properties of InGaN

The effects of thermal annealing and electron beam irradiation on the optical properties of $In_{0.14}Ga_{0.86}N$ films grown by MOCVD have been studied. No change in the luminescence characteristics were observed after annealing up to 700 °C for one hour. This is reasonable since the film was grown at 735 °C. A multi-fold increase in luminescence intensity was observed after annealing at 800 °C for 5 minutes. The improved luminescence intensity was found to be stable even after subsequent annealing at a lower temperature of 600 °C for 1 hour. It was found that low-energy electron beam irradiation at room temperature resulted in a similar increase in luminescence intensity. The improved CL intensity by electron radiation is reversed back to the as-grown level after subsequent annealing at 600 °C for 1 hour. The improvement in luminescence intensity has been attributed to the dissociation of N-H bonds from un-reacted ammonia that results from the low temperature growth. It is speculated that un-reacted ammonia act as non-radiative recombination centers, which are dissociated and removed when annealed at a temperature

greater than 800°C, or are locally dissociated by electron irradiation. This study shows mechanism that can significantly improve the luminescence efficiency of InGaN, which is important for InGaN-based optoelectronic devices.

As a future study, it is important to experimentally prove the dissociation of N-H bond and removal of H atoms after thermal annealing or after electron irradiation. However, hydrogen is prevalent in MOCVD-grown GaN, and its concentration is difficult to measure with SIMS. A possible experiment is to use Forward Rutherford Scattering to measure the H content, or to use Raman spectroscopy to measure the N-H bond characteristics before and after thermal annealing.

REFERENCES

1. F. A. Ponce and D. P. Bour, *Nitride-based semiconductors for blue and green light-emitting devices*, Nature 386, 351 (1997).

2. J. Wu, W. Walukiewicz, K. M. Yu, W. Shan, J. W. Ager, E. E. Haller, Hai Lu, William J. Schaff, W. K. Metzger, and S. Kurtz, *Superior radiation resistance of $In_{1-x}Ga_xN$ alloys: Full-solar-spectrum photovoltaic material system*, J. Appl. Phys. 94, 6477 (2003).

3. J. J. Williams, H. McFavilen, A. M. Fischer, D. Ding, S. R. Young, E. Vadiee, F. A. Ponce, C. Arena, C. B. Honsberg, and S. M. Goodnick, *Development of a high-band gap high temperature III-nitride solar cell for integration with concentrated solar power technology*, IEEE 44th Photovoltaic Specialists Conference (2017).

4. H. Amano et al, *The 2018 GaN power electronics roadmap*, J. Phys. D: Appl. Phys. 51, 163001 (2018).

5. F. A. Ponce, *Crystal defects and device performance in LEDs and LDs*, Chapter 4 in *Introduction to Nitride Semiconductor Blue Lasers and Light Emitting Diodes*, edited by S. Nakamura and S. F. Chichibu (Taylor and Francis Ltd., London, 2000).

6. D. Chandrasekhar, D. J. Smith, S. Strite, M. E. Lin, and H. Morkoc, *Characterization of Group III-nitride semiconductors by high-resolution electron microscopy*, J. Cryst. Growth, 152, 135 (1995).

7. N. Koide, H. Kato, M. Sassa, S. Yamasaki, K. Manabe, M. Hashimoto, H. Amano, K. Hiramatsu, and I. Akasaki, *Doping of GaN with Si and properties of blue m/i/n/n^+ GaN LED with Si-doped n^+-layer by MOVPE*, J. Crys. Grow. 115, 639 (1991).

8. W. Götz and N. M. Johnson, *Activation energies of Si donors in GaN*, Appl. Phys. Lett. 68, 3144 (1996).

9. J. I. Pankove, M. T. Duffy, E. A. Miller, and J. E. Berkeyheiser, *Luminescence of insulating Be-doped and Li-doped GaN*, J. Lumin. 8, 89 (1973).

10. J. I. Pankove, and J. A. Hutchby, *Photoluminescence of ion-implanted GaN*, J. Appl. Phys. 47, 5387 (1976).

11. H. P. Maruska, W. C. Rhines, and D. A. Stevenson, *Preparation of Mg-doped GaN diodes exhibiting violet electroluminescence*, Mat. Res. Bull. 7, 777 (1972).

12. O. Lagerstedt and B. Monemar, *Luminescence in epitaxial GaN:Cd*, J. Appl. Phys. 45, 2266 (1974).

13. H. Amano, M. Kito, K. Hiramatsu, and I. Akasaki, *P-Type conduction in Mg-doped GaN treated with low-energy electron beam irradiation (LEEBI)*, Jpn. J. Appl. Phys. 28, L2112 (1989).

14. S. Nakamura, T. Mukai, M. Senoh, and N. Iwasa, *Thermal Annealing Effects on P-Type Mg-Doped GaN Films*, Jpn. J. Appl. Phys. 31, L139 (1992).

15. M. S. Brandt, N. M. Johnson, R. J. Molnar, R. Singh, and T. D. Moustakas, *Hydrogenation of p -type gallium nitride*, Appl. Phys. Lett. 64, 2264(1994).

16. Y. Ohba and A. Hatano, Jpn. *H-atom incorporation in Mg-doped GaN grown by metalorganic chemical vapor deposition*, J. Appl. Phys. 33, L1367 (1994).

17. S. Nakamura, N. Iwasa, M. Senoh, and T. Mukai, *Hole compensation mechanism of p-type GaN films*, Jpn. J. Appl. Phys. 31, 1258 (1992).

18. W. Gotz, N. Johnson, J. Walker, D. Bour, H. Amano, and I. Akasaki, *Hydrogen passivation of Mg acceptors in GaN grown by metalorganic chemical vapor deposition*, Appl. Phys. Lett. 67, 2666 (1995).

19. W. Götz, N. M. Johnson, J. Walker, D. P. Bour, and R. A. Street, *Activation of acceptors in Mg - doped GaN grown by metalorganic chemical vapor deposition*, Appl. Phys. Lett. 68, 667 (1996).

20. Z. Liliental-Weber, M. Benamara, W. Swider, J. Washburn, I. Grzegory, S. Porowski, D. J. H. Lambert, C. J. Eiting, and R. D. Dupuis, *GaN:Mg: Similar defects in bulk crystals and layers grown on Al_2O_3 by metal-organic chemical-vapor deposition*, Appl. Phys. Lett. 75, 4159 (1999).

21. M. Hansen, L. F. Chen, J. S. Speck, and S. P. DenBaars, *Observation of Mg-rich precipitates in the p-Type doping of GaN-based laser diodes*, Phys. Stat. Sol. (b) 228, 353 (2001).

22. H. Obloh, K.H. Bachem, U. Kaufmann, M. Kunzer, M. Maier, A. Ramakrishnan, and P. Schlotter, *Self-compensation in Mg doped p-type GaN grown by MOCVD*, J. Cryst. Growth 195, 270 (1998).

23. I. C. Kizilyalli, A. P. Edwards, O. Aktas, T. Prunty, and D. Bour, *Vertical Power p-n Diodes Based on Bulk GaN*, IEEE Trans. Electron. Devices, 62 414 (2015).

24. U. K. Mishra, L. Shen, T. E. Kazior, and Y.-F. Wu, *GaN-Based RF Power Devices and Amplifiers*, Proceed. IEEE, 96 297 (2007).

25. K. Fu , H. Fu , X. Huang , H. Chen, T.-H. Yang, J. Montes, C. Yang, J. Zhou, and Y. Zhao, *Demonstration of 1.27 kV Etch-Then-Regrow GaN p-n Junctions With Low Leakage for GaN Power Electronics*, IEEE Electron Device Lett. 40, 1728 (2019).

26. S. Kucheyev, J. Williams, and S. Pearton, *Ion implantation into GaN*, Mat. Sci. Eng. R 33, 57 (2001).

27. J. K. Sheu and G. C. Chi, *The doping process and dopant characteristics of GaN*, J. Phys. Condens. Mat. 14, R657 (2002).

28. B. G. Yacobi and D. B. Holt, *Cathodoluminescence Microscopy of Inorganic Solids*, (Plenum Press, New York, 1990).

29. J. I. Goldstein, D. E. Newbury, P. Echlin, D. C. Joy, C. Fiori, and E. Lifshin, *Scanning Electron Microscopy and X-ray Microanalysis*, 3rd edn. (Plenum Press, New York, 1981).

30. K. Kanaya and S. Okayama, *Penetration and energy-loss theory of electrons in solid targets*, J. Phys. D: Appl. Phys. 5, 43 (1972).

31. E. H. Hall, *On a New Action of the Magnet on Electrical Current*, Amer. J. Math. 2, 287 (1879).

32. L. J. van der Pauw, *A Method of Measuring Specific Resistivity and Hall Effect of Discs of Arbitrary Shapes*, Philips Res. Repts. 13, 1 (1958).

33. F. A. Stevie, *Secondary Ion Mass Spectrometry: Applications for Depth Profiling and Surface Characterization*, Momentum Press (2016).

34. V. E. Krohn, *Emission of Negative Ions from Metal Surfaces Bombarded by Positive Cesium Ions*, J. Appl. Phys. 33, 3523 (1962).

35. P. Williams and C. A. Evans, *Anomalous enhancement of negative sputtered ion emission by oxygen*, Surf. Sci. 78, 324 (1978).

36. X. Li and J. J. Coleman, *Time-dependent study of low energy electron beam irradiation of Mg-doped GaN grown by metalorganic chemical vapor deposition*, Appl. Phys. Lett. 69, 1605 (1996).

37. O. Gelhausen, H. N. Klein, M. R. Phillips, and E. M. Goldys, *Influence of low-energy electron beam irradiation on defects in activated Mg-doped GaN*, Appl. Phys. Lett. 81, 3747 (2002).

38. H. Amano, M. Kitoh, K. Hiramatsu, and I. Akasaki, *Growth and Luminescence Properties of Mg-Doped GaN Prepared by MOVPE*, J. Electrochem. Soc. 137, 1639 (1990).

39. L. Shang, S. Ma, J. Liang, T. Li, C. Yu, X. Liu, and B. Xu, *The Properties of p-GaN with Different Cp_2Mg/Ga Ratios and Their Influence on Conductivity*, J. Electron. Mater. 45, 2697, (2016).

40. U. Kaufmann, M. Kunzer, M. Maier, H. Obloh, A. Ramakrishnan, B. Santic, and P. Schlotter, *Nature of the 2.8 eV photoluminescence band in Mg doped GaN*, Appl. Phys. Lett. 72, 1326 (1998).

41. U. Kaufmann, M. Kunzer, M. Maier, H. Obloh, A. Ramakrishnan, B. Santic, and P. Schlotter, *Origin of defect-related photoluminescence bands in doped and nominally undoped GaN*, Phys. Rev. B 59, 5561 (1999).

42. F. Shahedipour and B. W. Wessels, *Investigation of the formation of the 2.8 eV luminescence band in p-type GaN:Mg*, Appl. Phys. Lett. 76, 3011 (2000).

43. H. Obloh, K.H. Bachem, U. Kaufmann, M. Kunzer, M. Maier, A. Ramakrishnan, and P. Schlotter, *Self-compensation in Mg doped p-type GaN grown by MOCVD*, J. Cryst. Growth 195, 270 (1998).

44. A. M. Fischer, S. Srinivasan, F. A. Ponce, B. Monemar, F. Bertram, and J. Christen, *Time-resolved cathodoluminescence of Mg-doped GaN*, Appl. Phys. Lett. 93, 151901 (2008).

45. Y.-H. Kwon, S. K. Shee, G. H. Gainer, G. H. Park, S. J. Hwang, and J. J. Song, *Time-resolved study of yellow and blue luminescence in Si- and Mg-doped GaN*, Appl. Phys. Lett. 76, 840 (2000).

46. U. Kaufmann, P. Schlotter, H. Obloh, K. Köhler, and M. Maier, *Hole conductivity and compensation in epitaxial GaN:Mg layers*, Phys. Rev. B 62, 10867 (2000).

47. H. Fu, K. Fu, X. Huang , H. Chen, I. Baranowski, T.-H. Yang, J. Montes, and Y. Zhao, *High performance vertical GaN-on-GaN p-n power diodes with hydrogen-plasma-based edge termination*, IEEE Electron Device Lett. 39, 1018 (2018).

48. H. Fu, K. Fu, H. Liu, S. R. Alugubelli, X. Huang, H. Chen, J. Montes, T.-H. Yang, C. Yang, J. Zhou, F. A. Ponce, and Y. Zhao, *Implantation-and etching-free high voltage vertical GaN p–n diodes terminated by plasma-hydrogenated p-GaN: revealing the role of thermal annealing,* Appl. Phys. Express 12, 051015 (2019).

49. J. Yang, D. G. Zhao, D. S. Jiang, P. Chen, Z. S. Liu, L. C. Le, X. J. Li, X. G. He, J. P. Liu, S. M. Zhang, H. Wang, J. J. Zhu, and H. Yang, *Investigation on the compensation effect of residual carbon impurities in low temperature grown Mg doped GaN films*, J. Appl. Phys. 115, 163704 (2014).

50. S. Chowdhury and U. K. Mishra, *Lateral and Vertical Transistors Using the AlGaN/GaN Heterostructure*, IEEE Trans. Electron Devices 60, 3060 (2013).

51. I. C. Kizilyalli, A. P. Edwards, H. Nie, D. Disney, and D. Bour, *High voltage vertical GaN p-n diodes with avalanche capability*, IEEE Trans. Electron Devices 60, 3067 (2013).

52. H. Fu, X. Huang, H. Chen, Z. Lu, I. Baranowski, and Y. Zhao, *Ultra-low turn-on voltage and on-resistance vertical GaN-on-GaN Schottky power diodes with high mobility double drift layers,* Appl. Phys. Lett. 111, 152102 (2017).

53. M. Sun, Y. Zhang, X. Gao, and T. Palacios, *High-performance GaN vertical fin power transistors on bulk GaN substrates*, IEEE Electron Device Lett. 38, 509 (2017).

54. D. Ren, and P. D. Dapkus, *Anisotropic Mg incorporation in GaN growth on nonplanar templates,* Appl. Phys. Lett. 86, 121901 (2005).

55. S. C. Cruz, S. Keller, T. E. Mates, U. K. Mishra, and S. P. DenBaars, *Crystallographic orientation dependence of dopant and impurity incorporation in GaN films grown by metalorganic chemical vapor deposition*, J. Cryst. Growth 311, 3817 (2009).

56. A. Chakraborty, H. Xing, M. D. Craven, S. Keller, T. Mates, J. S. Speck, S. P. DenBaars, and U. K. Mishra, *Nonpolar a-plane p-type GaN and p-n Junction Diodes*, J. Appl. Phys. 96, 4494 (2004).

57. J. Wang, Y. Gao, S. Alam, and F. Scholz, *Mg doping of 3D semipolar InGaN/GaN-based light emitting diodes*, Phys. Status Solidi A 211, 2645 (2014).

58. D. Ji and S. Chowdhury, *Design of 1.2 kV power switches with low R_{ON} using GaN-based vertical JFET*, IEEE Trans. Electron Devices 62, 2571 (2015).

59. S. Nakamura, G. Fasol, and S. J. Pearton, "The Blue Laser Diode: The Complete Story" 2nd ed (Springer, Heidelberg, 2000).

60. Y. Zhao, H. Fu, G. T. Wang, and S. Nakamura, *Toward ultimate efficiency: progress and prospects on planar and 3D nanostructured nonpolar and semipolar InGaN light-emitting diodes*, Adv. Opt. Photonics 10, 246 (2018).

61. K. Hiramatsu, K. Nishiyama, M. Onishi, H. Mizutani, M. Narukawa, A. Motogaito, H. Miyake, Y. Iyechika, and T. Maeda, *Fabrication and characterization of low defect density GaN using facet-controlled epitaxial lateral overgrowth (FACELO)*, J. Cryst. Growth 221, 316 (2000).

62. B. Beaumont, S. Haffouz, and P. Gibart, *Magnesium induced changes in the selective growth of GaN by metalorganic vapor phase epitaxy*, Appl. Phys. Lett. 72, 921 (1998).

63. M. Leroux, N. Grandjean, B. Beaumont, G. Nataf, F. Semond, J. Massies, and P. Gibart, *Temperature quenching of photoluminescence intensities in undoped and doped GaN*, J. Appl. Phys. 86, 3721 (1999).

64. T. Suski, E. Litwin-Staszewska, R. Piotrzkowski, R. Czernecki, M. Krysko, S. Grzanka, G. Nowak, G. Franssen, L. H. Dmowski, M. Leszczynski, P. Perlin, B. Łucznik, I. Grzegory, and R. Jakieła, *Substrate misorientation induced strong increase in the hole concentration in Mg doped GaN grown by metalorganic vapor phase epitaxy*, Appl. Phys. Lett. 93, 172117 (2008).

65. L. Jiang, J. Liu, A. Tian, X. Ren, S. Huang, W. Zhou, L. Zhang, D. Li, S. Zhang, M. Ikeda, and H. Yang, *Influence of substrate misorientation on carbon impurity incorporation and electrical properties of p-GaN grown by metalorganic chemical vapor deposition*, Appl. Phys. Express 12, 055503 (2019).

66. I. C. Kizilyalli, D. P. Bour, T. R. Prunty, and G. Ye, "High power gallium nitride electronics using miscut substrates," US Patent No.10,347,736 B2 (9 July 2019).

67. S. R. Alugubelli, H. Fu, K. Fu, H. Liu, Y. Zhao, and F. A. Ponce, *Dopant profiling in p-i-n GaN structures using secondary electrons*, J. Appl. Phys. 126, 015704 (2019).

68. H. Liu, H. Fu, K. Fu, S. R. Alugubelli, P.-Y. Su , Y. Zhao, and F. A. Ponce, *Non-uniform Mg distribution in GaN epilayers grown on mesa structures for applications in GaN power electronics*, Appl. Phys. Lett. 114, 082102 (2019).

69. M. Shinohara and N. Inoue, *Behavior and mechanism of step bunching during metalorganic vapor phase epitaxy of GaAs*, Appl. Phys. Lett. 66, 1936 (1995).

70. J. Wu, W. Walukievicz, K. M. Yu, W. Shan, J. W. Ager III, E. E. Haller, H. Lu, W. J. Schaff, W. K. Metzer, and Sarah Kurtz, *Superior radiation resistance of $In_{1-x}Ga_xN$ alloys: Full-solar-spectrum photovoltaic material system*, J. Appl. Phys. 94, 6477 (2003).

71. A. M Fischer, Y. O. Wei, F. A. Ponce, M. Moseley, B. Gunning, and W. A. Doolittle, *Highly luminescent, high-indium-content InGaN film with uniform composition and full misfit-strain relaxation*, Appl. Phys. Lett. 103, 131101 (2013).

72. J. J. Williams, H. McFavilen, A. M. Fischer, D. Ding, S. Young, E. Vadiee, F. A. Ponce, C. Arena, C. B. Honsberg, and S. M. Goodnick, *Refractory InxGa1−xN Solar Cells for High-Temperature Applications*, IEEE J. Photovoltaics 7, 1646 (2017).

73. X. Huang, H. Fu, H. Chen, Z. Lu, I. Baranowski, J. Montes, T.-H. Yang, B. P. Gunning, D. Koleske, and Y. Zhao, *Reliability analysis of InGaN/GaN multi-quantum-well solar cells under thermal stress*, Appl. Phys. Lett. 111, 233511 (2017).

74. G. T. Thaler, D. D. Koleske, S. R. Lee, K.H. A. Bogart, and M. H.Crawford, *Thermal stability of thin InGaN films on GaN*, J. Cryst. Growth 312, 1817 (2010).

75. M. D. McCluskey, L. T. Romano, B. S. Krusor, D. P. Bour, N. M. Johnson, and S. Brennan, *Phase separation in InGaN/GaN multiple quantum wells*, Appl. Phys. Lett. 72, 1730 (1998).

76. C.-C. Chuo, C.-M. Lee, T.-E. Nee, and J.-I. Chyi, *Effects of thermal annealing on the luminescence and structural properties of high indium-content InGaN/GaN quantum wells*, Appl. Phys. Lett. 76, 3902 (2000).

77. C.-C. Chuo, M. N. Chang, F.-M. Pan, C.-M. Lee, and J.-I. Chyi, *Effect of composition inhomogeneity on the photoluminescence of InGaN/GaN multiple quantum wells upon thermal annealing*, Appl. Phys. Lett. 80, 1138 (2002).

78. G. Li, S. J. Chua, J. H. Teng, W. Wang, Z. C. Feng, Y. H. Huang, and T. Osipowicz, *Blueshift of $In_{0.2}Ga_{0.8}N$/GaN single quantum well band gap energy by rapid thermal annealing*, J. Vac. Sci. Technol. B 17, 1507 (1999).

79. U. Jahn, S. Dhar, H. Kostial, I. M. Watson, and K. Fujiwara, *Low-energy electron-beam irradiation of GaN-based quantum well structures*, Phys. Status Solidi C 0, 2223 (2003).

80. N. M. Shmidt, P. S. Vergeles, E. E. Yakimov, E. B. Yakimov, *Effect of low-energy electron irradiation on the cathodoluminescence of multiple quantum well (MQW) InGaN/GaN structures*, Solid State Comm. 151, 208 (2011).

81. P. S. Vergeles, N. M. Shmidt, E. E. Yakimov, and E. B. Yakimov, *Effect of low energy electron irradiation on optical properties of InGaN/GaN light emitting structures*, Phys. Status Solidi C 8, 1265 (2011).

82. Y. Kuznetsova, and M. Zamoryanskaya, *Unstable Luminescence of Nitrides under Electron-Beam Irradiation*, Japan. J. Appl. Phys. 52, 08JJ06 (2013).

83. P. Chen, R. Zhang, X.F. Xu, Y.G. Zhou, Z.Z. Chen, S.Y. Xie, W.P. Li, and Y.D. Zheng, *The oxidation of gallium nitride epilayers in dry oxygen*, Appl. Phys. A 71, 191 (2000).

84. D. Song, L. Li, B. Li, Y. Sui, and A. Shen, *Band gap engineering of N-alloyed Ga_2O_3 thin films*, AIP Advances 6, 065016 (2016).

85. A. White, and W. Melville, *The decomposition of ammonia at high temperatures*, J. Am. Chem. Soc. 27, 373 (1905).

86. C. H. Kunsman, *The thermal decomposition of ammonia on tungsten, molybdenum, and nickel*, J. Am. Chem. Soc. 50, 2100 (1928).

87. F. A. Ponce, D. P. Bour, W. Götz, and P. J. Wright, *Spatial distribution of the luminescence in GaN thin films*, Appl. Phys. Lett. 68, 57 (1996).

88. S. Nakamura, *GaN growth using GaN buffer layer*, Jpn. J. Appl. Phys. 30, 1705 (1991).

APPENDIX A

LIST OF PUBLICATIONS DURING THE STUDY TOWARDS THE DOCTORAL DEGREE

C. Yang, H. Fu, P.-Y. Su, H. Liu, K. Fu, X. Huang, T.-H. Yang, H. Chen, J. Zhou, X. Deng, J. Montes, X. Qi, F. A. Ponce, and Y. Zhao, *Demonstration of GaN-based metal-insulator-semiconductor junction by hydrogen plasma treatment*, submitted to Appl. Phys. Lett.

P.-Y. Su*, H. Liu*, C. Yang, K. Fu, H. Fu, Y. Zhao, and F. A. Ponce, *Lateral and vertical growth of Mg-doped GaN on trench-patterned GaN films*, submitted to Appl. Phys. Lett.

P.-Y. Su, H. Liu, S. Wang, Z. Wu, R. Liu, and F. A. Ponce, *The effect of low-angle off-axis GaN substrate orientation on the surface morphology of Mg-doped GaN epilayers*, submitted to J. Appl. Phys.

H. Liu, P.-Y. Su, Z. Wu, R. Liu, and F. A. Ponce, *Influence of substrate miscut angle on the optical properties of Mg-doped GaN*, J. Appl. Phys. **127**, 195701 (2020).

A. Chikhalkar, A. Gangopadhyay, H. Liu, C. Zhang, F. A. Ponce, D. J. Smith, C. Honsberg, and R. R. King, *Investigation of polycrystalline $GaxIn_{1-x}P$ for potential use as a solar cell absorber with tunable bandgap*, J. Appl. Phys. **127**, 073102 (2020).

S. R. Alugubelli, H. Fu, K. Fu, H. Liu, Y. Zhao, M. R. McCartney, and F. A. Ponce, *Determination of electronic band structure by electron holography of etched-and-regrown interfaces in GaN p-i-n diodes*, Appl. Phys. Lett. **115**, 201602 (2019).

H. Liu, H. Fu, K. Fu, S. R. Alugubelli, P.-Y. Su, Y. Zhao, and F. A. Ponce, *Non-uniform Mg distribution in GaN epilayers grown on mesa structures for applications in GaN power electronics*, Appl. Phys. Lett. **114**, 082102 (2019).

S. R. Alugubelli, H. Fu, K. Fu, H. Liu, Y. Zhao, and F. A. Ponce, *Dopant profiling in p-i-n GaN structures using secondary electrons*, J. Appl. Phys. **126**, 015704 (2019).

H. Fu, K. Fu, H. Liu, S. R. Alugubelli, X. Huang, H. Chen, J. Montes, T.-H. Yang, C. Yang, J. Zhou, F. A. Ponce, and Y. Zhao, *Implantation-and etching-free high voltage vertical GaN p–n diodes terminated by plasma-hydrogenated p-GaN: revealing the role of thermal annealing*, Appl. Phys. Express **12**, 051015 (2019).

P.-Y. Su, H. Liu, R. M. S. Kawabata, E. C. Weiner, R. Jakomin, M. P. Pires, R. R. King, P. L. Souza, and F. A. Ponce, *Effect of InAs quantum dots capped with GaAs on atomic-scale ordering in $Ga_{0.5}In_{0.5}P$*, J. Appl. Phys. **125**, 053104 (2019).

K. Fu, H. Fu, H. Liu, S. R. Alugubelli, T.-H. Yang, X. Huang, H. Chen, I. Baranowski, J. Montes,F. A. Ponce, and Yuji Zhao, *Investigation of GaN-on-GaN vertical p-n diode with regrown p-GaN by metalorganic chemical vapor deposition*, Appl. Phys. Lett. **113**, 233502 (2018).

H. Fu, X. Zhang, K. Fu, H. Liu, S. R. Alugubelli, X. Huan, H. Chen, I. Baranowski, T.-H. Yang, K. Xu, F. A. Ponce, B. Zhang, and Y. Zhao, *Nonpolar vertical GaN-on-GaN p-n didodes grown on free-standing (10-10) m-plane GaN substrates*, Appl. Phys. Express **11**, 111003 (2018).

S. Wang, H. Xie, H. Liu, A. M. Fischer, H. McFavilen, and F. A. Ponce, *Dislocation baskets in thick $In_xGa_{1-x}N$ epilayers*, J. Appl. Phys. **124**, 105701 (2018).

D. Swanson, C. Reich, A. Abbas, T. Shimpi, H. Liu, F. A. Ponce, J. M. Walls, Y.-H. Zhang, W. K. Metzger, W. S. Sampath, and Z. C. Holman, *CdCl2 passivation of polycrystalline CdMgTe and CdZnTe absorbers for tandem photovoltaic cells*, J. Appl. Phys. **123**, 203101 (2018).

X. Li, S. Wang, H. Liu, F. A. Ponce, T. Detchprohm, and R. D. Dupuis, *100-nm thick single-phase wurtzite BAlN films with boron contents over 10%*, Phys. Status Solidi B **8**, 1600699 (2017).

H. Xie, R. Prioli, G. Torelly, H. Liu, A. M. Fischer, R. Jakomin, R. Mourão, R. M. S. Kawabata, M. P. Pires, P. L. Souza, and F. A. Ponce, *Correlation between size distribution and luminescence properties of spool-shaped InAs quantum dots*, Semicon. Sci. Technol **32**, 055013 (2017).